Association between Natural Killer Cell Education and Cellular Glucose Metabolism in Human Natural Killer Cells

Dissertation

with the aim of achieving a doctoral degree at the Faculty of Mathematics, Informatics and Natural Sciences Department of Chemistry, University of Hamburg

submitted by

Caroline Pfeifer

Hamburg, 29th of October, 2018

Dissertationsgutachter / *dissertation reviewer:*

1. Gutachter / *first reviewer*: **Prof. Dr. Marcus Altfeld**,

Department of Virus Immunology, Heinrich Pette Institute (HPI), Leibniz-Institute for Experimental Virology, Hamburg, Germany

2. Gutachter / *second reviewer*: **Prof. Dr. Michael Kolbe**,

Department of Structural Infectionbiology, Helmholtz Centre for Infection Research, Centre for Structural Systems Biology (CSSB), Hamburg, Germany

vorgelegt von / *submitted by*: **Caroline Pfeifer**

vorgelegt am / *submitted on*: **29th of October, 2018**

Datum der Disputation / *date of thesis defense*: **18th December, 2018**

This work was done in the period from

1st of September 2015 until 30st of September 2018

in the research department Virus Immunology of Prof. Dr. med. Marcus Altfeld

at the Heinrich Pette Institute, Leibniz Institute for Experimental Virology, Hamburg.

Diese Arbeit wurde im Zeitraum vom

1. September 2015 bis zum 30. September 2018

am Heinrich-Pette Institut Hamburg

in der Arbeitsgruppe Virus Immunologie von Prof. Dr. Marcus Altfeld angefertigt.

Table of contents

Zusammenfassung

Natürliche Killer (NK)-Zellen sind Teil des angeborenen Immunsystems und werden zu der Gruppe der Lymphozyten gezählt. Sie besitzen die Fähigkeit abnormale Zellen, wie beispielsweise Tumorzellen oder virusinfizierte Zellen von normalen, körpereigenen Zellen zu unterscheiden. Dies geschieht mit Hilfe spezieller inhibitorischer und aktivierender Rezeptoren auf der Zelloberfläche dieser Zellen. Inhibitorische Rezeptoren vermitteln den Zellen eine Toleranz gegenüber körpereigenen normalen Zellen, während aktivierende Rezeptoren die Zellen zur Ausübung von zytotoxischen Funktionen anregen, welche zum Tod der Zielzelle führen können. Inhibitorische Rezeptoren, welche an körpereigene Moleküle binden, übertragen dabei eine funktionelle Kompetenz, welche es den Zellen erlaubt auf aktivierende Signale zu reagieren. Fehlt den Zellen diese funktionelle Kompetenz, bleiben sie passiv. Dieser Prozess ist auch als NK-Zell Lizensierung bekannt. Dabei weisen lizensierte NK-Zellen bei Stimulation eine erhöhte Funktion gegenüber unlizensierten NK-Zellen auf. Über die zugrunde liegenden molekularen Mechanismen, welche zu funktionellen Unterschieden zwischen lizensierten und unlizensierten NK-Zellen führen, ist nur wenig bekannt. Eine zunehmende Anzahl von Studien konnte zeigen, dass die Funktionen von Immunzellen maßgeblich durch zelluläre Stoffwechselwege beeinflusst werden können. Veränderungen innerhalb dieser Stoffwechselwege könnten daher eine Rolle bei der Übertragung von funktioneller Kompetenz in lizensierten NK-Zellen spielen. Aus diesem Grund war es das Ziel dieser Arbeit, das glykolytische Profil von lizensierten und unlizensierten NK-Zellen zu bestimmen und miteinander zu vergleichen. Dafür wurden primäre human NK-Zellen aus Vollblut isoliert und anschließend mit Zielzelllinien stimuliert. Mit Hilfe von durchflusszytometrischen Methoden konnte die funktionelle Aktivität sowie die Expression von inhibitorischen Rezeptoren bestimmt werden. Basierend auf diesen funktionellen und phänotypischen Analysen, wurden NK-Zellen in lizensierte und unlizensierte Untergruppen eingeteilt. Für die Bestimmung des glykolytischen Profils wurden lizensierte und unlizensierte NK-Zellen auf die Expression des Glukosetransporters Glut1 untersucht. Mittels Fluoreszenz-aktivierter Zellsortierung konnten lizensierte und unlizensierte NK-Zellen isoliert und die glykolytische Aktivität in einem Seahorse XF Glykolyse Stresstest gemessen werden. Dabei konnte gezeigt werden, dass lizensierte NK-Zellen erhöhte Funktion gegenüber unlizensierten NK-Zellen besitzen. Lizensierte NK-Zellen wiesen darüber hinaus eine

gesteigerte Expression des Glukosetransporters Glut1 auf. Zudem zeigten lizensierte NK-Zellen ein erhöhtes glykolytisches Profil. Die Ergebnisse dieser Arbeit zeigten, dass lizensierte NK-Zellen ein charakteristisches metabolisches Profil besitzen, welches ein mögliches Erklärungsmodell für die funktionellen Unterschiede zwischen lizensierten und unlizensierten NK-Zellen liefert.

Abstract

Natural killer (NK) cells express activating and inhibitory receptors to distinguish between healthy and aberrant cells. Whereas activating receptors detect stress-ligands on virus-infected or malignant cells, inhibitory receptors bind to self-molecules that are expressed by all nucleated host cells. Inhibitory receptors that bind to self-molecules mediate self-tolerance and transfer functional competence to NK cells, allowing these cells to respond upon activation. This process is known as NK-cell education. Thereby, educated NK cells exhibit increased responsiveness upon stimulation while being tolerant towards healthy host cells at the same time. In contrast, uneducated NK cells, that lack inhibitory receptors for self-molecules, have been shown to be hyporesponsive upon stimulation. To date, little is known about the underlying molecular mechanisms leading to functional differences between educated and uneducated NK cells. An increasing number of studies have shown that immune cell functions can be directly influenced by cellular metabolic pathways. Changes within these metabolic pathways may therefore play a role in NK-cell education. For this reason, the aim of this work was to determine the glycolytic profiles of educated and uneducated NK cells. Primary human NK cells were isolated and co-cultured with the target cell lines K-562 and 721.221. NK-cell function and the expression of inhibitory receptors was assessed via flow cytometry. Based on functional and phenotypical analysis, NK cells were stratified into educated and uneducated NK-cell subsets. In order to determine the glycolytic profile of educated and uneducated NK cells, these subsets were examined for the expression of the glucose transporter Glut1. Using fluorescence-activated cell sorting, NK cells were divided into educated and uneducated NK-cell populations, which were subsequently analyzed for their glycolytic activity in a Seahorse XF glycolysis stress test. Data revealed, that educated NK cells exhibited an increased functional capacity upon stimulation with target cell lines compared to uneducated NK cells. Furthermore, educated NK cells displayed an increased surface expression of the glucose transporter Glut1. In addition, educated NK cells possessed an elevated glycolytic profile. The results of this work showed that educated NK cells display a characteristic metabolic profile that provides a potential model for the underlying mechanisms that lead to functional differences between educated and uneducated NK cells.

Index of abbreviations

Acronym	Definition
2-DG	2-Deoxy-D-glucose
3PG	3-phosphoglycerate
ACC	Acceleration
Acetyl-CoA	Acetyl coenzyme A
ADCC	Antibody-dependent cell-mediated cytotoxicity
ADP	Adenosine diphosphate
APC	Antigen-presenting cell
APC	Allophycocyanin
ATP	Adenosine triphosphate
BP-filter	Bandpass filter
BV	Brilliant Violet
CD	Cluster of differentiation
CS&T	Cytometer setup and tracking
DAP12	DNAX activation protein of 12kDa
DC	Dendritic cells
DECEL	Deceleration
DMSO	Dimethyl sulfoxide
DNA	Deoxyribonucleic acid
DPBS	Dulbecco's phosphate buffered saline
EDTA	Ethylenediaminetetraacetic acid
eGFP	Enhanced green fluorescent protein
ETC	Electron transport chain
FACS	Fluorescence-activated cell sorting
FAD	Flavin adenine dinucleotide, oxidized form
FADH	Flavin-Adenin-Dinukleotid, reduced form
FAO	Fatty acid oxidation
FAS	Fatty acid synthase
FasL	Fas ligand
FBS	Fetal bovine serum
Fc region	Fragment crystallizable region
FCS-file	Flow cytometry standard file
FcγRIII	Fcγ receptor III
FITC	Fluorescein isothiocyanate
FMO	Fluorescence mius one
FSC	Forward scatter

HBSS	Hank's balanced salt solution
HIF1α	Hypoxia-inducible factor 1a
HLA	Human leukocyte antigen
HTLV	Human T cell leukemia virus
IFN-γ	Interferon gamma
IgG	Immunoglobulin G
iKIR	Inhibitory killer-cell immunoglobulin-like receptor
IL-15	Interleukin-15
ILC	Innate lymphoid cells
ITAM	Tyrosine-based activation motif
ITIM	Immunoreceptor tyrosine-based inhibition motif
KIR	Killer-cell immunoglobulin-like receptor
LN	Liquid nitrogen
LP-filter	Longpass filter
LRC	Leukocyte receptor complex
MHC	Major histocompatibility complex
mTOR	Mammalian target of rapamycin
mTORC1	Mammalian target of rapamycin complex 1
mTORC2	Mammalian target of rapamycin complex 2
NAD^+	Nicotinamide adenine dinucleotide, oxidized form
NADH	Nicotinamide adenine dinucleotide, reduced form
NK cell	Natural Killer cell
NKC	Natural killer gene complex
NKG	NK cell group
OXPHOS	Oxidative phosphorylation
PBMC	Peripheral blood mononuclear cell
PDC	Pyruvate dehydrogenase complex
PDK1	Phosphatidylinositide 3-kinase-dependent kinase
PFA	Paraformaldehyde
P_i	Inorganic phosphate
PI3K	Phosphatidylinositide 3-kinase
PIP2	Phosphatidylinositol (4,5)-bisphosphate
PIP3	phosphatidylinositol (3,4,5)-trisphosphate
PKB	Protein kinase B
PKM2	Pyruvate kinase
PMT	Photomultiplier tube
RBD	Receptor-binding domain
RCF	Relative centrifugal force

RFI	Relative fluorescence intensity
RHEB	RAS homolog enriched in brain
RPMI	Roswell park memorial institute
SHP-1	Src homology region 2 domain-containing phosphatase-1
SSC	Side scatter
Syk	Spleen tyrosine kinase
TCR	T cell receptor
TfR1	Transferrin receptor protein 1
TNF-α	Tumor necrosis factor alpha
TRAIL	Tumor necrosis factor related apoptosis inducing ligand
WBS	White blood cells
ZAP70	Zeta-chain-associated protein kinase 70

List of tables

Table of figures

1 Introduction

1.1 The human immune system

The immune system is a defense system that protects an organism of malignancies and disease-causing microorganisms or pathogens, such as viruses, bacteria and fungi (1). It is classically divided into innate and adaptive immunity. The innate immune system is composed of a variety of myeolid and lymphoid cells that can rapidly eradicate invading pathogens by implementing various effector functions. The main cells of the innate immune system are phagocytic leukocytes, granulocytes, dendritic cells and natural killer (NK) cells. Adaptive immunity, however, develops during the lifetime of an individual and is mainly characterized by two types of lymphocytes, B and T cells (2) (**Figure 1**). While the innate immune system relies on recognition of invariant patterns to detect and eliminate pathogens, cells of the adaptive immune system carry highly specific antigen receptors that recognize unique antigen-specific structures. Additionally, antigen-reactive lymphocytes acquire the property of immunological memory, which enhances protection against reinfection by the same pathogen.

1.2 Innate and adaptive immunity

Innate immunity represents the first line of defense against pathogens by preventing infection of the host (3). Epithelial surfaces provide a physical barrier against pathogen entry by isolating the internal environment from external factors and impeding pathogen spreading through the secretion of antimicrobial enzymes and peptides. Pathogens that have crossed the epithelial surface, encounter a major component of the innate immunity known as the complement system, which comprises soluble proteins present in the blood and other body fluids (4). Thus, invading pathogens are coated with antibodies or complement proteins that can be detected by phagocytic cells, which in turn will destroy and ingest the labeled pathogen. Phagocytic cells, such as macrophages and dendritic cells, that have internalized pathogens, can present pathogen-derived fragments on their cell surface and thereby function as antigen-presenting cells (APCs). At the same time, the stimulation of innate sensors on innate cells leads to the release of pro-inflammatory chemokines and cytokines, which recruit other immune cells to the sites of infection. Moreover, NK cells play an important role in the recognition and killing of cancer or virus-infected host cells. They

possess specialized surface receptors to distinguish between healthy and abberrant cells based on the expression of human leukocyte antigen (HLA) class I molecules and stress-ligands that are upregulated on infected cells. Once NK cells are activated they are able to exert cytotoxic effector functions that lead to the death of the target cell.

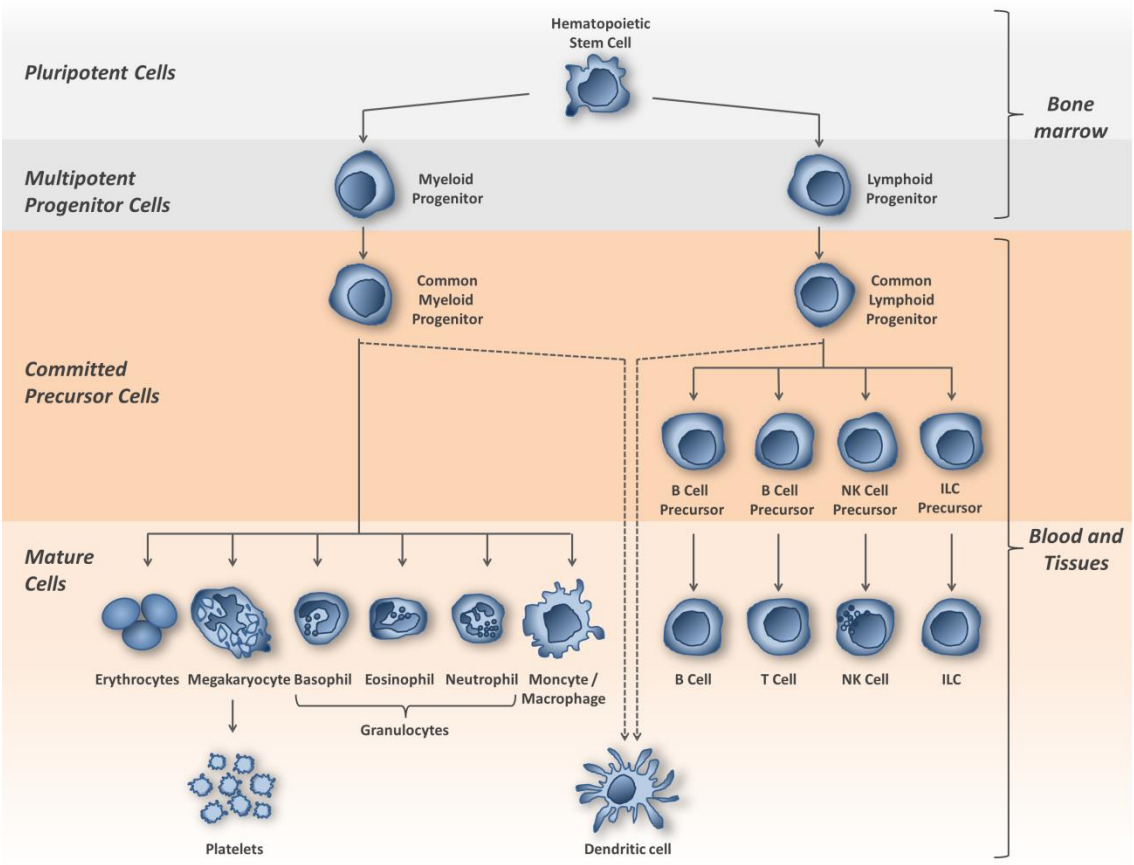

Figure 1: Haematopoiesis of human immune cells

Schematic illustration of the haematopoiesis of human immune cells. Cells of the immune system arise from pluripotent hematopoietic stem cells in the bone marrow, which divide into two types of multipotent stem cells. The myeloid progenitor gives rise to the myeloid lineage, which comprises erythrocytes, megakaryocytes, granulocytes, and monocytes. The lymphoid lineage gives rise to B and T cells, natural killer (NK) cells, and innate lymphoid cells (ILCs) (5). B and T cells are distinguished from the rest of the lymphocytes as they express antigen-specific receptors and are distinguished among each other by having different sites of differentiation – the bone marrow and thymus respectively. Unlike B and T lymphocytes, NK cells and ILCs lack antigen-specific receptors. The majority of dendritic cells arise from the common myeloid progenitor, but some may also derive from the common lymphoid progenitor cells. Monocytes can enter tissues where they can differentiate into phagocytic macrophages or dendritic cells. Finally, megakaryocytes can produce platelets, which are important for blood clotting (the figure was created based on (1)).

Upon inflammation, increased fluid in the tissues facilitates the movement of pathogen-bearing APCs to the lymph nodes. Once an APC arrived in the lymph node, it encounters naïve B and T cells. The ligation between the antigen presented by the APC and the antigen-specific B and T cell receptor leads to the maturation and activation of B and T cells. Thereby, APCs function as a bridge between the innate and adaptive immunity.

Although the innate immune system represents a defense mechanism that is essential for the host's control against many common pathogens, there are some pathogens that cannot be recognized by innate sensors (1). The defense system of innate immunity is based on several different germline-encoded receptors that recognize surface molecules that are common to many pathogens and have been conserved over the evolutionary course. Some pathogens, however, have evolved strategies to escape the detection through innate sensors. Lymphocytes of the adaptive immune response have evolved to overcome the limitation faced by the innate immune system. Instead of expressing several different receptors which target invariant surface features of various pathogens, naïve B and T cells carry specialized receptors that only show specificity for a single antigen. A unique gene-rearrangement mechanism that takes place during the development of these cells determines the specificity of these receptors. In that way, the receptors of the adaptive immune system can recognize an almost infinite number of antigens targeting each different pathogen specifically. Even though an individual lymphocyte carries receptors of only one specificity, the specificity of each lymphocyte is different, which creates a unique lymphocyte receptor repertoire in every individual. Furthermore, during the lifetime of an individual, these lymphocytes undergo a process of clonal selection. Thereby, only those lymphocytes that effectively bind to an antigen which is targeted by their receptor will be activated. Activated lymphocytes will then proliferate and differentiate into effector cells. This mechanism is called clonal expansion. After the antigen has been eliminated an increased number of activated antigen-specific B and T cells persist in the body known as memory cells. These cells can be reactivated much more quickly than naïve lymphocytes. After reinfection with the same pathogen, a more rapid and effective response can be realized by these cells, which contributes to the immunological memory of an individual and provides lasting protective immunity in the host.

1.3 Natural killer cells

NK cells were first described in the early 1970s as lymphocytes that were able to lyse certain tumor cell targets in mice (6–8) and humans (9). Those early studies reported that the observed antitumor effect was mediated by a unique subpopulation of non-adherent lymphoid cells that were lacking any known T- or B-lymphocyte cell-surface markers. Based on the "natural" cytotoxic activity this subpopulation was termed natural killer cells (8). NK cells represent around 5-15% of lymphocytes in peripheral blood and are present under physiological conditions in the bone marrow, liver, uterus, spleen, gut and lungs as well as to a lesser extent in secondary lymphoid tissue, mucosa-associated lymphoid tissue, and the thymus (10–12).

1.3.1 NK-cell receptors and functions

NK cells are effector lymphocytes that belong to the first-line of defense against viral infections (13) and malignant cells (14). To sense and respond to pathogens that infiltrated the host, NK cells possess a variety of surface receptors, which regulate their activity. Unlike T cells, which express highly specific antigen receptors that are generated by somatic gene rearrangements, NK cells express a number of germline-encoded receptors that can recognize molecules on the surface of infected or transformed cells (1) (**Figure 2**). NK cells express a variety of activating receptors which mainly recognize cellular stress ligands upregulated on malignantly transformed or virus-infected host cells. Engagement of activating receptors with stress-induced ligands will increase the probability that an NK cell will release cytokines and chemokines, such as interferon-γ (IFN-γ) or tumor necrosis factor-α (TNF-α). These molecules function as signaling proteins regulating maturation, growth, and responsiveness of other immune cells. At the same time, NK cells can also be stimulated by cytokines. Accordingly, they express cytokine receptors that bind cytokines which are produced by other immune cells, such as T cells or dendritic cells (DCs) (15). Thus, this immunological cross-talk connects the innate and adaptive immunity and contributes to a control of viral replication and the elimination of aberrant cells.

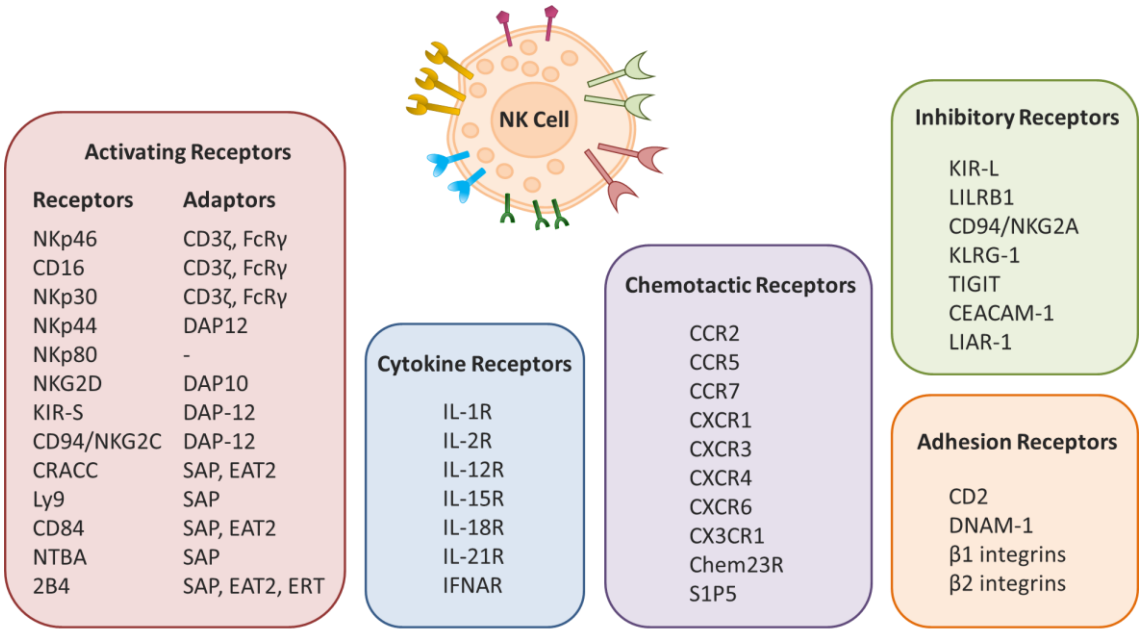

Figure 2: Human NK-cell receptor repertoire

Illustration of the human NK-cell receptor repertoire. NK cells are lymphocytes of the innate immune system that can detect virus-infected or malignant cells. To be able to distinguish between healthy and abnormal cells, they express numerous receptors on their cell surface that can be grouped into activating (red), inhibitory (green), cytokine (blue), chemotactic (purple) and adhesion receptors (orange). The integration of signals that they receive upon ligand binding controls NK-cell function. Thereby, NK cells can contribute to the protection against pathogens and shape the adaptive immune response (the figure was created based on (16)).

More important, NK cells exert effector functions that can directly kill target cells. Like cytotoxic T cells, NK cells store cytolytic proteins, such as perforin and granzymes in intracellular secretory granules in their cytosol. Upon activation, these cytolytic proteins are released through directed exocytosis towards the target cell, which can lead to target cell lysis. This is achieved by Fcγ receptors, such as FcγRIII, which are expressed on the surface of NK cells. These receptors recognize the Fc portion of immunoglobulin G (IgG) antibodies bound to the surface of pathogen-infected target cells. Engagement of the FcγRIII with IgG activates NK cells to release cytokines and to exert their cytotoxic effector functions (17). This process is known as antibody-dependent cell-mediated cytotoxicity (ADCC) (18). A second way to induce death of a target cell is mediated through expression of membrane-bound death ligands such as the TNF-related apoptosis-inducing ligand (TRAIL) or Fas ligand (Fas-L). These ligands bind to death-cell receptors (Fas-R or TRAIL-R) on the surface of target cells resulting in receptor aggregation and recruitment of adaptor proteins, which in turn will initiate death of the target cell through caspase-dependent apoptosis (19) (**Figure 3**).

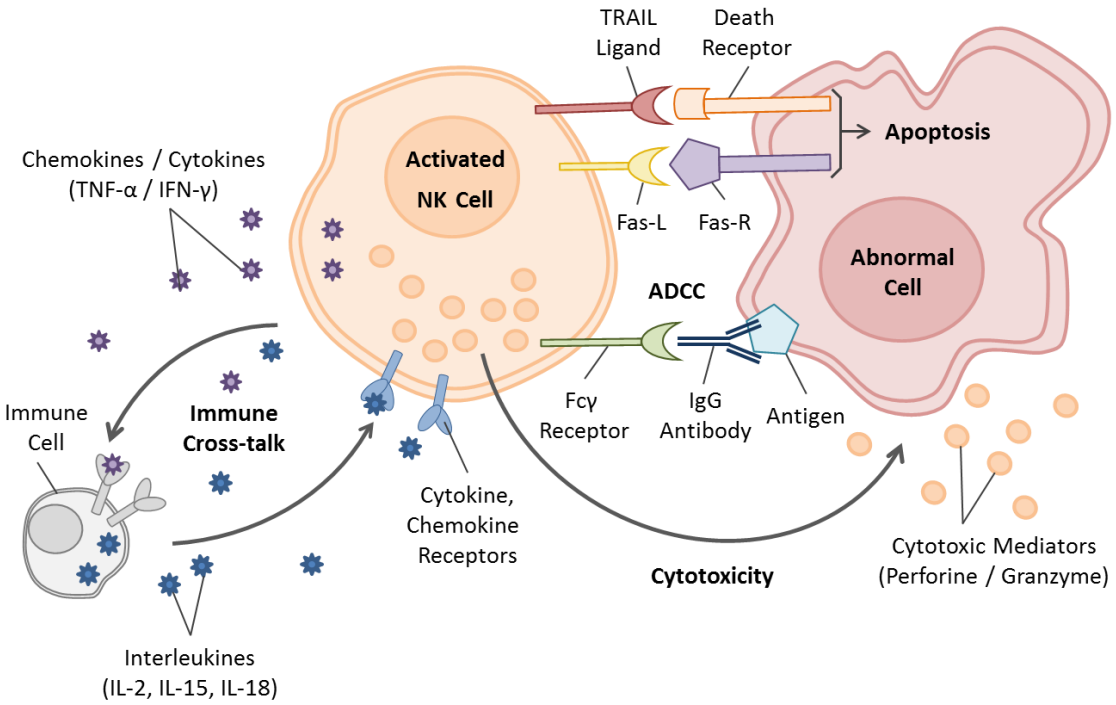

Figure 3: The cytotoxic effector functions of NK cells

Schematic representation of the cytotoxic effector functions of NK cells upon target cell regognition. NK cells can detect virus-infected or malignant cells. Various receptors and ligands that exist on the surface of NK cells can bind to stress molecules expressed by abnormal cells. NK cells express death ligands such as the TNF-related apoptosis-inducing ligand (TRAIL) or Fas ligand (Fas-L) which bind to death-cell receptors (Fas-R or TRAIL-R) on the surface of target cells and initiate caspase-dependent apoptosis in that cell. Moreover, NK cells express Fcγ receptors, such as FcγRIII, that recognize immunoglobulin G (IgG) antibodies bound to pathogen-infected target cells. NK-cell activation via Fcγ receptors leads to the release of cytotoxic mediators, such as granzymes and perforines that induce target cell lysis. This process is known as antibody-dependent cell-mediated cytotoxicity (ADCC). Activated NK cells will release cytokines, such as IFN-γ and TNF-α. Other immune cells in the surrounding can be stimulated through these cytokines resulting in maturation, growth, and an enhanced responsiveness towards pathogens. On the other hand, NK cells can get stimulated through cytokines that are released from immune cells, such as DCs, macrophages and T cells contributing to the cross-talk that links innate and adaptive immunity.

The important role of NK cells in the immune defense against pathogens becomes apparent in NK cell–deficient patients. NK cell deficiencies, however, are very rare and are characterized by a reduced quantity of NK cells among peripheral blood lymphocytes or a normal distribution in quantity but with severe defects within the implementation of effector functions (20). Individuals with NK-cell deficiencies are extremely susceptible to viral infections, especially to herpesvirus and papillomavirus infections (21). Both of these virus families have developed strategies to evade cytotoxic T cell responses, emphasizing the essential role for NK cells in antiviral defense.

1.3.2 Self-tolerance

An important feature of NK cells is their ability to distinguish between abnormal and healthy cells. Opposing signals received by a diverse set of activating and inhibitory NK-cell receptors determine, whether a cell that is interacting with an NK cell will be attacked or not. NK cells must be triggered by activating receptors to be able to lyse target cells or to produce effector cytokines. However, some healthy cells that are not diseased, express ligands that can bind to activating receptors on the surface of NK cells (22). If the stimulation through activating ligands on healthy cells were not counteracted, NK cells would possibly show autoimmune reactivity towards self lymphoid cells (23,24). Healthy cells express HLA class I molecules on their surface that serve as ligands for inhibitory NK-cell receptors. As these receptors bind to surface HLA class I, a signal is transferred into the cell, preventing NK cells from target cell killing (25,26). Thereby, NK cells are able to exhibit self-tolerance towards healthy host cells (**Figure 4**). This is in contrast to malignant or virus-infected cells, which may downregulate HLA class I molecules to evade recognition by T cells (27). A target cell that has lost expression of self-HLA class I molecules due to infection, delivers activating signals that are unopposed, which results in NK-cell activation and target-cell lysis. This phenomenon is known as missing-self recognition. As a result of transformation or infection, stimulatory ligands are induced to a higher extent compared to healthy cells, so that the signals derived from inhibitory receptors are overcome. Self-inhibitory signals and an increased expression of stress- or virus-induced ligands for activating NK-cell receptors tip the balance towards NK-cell activation, which is described as stress-induced self recognition. As NK cells become activated, they exert their effector functions through the release of cytotoxic molecules and moreover by the production of pro-inflammatory cytokines that can stimulate other immune cells to attack the pathogen (28).

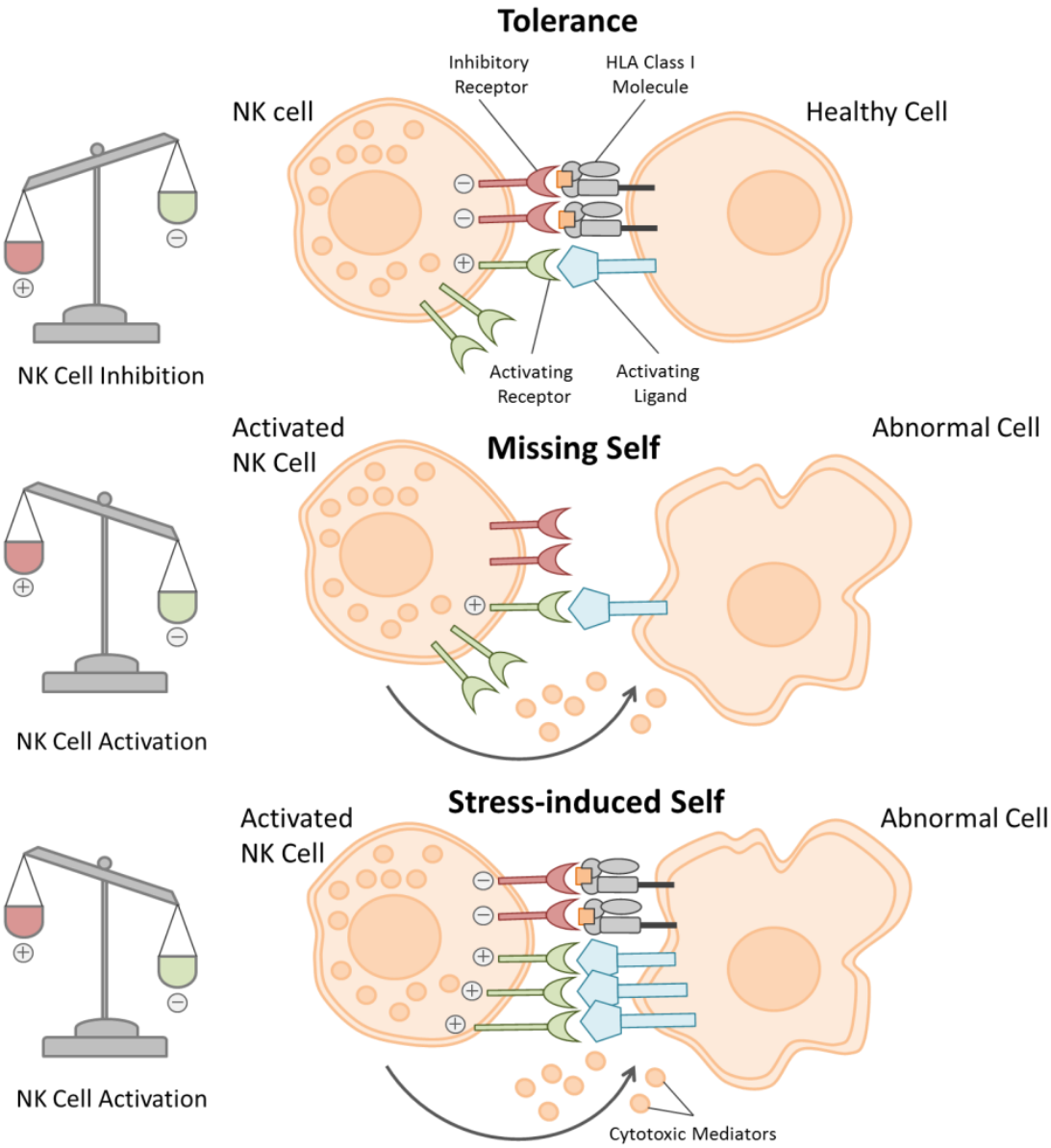

Figure 4: Concepts of NK cell activation and inhibition

Schematic illustration of NK-cell activation and inhibition. NK cells express inhibitory and activating receptors on their cell surface to discriminate between self and altered-self. Based on the receptor type, engagement with their cognate ligand transfers a signal into the cell that can be either activating or inhibitory. Balancing the signals that are received upon receptor ligation determines NK-cell reactivity. **Tolerance:** NK cells are tolerant towards healthy host cells expressing plenty of HLA class I molecules, as the strength of the inhibitory signal is overruling the activating signal. **Missing self**: Tumor cells or infected cells may downregulate HLA class I molecules, leading to NK-cell activation and target cell killing, due to loss of HLA class I molecules. **Stressed self**: Virus-infected or stressed cells upregulate activating ligands for NK cells, triggering NK-cell activation and elimination of the target cell (the figure was created based on (28)).

1.3.3 NK-cell receptor gene complexes

NK-cell function is well orchestrated by the integration of various signals perceived through several germline-encoded inhibitory and activating receptors expressed on the cell surface of NK cells (29). The genes that encode for NK-cell receptors are found within two main clusters on different chromosomes: the natural killer complex (NKC) on chromosome 12p13.1 and the leukocyte receptor complex (LRC) on chromosome 19q13.4 (30) (**Figure 5**). The NKC encodes for genes of the NKG2 family (31), whereas the LRC includes the KIR family. The NKC family is a group of C-type lectin-like receptors expressed on NK cells and T cell subsets (32–34). The NKG2 receptors are type II transmembrane proteins, where some family members such as NKG2A, NKG2C, and NKG2E form a heterodimer with CD94, another lectin-like protein encoded by the NKC (35). The NKG2 family is composed of inhibitory and activating receptors (36). CD94/NKG2C is an activating receptor that associates with DAP12 via positively charged residues in the transmembrane region (37), whereas CD94/NKG2A is an inhibitory receptor. Both receptors bind to the non-classical HLA class I molecule HLA-E, mediating an activating or inhibitory signal into the cell respectively (35,38,39).

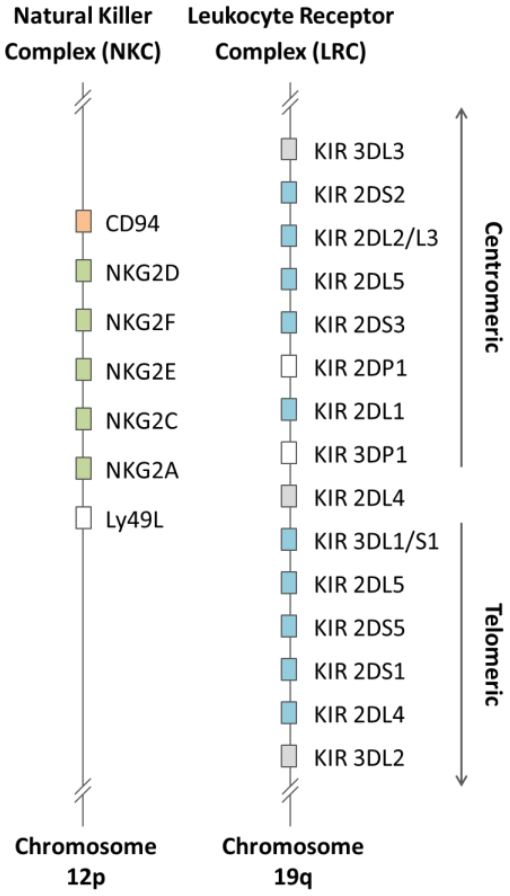

Figure 5: The NKC and LRC gene complexes in humans

Schematic overview of the genes encoded in the Natural Killer Complex (NKC) (left panel) on chromosome 12p and the Leukocyte Receptor Complex (LRC) (right panel) on chromosome 19q in humans. The NKC encodes for CD94 (orange), NKG2 family members (green), and the pseudogene Ly49L (white) whereas the LRC encodes for killer-cell immunoglobulin-like receptor (KIR) genes. The framework genes KIR3DL3 and KIR3DL2 (grey) represent the boundaries of the LRC. The gene for KIR2DL4 (grey) is located in the middle of the KIR cluster and is separating the centromeric-faced and telomeric-faced parts from each other. The LRC contains two pseudogenes KIR2DP1 and KIR3DP1 (white). Intergenic sequences separate the genes.

1.3.4 Killer-cell immunoglobulin-like receptors (KIRs)

In humans, the main NK-cell receptors for HLA class I molecules belong to the Killer-cell immunoglobulin-like receptor (KIR) gene family. This gene family encodes for activating and inhibitory surface receptors, consisting of type I transmembrane glycoproteins and extracellular immunoglobulin (Ig)-like domains. These receptors are expressed on NK cells and T cell subsets (40). The KIR gene cluster is characterized by differences within the gene content and allelic polymorphism between individual haplotypes (41). Each KIR can possess either two (KIR2D) or three (KIR3D) extracellular Ig-like domains. Upon receptor engagement, specific intracellular motifs mediate activating or inhibitory signals into the cell. Activating KIRs possess short cytoplasmic tails that are associated with adaptor molecules (such as DAP12), carrying immunoreceptor tyrosine-based activating motifs (ITAMs), whereas inhibitory KIRs have long cytoplasmic tails bearing immunoreceptor tyrosine-based inhibitory motifs (ITIMs) (42) (**Figure 6**). Upon ligand binding, tyrosines in the ITIMs become phosphorylated and can therefore associate with intracellular phosphatases (such as SHP-1), which results in the transfer of an inhibitory signal into the cell (43). On the contrary, activating receptors that bind their cognate ligand, phosphorylate ITAMs by Src-kinase family members, forming a binding site for tyrosine kinases ZAP70 and Syk, which leads to transfer of an activating signal (43).

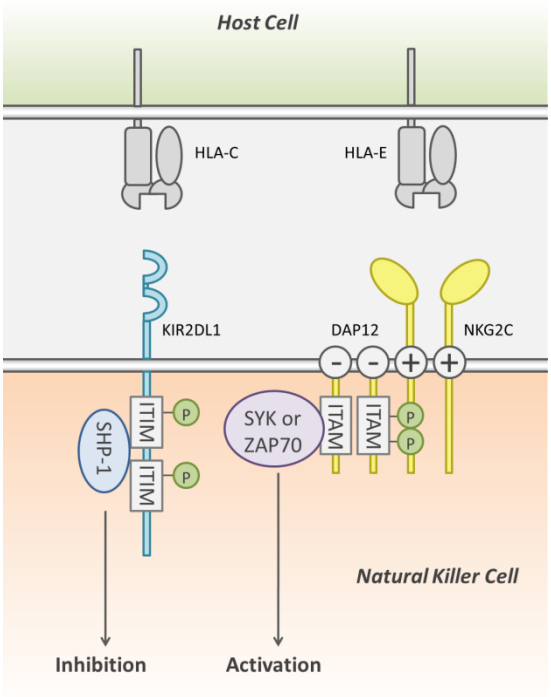

Figure 6: Inhibitory and activating NK-cell receptors

Schematic overview of an inhibitory and an activating NK-cell receptor and the resulting signal after binding with their cognate HLA class I ligand on host cells. Inhibitory receptors, such as the KIR2DL1 possess two immunoreceptor tyrosine-based inhibition motifs (ITIMs) within their cytoplasmic tail. Upon engagement with their cognate HLA ligand, these motifs become phosphorylated and bind to tyrosine phosphate SHP-1 leading to an inhibitory signal. Activating receptors, such as NKG2C that are associated with DAP12, which carries an immunoreceptor tyrosine-based activating motif (ITAM) in its cytoplasmic tail. Receptor engagement with HLA-E, leads to a phosphorylation of tyrosines in the ITAM motif by Src-kinase family members. Phosphorylated ITAMs are subsequently bound by the tyrosine kinases Syk and ZAP70 leading to an activation signal (the figure was created based on (43)).

1.4 Regulation of NK-cell activity

1.4.1 HLA class I molecules

In humans, HLA class I molecules[1] are encoded by the human leukocyte antigen (HLA) gene complex and are expressed on the surface of all nucleated cells (44). Based on their ability to present antigens on the cell surface for the recognition by T cells, they play a crucial role in the adaptive immunity (1). HLA class I molecules are heterodimers composed of two polypeptides, the α-chain and β_2-microglobulin (β_2m), whereas a groove in-between the two helices facilitates peptide binding (**Figure 7**). The α-chain is highly polymorphic and encoded by genes from the class I HLA locus on chromosome 6, whereas β_2m is not polymorphic and encoded by the β_2m gene on chromosome 15. In the human population, there are three classical class I α-chain genes (HLA-A, -B, and –C), which are characterized multiple allele-variants. In addition, most individuals are heterozygous for each gene. The particular combination of HLA alleles found on a single chromosome is termed HLA haplotype. Allelic variations can affect the nature and composition of the peptide-binding groove and thus modulate the peptide repertoire that is presented on the surface (45). The HLA class I α-chain folds and assembles with β2m in the lumen of the endoplasmic reticulum (ER), where it is loaded with pathogen-derived peptides. Peptide-loaded HLA class I molecules will be released from the ER and further transported via the Golgi apparatus to the plasma membrane (**Figure 7**). Once the peptide-loaded HLA class I molecules have arrived on the surface, they present their antigen to cytotoxic $CD8^+$ T cells. T cell receptors (TCR) on the surface of $CD8^+$ T cells, which possess a specificity for the presented antigen can bind to the HLA class I molecule leading to T cell activation. Furthermore, inhibitory NK-cell receptors have been shown to exhibit a degree of peptide specificity as well. Nevertheless, this specificity is much broader than the peptide specificity of TCRs, with NK-cell receptors recognizing peptide motifs, rather than individual peptides (46–49). This peptide selectivity has been confirmed for all inhibitory killer cell immunoglobulin-like receptors (KIRs) tested to date, particular activating KIRs, and also members of the C-type lectin-like receptor family (50). During viral infections and tumorgenesis, viral or tumor antigens can be presented by HLA class I molecules to cytotoxic effector T cells. However, it has been shown that the peptide presentation

[1] HLA class I molecules are the human pendant to *major histocompatibility complex (MHC)* class I molecules, that are found in all modern species of jawed vertebrates (1).

process can be altered during viral infections, resulting in modifications within the peptide repertoire that is presented by HLA class I molecules (51). The recognition of changes in peptide repertoire by NK cells might confer a selective advantage to the host, but the significance of these observations still has to be elucidated.

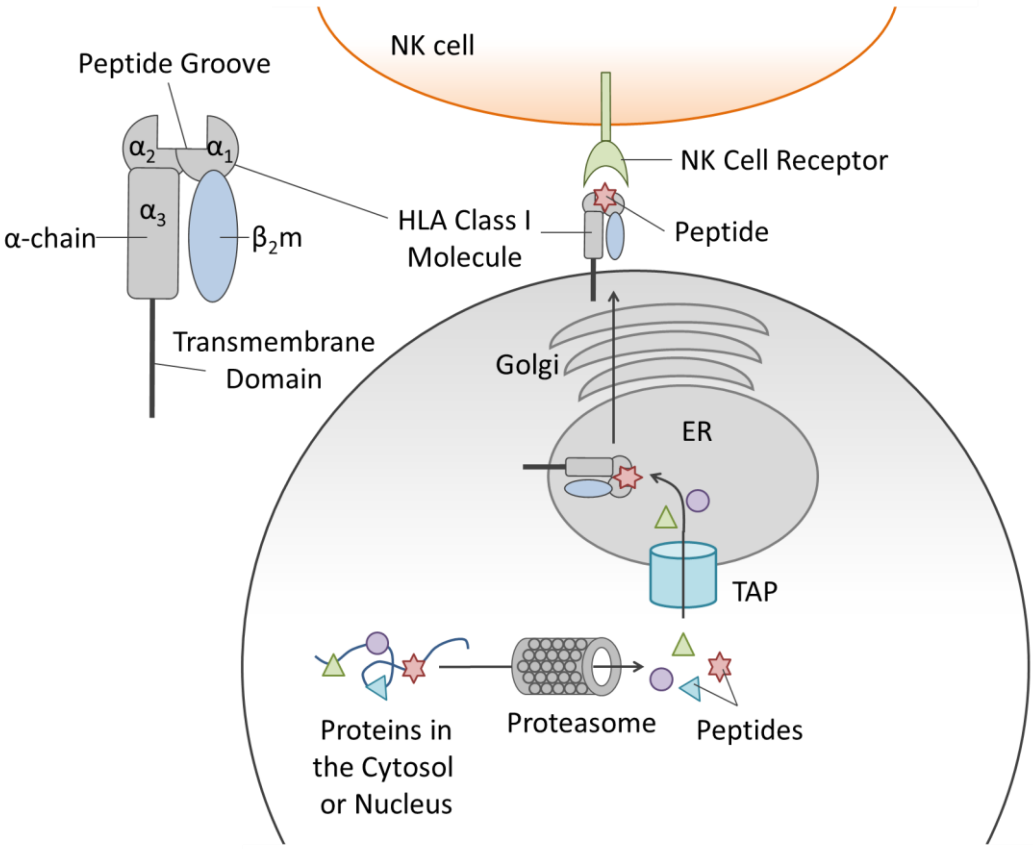

Figure 7: HLA class I molecule and the antigen presentation pathway

Schematic figure of an HLA class I molecule and the antigen presentation pathway. HLA class I molecules are composed of two polypeptides, the α-chain and β_2-microglobulin (β_2m). Transmembrane helices anchor the α-chain of the molecule in the membrane. The first step in the antigen presentation pathway of HLA class I molecules, is the degradation of antigens by the proteasome in the cytosol. The resulting peptides are translocated via transporter associated with antigen presentation (TAP) into the lumen of the endoplasmic reticulum (ER) and are subsequently loaded onto HLA class I molecules. Peptide-loaded HLA class I molecules will be released from the ER and transported via the Golgi apparatus to the plasma membrane. Surface HLA class I molecules can be recognized by NK cells or cytotoxic $CD8^+$ T cells (the figure was created based on (52)).

1.4.2 HLA class I molecules as ligands for NK-cell receptors

KIR receptors recognize specific motifs of HLA class I molecules (53). These molecules are encoded by highly polymorphic genes of the HLA class I gene complex. HLA-C is the dominant HLA class I locus that expresses ligands for many KIR receptors (54). The inhibitory receptors KIR2DL1, KIR2DL2, KIR2DL3 recognize different epitopes on HLA-C molecules (55,56). Based on sequence polymorphism at amino acid position 80, HLA-C molecules can be subdivided into two principal groups: HLA-C group 2 (Lys^{80}) and HLA-C group 1 (Asn^{80}) (57,58). KIR2DL1 binds exclusively to *C2* allotypes, whereas KIR2DL3 recognizes *C1* molecules. KIR2DL2 shows affinities for both groups (59). Contrarily, HLA-A and HLA-B molecules that carry a *Bw4* epitope function as ligands for KIR3DL1 (60,61). **Figure 8** illustrates the KIRs and their specificity for HLA class I ligands in humans.

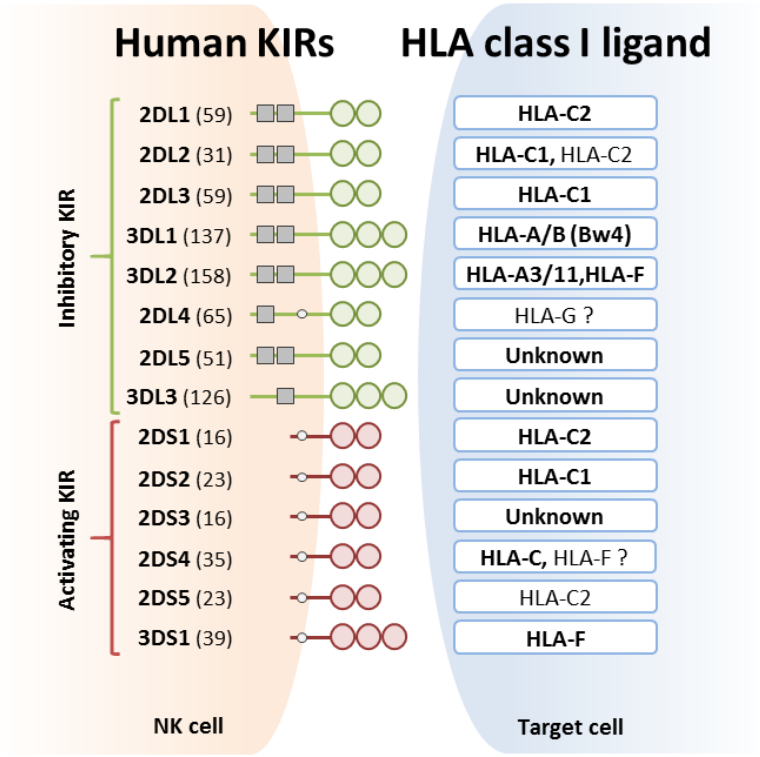

Figure 8: Human KIRs and their interactions with HLA class I ligands

Schematic representation of human KIRs and their HLA class I ligands. KIRs can be activating (red) or inhibitory (green) receptor types that comprise either two (2D) or three (3D) extracellular immunoglobulin-like domains (illustrated in circles) and and either a long (L) or short (S) cytoplasmic tail. The ITIM motifs in the cytoplasmic tails of inhibitory KIRs are shown as grey boxes. The positively charged residues in the transmembrane regions of KIRs are shown as small grey circles. The number of protein sequence variants characterized to date for each KIR receptor is stated in brackets. This data was extracted from the IPD-KIR database (http://www.ebi.ac.uk/ipd/kir/stats.html; 2.7.0 (July 2017) (the figure was created based on (54)).

1.4.3 NK-cell education

The intrinsic cytotoxic capacity of NK cells has to be tightly regulated to protect autologous cells from being attacked by NK cells. The engagement of inhibitory NK-cell receptors with self-HLA class I molecules on healthy cells prevents NK cells from killing and mediates self-tolerance (25). For this reason, it was previously assumed that mature peripheral blood NK cells must express at least one inhibitory receptor for self-HLA class I molecules to avoid autoreactivity (62). Nevertheless, it has been shown that a subset of NK cells, which is lacking expression of HLA-specific inhibitory receptors is not autoreactive even though the inhibitory signal is absent in those cells (63–65). Upon stimulation, these cells were rather hyporesponsive towards HLA class I deficient target cells, which was reflected by reduced degranulation and target cell killing. This observation led to the proposition that NK cells depend on the engagement of inhibitory receptors with self-HLA class I molecules to acquire their full functional competence (**Figure 9**). The process through which an NK cell is programmed for reactivity is known as NK-cell education. To date, there are three different models that describe how NK-cell education might be achieved (66). The arming model postulates that NK cells binding to self-HLA molecules are endowed with a high effector potential and NK cells that fail to bind self-HLA molecules are programmed for lower reactivity. The disarming model, on the other hand, describes that all developing NK cells are equally capable to exert strong effector responses, but are situated in an anergic state due to constitutive activation by activating receptors. However, only NK cells that engage self-HLA molecules are released from the activation-induced anergy, while those that lack engagement with self, lose effector potential and become hyporesponsive. A third, quantitative NK cell model describes that the avidity[2] of the total interactions between inhibitory receptors and HLA-molecules determines the level of reactivity of each NK cell (67). This model is also known as the rheostat model: those NK cells with fewer binding interactions through inhibitory receptors exhibit a low effector potential, whereas those with high numbers of interactions develop a strong reactivity. Due to cumulative signals received from multiple inhibitory receptor types, their expression levels and their affinities to self-HLA molecules NK cells experience an HLA-binding spectrum from no binding at

[2] The term *avidity* describes the strength of a multiple bond between a receptor and a ligand. The strength of a single bond is called *affinity*. The *avidity* is thus the sum of all affinities between receptor and ligand (1).

all via weak to strong binding (68). In other words, the strength of inhibitory signals received by the engagement of inhibitory receptors with self-HLA molecules tunes the reactivity of an individual NK cell (69). In summary, the functional diversity of NK cells is tuned by the combination of inhibitory receptors and the expression of cognate self-HLA molecules in an individual.

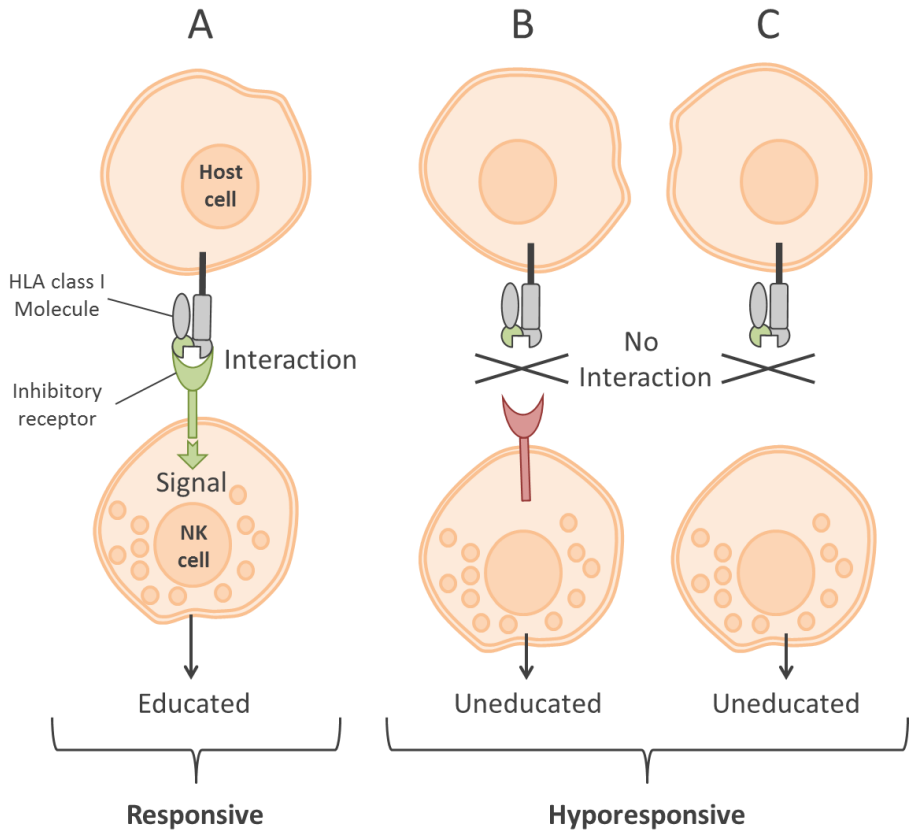

Figure 9: NK-cell education

Schematic overview of the concepts of NK-cell education. (A) NK cells expressing inhibitory receptors for self-HLA class I molecules on host cells receive signals upon receptor engagement that lead to NK-cell education. Educated NK cells gain functional competence and are responsive towards target cells that express stimulating ligands. (B) NK cells, which express inhibitory receptors that cannot bind to self-HLA class I molecules on host cells fail the interaction and will therefore not be educated. (C) NK cells that lack the expression of inhibitory receptors cannot get educated and become hyporesponsive. Uneducated NK cells are hyporesponsive towards target cells.

1.5 Cellular Metabolism

1.5.1 Glycolysis

Glycolysis is the major pathway of glucose metabolism in the cell. In eukaryotic cells, glycolysis can occur aerobically or anaerobically depending on whether oxygen is available or not. Glycolysis takes place in the cytosol and is defined by the breakdown of glucose to pyruvate which is accompanied by the generation of two adenosine triphosphate (ATP) molecules. During early evolutionary times, this metabolic pathway enabled organisms to utilize nutrients in an oxigen-free environment. With the emergence of an oxidative atmosphere and the formation of mitochondria, glycolysis is now used by many microorganisms and higher organisms only as a preparative way for aerobic respiration taking place in mitochondria (70). In the presence of oxygen, glycolysis ends with the production of pyruvate, which then enters mitochondria in order to be fully oxidized by the citric acid cycle. In general, glucose enters the cell from the blood stream through specific nutrient transporters that are embedded in the cell membrane. Although glucose is the most widely used monosaccharide in glycolysis, others, such as fructose or galactose can also be important fuels (71). The glycolytic pathway can be structured into three stages: stage (I) the enzyme hexokinase traps glucose in the cell and starts glycolysis, stage (II) one C_6-molecule is split into two C_3-fragments and stage (III) the formation of ATP (**Figure 10**). During glycolysis, ATP is generated via a metabolic reaction named substrate-level phosphorylation. Thereby, a phosphoryl group (PO_3) is directly transferred from phosphoenolpyruvate to adenosine diphosphate (ADP) at the end of stage III. This reaction is catalyzed by the enzyme pyruvate kinase resulting in the formation of two molecules of ATP and two molecules of pyruvate. Pyruvate can then either be transferred to mitochondria for the initiation of the citric acid cycle or further converted to lactate under anaerobic conditions. The reduction of pyruvate to form lactate is catalyzed by the enzyme lactate dehydrogenase. Lactate can be transferred into the liver fueling gluconeogenesis resulting in the generation of glucose, which can be used again in the glycolytic pathway (72). However, only a fraction of the energy of glucose is released under anaerobic conversion of pyruvate into lactate. Much more energy can be extracted under aerobic conditions when pyruvate is transformed to acetyl coenzyme A (acetyl-CoA) fueling the citric acid cycle and the electron transport chain (ETC) in mitochondria.

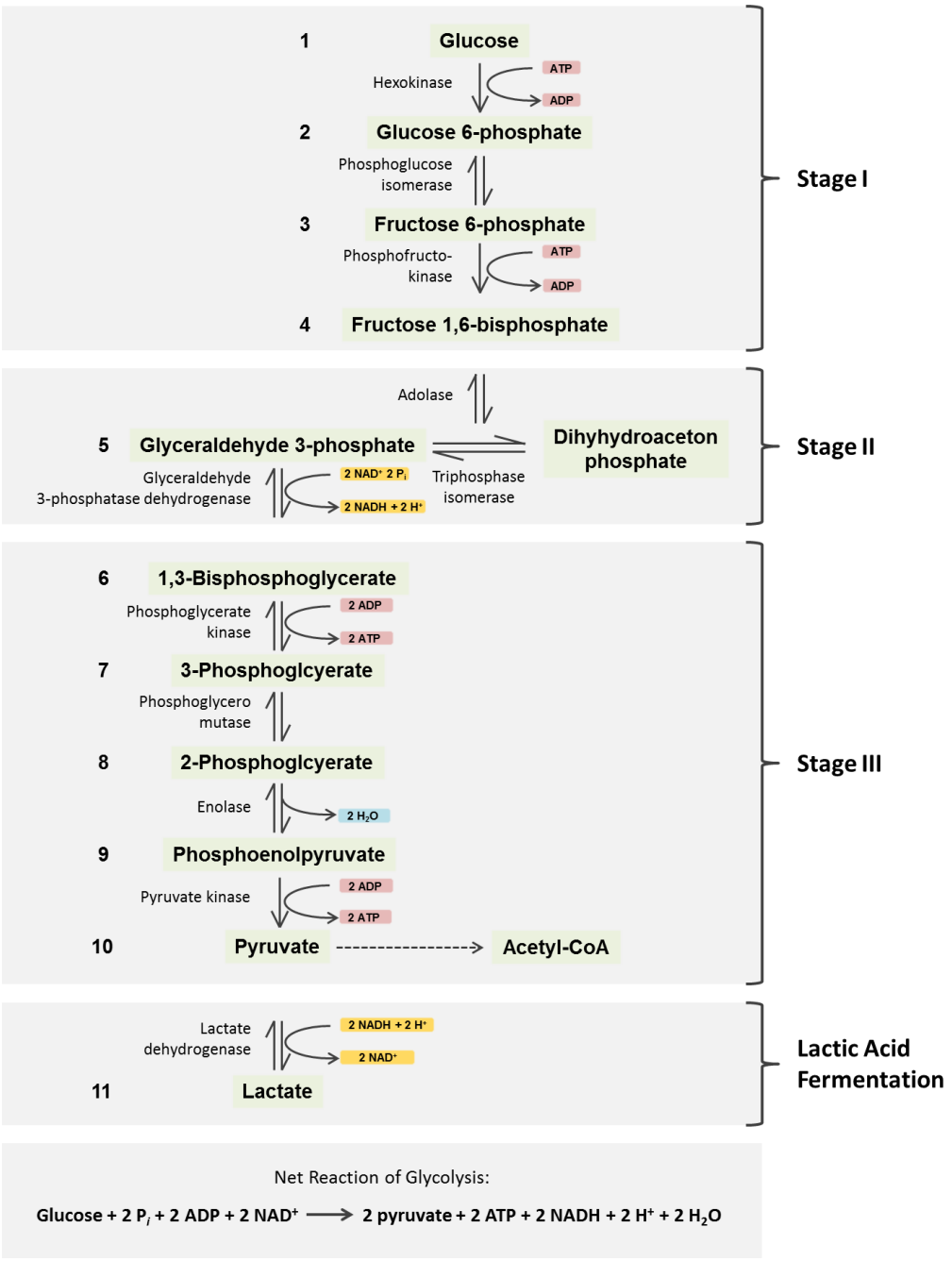

Figure 10: The glycolytic pathway

Schematic overview of the stages of the glycolytic pathway. Glycolysis is a metabolic pathway that takes place in the cytosol of a cell. The glycolytic pathway can be divided into three stages: stage (I) glucose is trapped and destabilized to glucose-6-phosphate, which cannot diffuse back through the membrane because of its negative charges, stage (II) two three-carbon molecules are generated by the cleavage of one six-carbon sugar and finally stage (III) formation of two molecules of pyruvate and two ATP molecules. Under aerobic conditions, this pathway ends at the formation of pyruvate. Pyruvate is subsequently transferred into mitochondria where it is converted to acetyl-CoA fueling the citric acid cycle. Under anaerobic conditions, however, two molecules of pyruvate serve as a source to produce two molecules of lactate via lactic acid fermentation. Adenosine triphosphate (ATP), adenosine diphosphate (ADP), proton (H^+), reduced form of nicotinamide adenine dinucleotide ($NADH+H^+$), oxidized form of nicotinamide adenine dinucleotide (NAD^+) (the figure was created based on (71).

1.5.2 Cellular respiration

Mitochondria produce the major amount of ATP needed by an aerobic cell and therefore play a central role in providing the energy that is required for biochemical processes by an organism. To meet the high energy demand, most eukaryotic cells, except erythrocytes, contain between 500 and 1500 mitochondria in their cytoplasm (70). For most cells, glucose is the primary source of energy. The glycolytic pathway metabolizes glucose to pyruvate. Pyruvate is an energy-rich compound which is a key molecule in the network of various metabolic pathways. In an aerobic environment, pyruvate is transported into mitochondria. Specific pyruvate carriers transport the molecule into the mitochondrial matrix (73), where it is transformed to acetyl-CoA by an irreversible process called pyruvate decarboxylation. Acetyl-CoA can then be used by the citric acid cycle to fuel cellular respiration. Thus, glycolysis and cellular respiration are linked by oxidative decarboxylation of pyruvate to acetyl-CoA (**Figure 11)**. Acetyl-CoA then enters the citric acid cycle, where it is completely oxidized by a chain of enzymes leading to formation of carbon dioxide (CO_2), protons (H^+), energy rich coenzymes (NADH/ $FADH_2$) and two molecules of ATP. Furthermore, NADH and $FADH_2$ are recycled by mitochondrial respiration complexes (complex I-IV) to generate a proton gradient across the inner mitochondrial membrane which drives ATP production (74). The majority of ATP is produced by the proton-driven ATP-synthase, which is a fundamental enzyme of cellular respiration. Synthesizing ATP from ADP and inorganic phosphate (P_i) requires energy itself. For that reason, synthesis of ATP is coupled to an electrochemical gradient maintained by the ETC. The complex interplay between ATP-synthesis via ADP phosphorylation, which is energetically coupled to a proton gradient maintained by the ETC by oxidizing products from the citric acid cycle, is known as oxidative phosphorylation (OXPHOS). Thereby, the cell can use glucose as a highly efficient energy source, with a theoretical yield of up to 38 ATP molecules per glucose molecule (74). Most of the ATP, which is synthesized in the mitochondrial matrix will be used for cellular processes in the cytosol. As the inner mitochondrial membrane is much less permeable to ions and small molecules than the outer mitochondrial membrane, ATP must be exported from its site of synthesis to the cytosol. Therefore, the inner mitochondrial membrane contains an antiporter, the ADP/ATP translocase, which is an integral membrane protein exchanging newly synthesized ATP from the mitochondrial matrix for ADP in the intermembrane space. The outer membrane of the mitochondrion, however, contains porins which allow ATP,

small molecules and ions to trespass. Overall, cellular respiration is understood as the integration of several metabolic processes that convert biochemical energy from nutrients under consumption of oxygen into ATP.

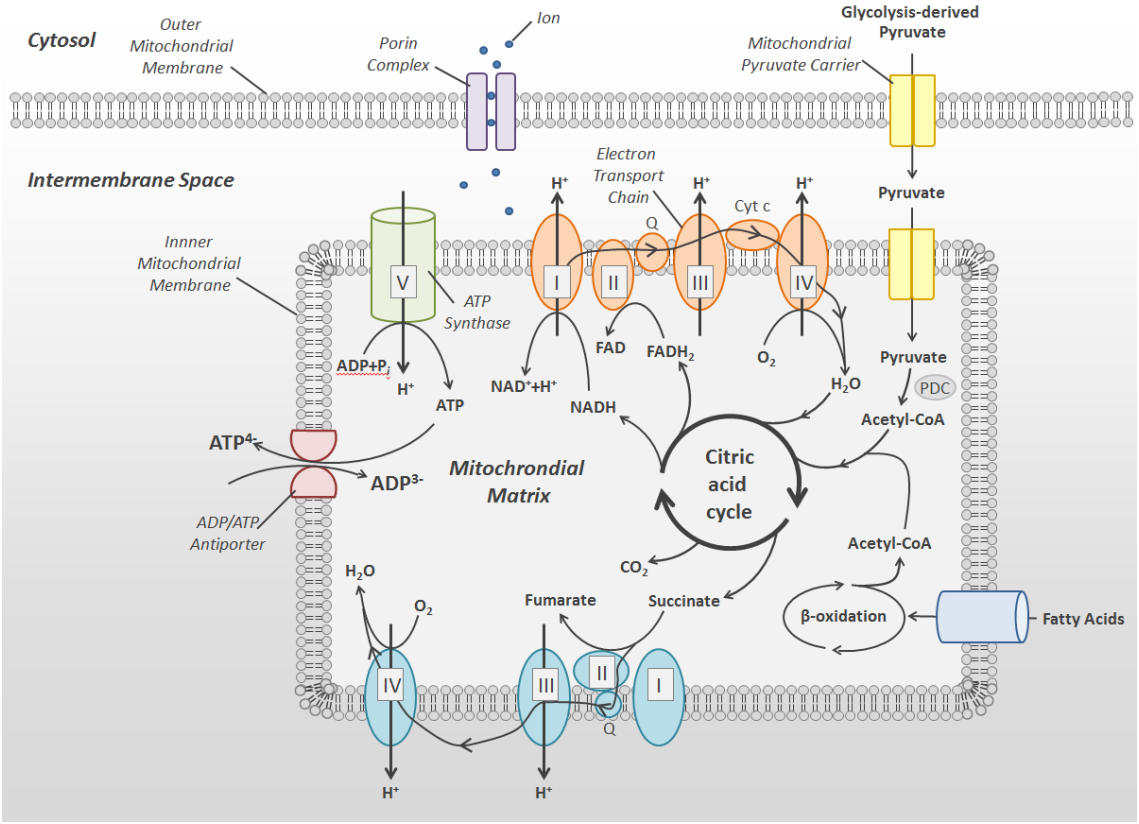

Figure 11: Mitochondrial respiration

Schematic illustration of cellular respiration in the mitochondria. Cellular respiration is understood as the interplay between different metabolic reactions and processes that take place in the cells of an organism. Thereby, biochemical energy from nutrients is transformed into ATP serving as energy source for cellular activity. The previous breakdown of glucose in the cytosol via the glycolytic pathway yields in the formation of two pyruvate molecules, which are further transported via specific pyruvate carriers into the mitochondrial matrix where they are oxidized to acetyl-CoA by the pyruvate dehydrogenase complex (PDC). Acetyl-CoA then enters the citric acid cycle, where it oxidized by a set of enzymes. The citric acid cycle provides energy-rich molecules, such as NADH or $FADH_2$, which can be used by the electron transport chain (ETC) to generate an electrochemical gradient along the inner mitochondrial membrane. The oxidation of NADH or $FADH_2$ provides the energy that is needed to transport protons (H+) from the mitochondrial matrix to the intermembrane space. This proton gradient can then be used by the ATP-synthase to drive the synthesis of ATP via the phosphorylation of ADP. The citric acid cycle can alternatively be fueled by fatty acids that are transported into the mitochondrial matrix where they are transformed to acetyl-CoA through a process called β-oxidation. Adenosine triphosphate (ATP), adenosine diphosphate (ADP), inorganic phosphate (P_i), proton (H^+), reduced form of nicotinamide adenine dinucleotide ($NADH+H^+$), oxidized form of nicotinamide adenine dinucleotide (NAD^+), flavin adenine dinucleotide (FAD), reduced form of flavin adenine dinucleotide ($FADH_2$), complex I-IV are part of the ETC, complex V illustrates the ATP Synthase (the figure was created based on (71).

1.6 Metabolism in immune cells

Cellular metabolism is understood as an elementary process that is required to provide sufficient energy and biological molecules to comply with the bioenergetic and biosynthetic demands of a cell (75). Immune cells are constantly exposed to a broad range of environmental stressors and need to rapidly adapt to altering circumstances in their environment to protect the host against infection and cancer. In order to function properly and without delay, immune cells need to synchronize cellular activation and proliferation along with their effector functions (76). For this reason, cellular metabolism needs to be flexible to meet the changing cellular demands not only by providing sufficient energy, but also in terms of biosynthesis. Recent research has demonstrated that immune cell activation leads to a switch in metabolic pathways supporting functional plasticity of the cell (77). A novel field of investigation that addresses the question of how metabolic pathways can influence and regulate immune cells is known as "immunometabolism". During the last years, a lot of knowledge was gained regarding the metabolic regulation of T-cell function (78,79). However, until today there is little knowledge about the metabolic regulation of NK-cell activation or effector function, and studies in the field of NK-cell metabolism are just beginning to emerge. Nevertheless, the knowledge about T cell metabolism might guide studies on NK cell metabolism, since NK cells and T cells arise from a common progenitor cell and share complementary roles in their defense against pathogens.

Mature naïve T cells exit from the thymus into the periphery and circulate through the body. As quiescent cells, they primarily use glucose-derived pyruvate in their mitochondria through OXPHOS or fatty acid oxidation (FAO) to generate energy in form of ATP (80). In the lymphoid organs, T cell receptor (TCR) ligation and binding to costimulatory molecules leads to activation of these cells. In contrast to quiescent cells, pro-inflammatory lymphocytes have an increased energy demand to fuel biosynthetic processes that can promote cellular growth, proliferation and synthesis of effector molecules. T cell activation induces rapid metabolic remodeling resulting in anabolic growth and biomass accumulation (79). This remodeling process is marked by a switch from a quiescent metabolic state, where the cells primarily use OXPHOS, to an activated metabolic state that is characterized by the engagement of anaerobic glycolysis. Although anaerobic glycolysis is less efficient than OXPHOS regarding the yield of ATP per molecule of glucose, anaerobic glycolysis can give rise to metabolic

intermediates which are important for cell growth and proliferation (81). For example, glucose-6-phosphate and 3-phosphoglycerate (3PG), which are produced during glycolysis, can be further metabolized in the pentose phosphate and serine biosynthesis pathways and thereby serve as precursors for nucleotides and amino acids (79) (**Figure** 12).

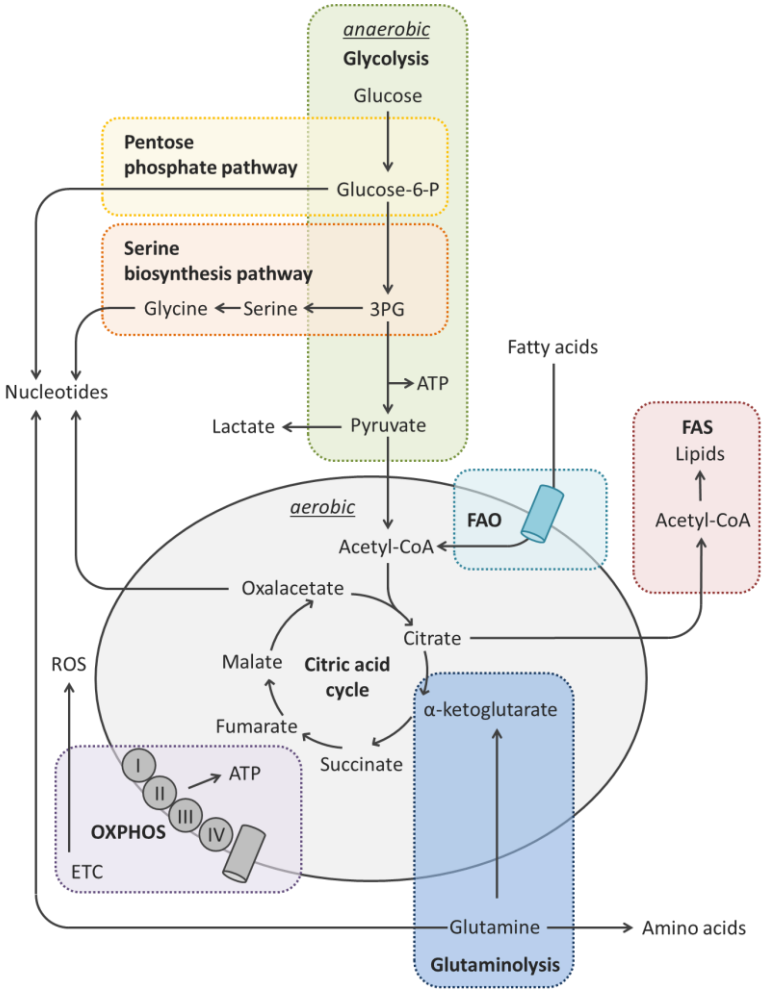

Figure 12: Principal pathways involved in glucose catabolism

The figure illustrates distinct intracellular metabolic pathways that generate energy and provide precursors for the production of biomolecules. Anaerobic glycolysis is the breakdown of glucose to lactate, whereas aerobic glycolysis ends with the production of pyruvate, which subsequently fuels the citric acid cycle after being converted to acetyl-CoA. The breakdown of substrates within the citric acid cycle provides reducing equivalents for oxidative phosphorylation (OXPHOS) within the electron transport chain (ETC) and oxalacetate, which can be used to generate nucleotides. Furthermore, glucose-derived citrate is exported back to the cytosol generating acetyl-coA for lipid-synthesis via the multi-enzyme protein fatty acid synthase (FAS). Other substrates can also be metabolized in the citric acid cycle, such as glutamine via the glutaminolysis or fatty acids via fatty acid oxidation (FAO) or also called β-oxidation (the figure was created based on (79)).

These metabolic changes are accompanied by an increased expression of glycolytic enzymes such as lactate dehydrogenase, which promotes the conversion of pyruvate into lactate (82). In addition, the activation of T cells is accompanied by an upregulation of nutrient transporters on their cell surface to facilitate nutrient uptake into the cell (83,84). As glucose is a key metabolic substrate for T cells, the glucose transporter Glut1 is upregulated on the surface of activated cells (85–87). The concept of substantial metabolic changes upon immune cell activation is known as metabolic reprogramming (**Figure 13**).

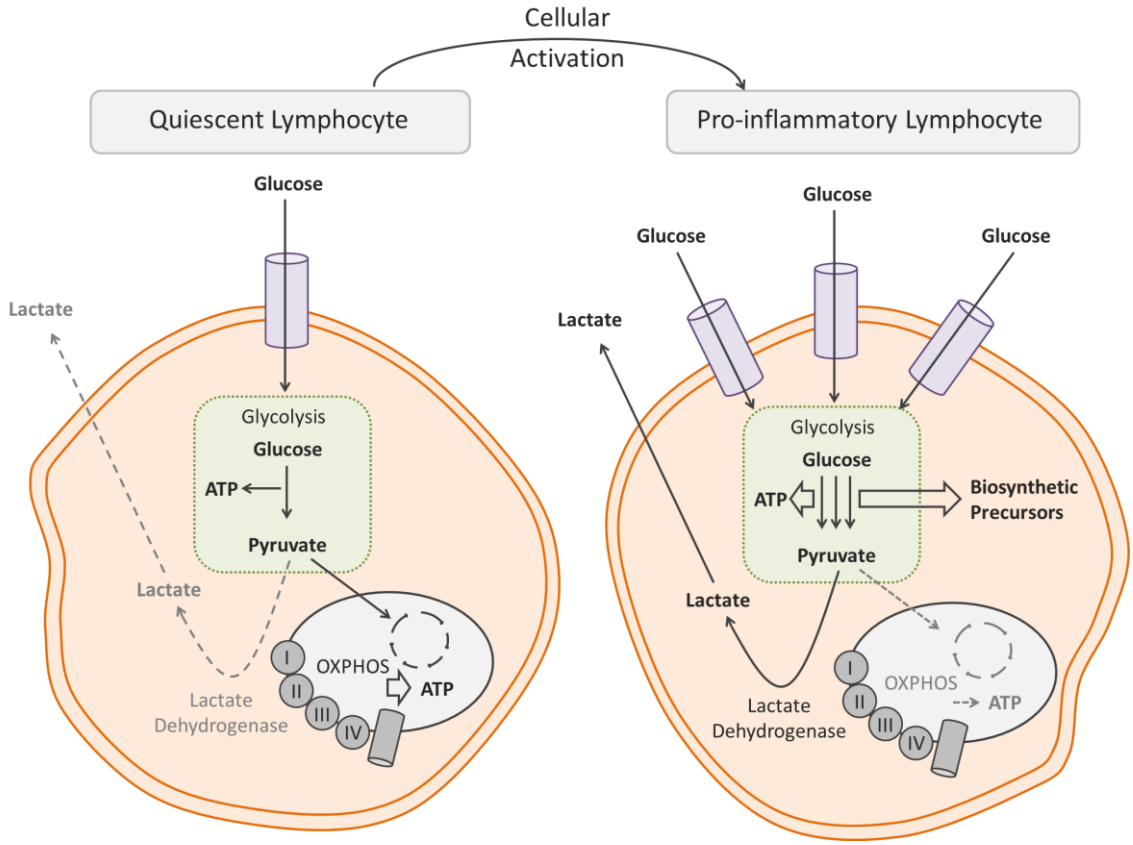

Figure 13: Metabolic reprogramming of pro-inflammatory lymphocytes

Schematic overview of metabolic reprogramming in lymphocytes upon activation. Quiescent lymphocytes use low amounts of glucose via the glycolytic pathway to generate pyruvate. Pyruvate is preferentially transported into the mitochondria, where it is fully oxidized to CO_2 within the citric acid cycle fueling OXPHOS and the subsequent formation of ATP. Upon immune activation, these cells now have an increased demand for glucose to maintain the biosynthetic processes that allow cellular growth, proliferation and the synthesis of effector molecules. Therefore, pro-inflammatory lymphocytes upregulate the expression of glucose transporters on their cell surface to facilitate glucose uptake and glycolytic flux. In order to prevent the accumulation of pyruvate, which would lead to the inhibition of the glycolytic pathway, pyruvate is converted to lactate and exported from the cell. Due to this process, high rates of glycolysis can be maintained. At the same time, high levels of glycolytic flux result in increased amounts of glycolytic intermediates that can fuel other biosynthetic pathways and therefore lead to the production of amino acids, lipids and nucleotides as well as to the generation of biomass (the figure was created based on (75)).

1.7 Hypothesis and aims

The molecular mechanisms underlying the functional superiority of educated NK cells remain insufficiently understood. New insights from the field of immunometabolism show that immune cells can undergo metabolic reprogramming upon transition from a quiescent to an activated state (77). I hypothesized that metabolic reprogramming serves as mechanism for differences in the responsiveness of educated and uneducated NK cells. To test this hypotesis, metabolic analyses of these distinct NK-cell populations were performed in this study.

2 Material and Methods

2.1 Material

2.1.1 Antibodies

Antibody	Conjugate	Clone	Source	Catalogue Number, Research Resource Identifier (RRID)
Glut1 receptor binding protein (RBD)	Enhanced Green Fluorescent Protein (eGFP)	/	Metafora Biosystems, Évry, France	Cat.#GLUT1-G100
α-human CD107a	Brilliant Violet 510 (BV510)	H4A3	Biolegend, Inc., San Diego, California, USA	Cat.#328632, RRID:AB_2562648
α-human CD14	Peridinin-Chlorophyll Protein Cyanine 5.5 (PerCP-Cy5.5)	HCD14	Biolegend, Inc., San Diego, California, USA	Cat.#325622, RRID:AB_893250
α-human CD16	Brilliant Violet 785 (BV785)	3G8	Biolegend, Inc., San Diego, California, USA	Cat.#302046, RRID:AB_2563803
α-human CD19	Peridinin-Chlorophyll Protein Cyanine 5.5 (PerCP-Cy5.5)	HIB19	Biolegend, Inc., San Diego, California, USA	Cat.#302230, RRID:AB_2073119
α-human CD3	Peridinin-Chlorophyll Protein Cyanine 5.5 (PerCP-Cy5.5)	UCHT1	Biolegend, Inc., San Diego, California, USA	Cat.#300430, RRID:AB_893299
α-human CD56	Brilliant Violet 395 (BUV395)	NCAM16.2	BD Bioscience, Franklin Lakes, New Jersey, USA	Cat.#563554, RRID:AB_2687886
α-human KIR2DL1/S5	Allophycocyanin (APC)	143211	R&D Systems; Minneapolis, Minnesota, USA	Cat.#FAB1844A-100, RRID:AB_416855
α-human KIR2DL1/S5	Fluorescein isothio-cyanate (FITC)	143211	R&D Systems; Minneapolis, Minnesota, USA	Cat.#FAB1844F-100, RRID:AB_2130402
α-human KIR2DL2/ L3/S2	Phycoerythrin (PE)	DX27	Biolegend, Inc., San Diego, California, USA	Cat.#312606, RRID:AB_2130554
α-human KIR2DL3	Allophycocyanin (APC)	180701	R&D Systems; Minneapolis, Minnesota, USA	Cat.#FAB2014A-100, RRID:AB_416869
α-human KIR3DL1	Brilliant Violet 421 (BV421)	DX9	Biolegend, Inc., San Diego, California, USA	Cat.#312714, RRID:AB_2561652
α-human NKG2A	Phycoerythrin-Cyanine7 (PE-Cy7)	Z199	Beckman Coulter, Brea, California, USA	Cat.#B10246, RRID:AB_2687887

2.1.2 Buffers, media and solutions

Buffer	Composition
Cell line cultivation medium	RPMI-1640 Medium supplemented with 10% (v/v) FBS, 10 units/ml penicillin and 1 mg/ml streptomycin
PBMC cultivation medium	RPMI-1640 Medium supplemented with 10% (v/v) FBS
Fixation buffer	DPBS supplemented with 2% (v/v) PFA
Cryopreservation medium	FBS supplemented with 10% (v/v) DMSO
NK-cell isolation buffer	DPBS supplemented with 2% (v/v) FBS and 1 mM EDTA
RBD acquisition buffer	DPBS supplemented with 2% (v/v) FBS, 0.09% (v/v) NaN_3, 1 mM EDTA and 1% (v/v) PFA
RBD labeling buffer	RPMI-1640 supplemented with 10% (v/v) FBS, 0.09% NaN_3 and 1 mM EDTA

Sorting buffer	RPMI-1640 without phenol red, supplemented with 5% FBS
Staining buffer	DPBS supplemented with 2% FBS

2.1.3 Cell lines

Cell line	Source	Species of origin	Category	Disease	Sex of cell	Catalogue Number, Research Resource Identifier (RRID)
K-562	DSMZ	Homo sapiens (Human)	Cancer cell line	Chronic myelogenous leukemia, BCR-ABL1 positive	Female	DSMZ Cat.#ACC 10. RRID:CVCL_0004
LCL 721.221	ATCC	Homo sapiens (Human)	Transformed cell line	/	Female	ATCC Cat.#CRL-1855, RRID:CVCL_6263

2.1.4 Chemicals and consumables

Product	Source	Catalogue Number
Accudrop beads	BD Biosciences, Franklin Lakes, New Jersey, USA	Cat.#345249
Anti-mouse Ig, κ/negative control compensation particles set	BD Biosciences, Franklin Lakes, New Jersey, USA	Cat.#552843
Aqua ad iniectabilia	B. Braun, Melsungen, Germany	Cat.#2351744
ArC Amine Reactive Compensation Bead Kit	Thermo Fisher Scientific, Waltham, Massachusetts, USA	Cat.#A10346
BD GolgiStop	BD Biosciences, Franklin Lakes, New Jersey, USA	Cat.#554724
Biocoll	Biochrom GmbH, Berlin, Germany	Cat.#L6115
CS&T research beads	BD Biosciences, Franklin Lakes, New Jersey, USA	Cat.#655051
Dulbecco's phosphate buffered saline (DPBS)	Sigma Aldrich, St. Louis, Missouri, USA	Cat.#D8537-6x500ML
Dymethyl sulfoxide (DMSO)	Sigma Aldrich, St. Louis, Missouri, USA	Cat.#D5879-1L-M
Ethylenediaminetetraacetic acid (EDTA)	Sigma Aldrich, St. Louis, Missouri, USA	Cat.#03690-100ml
Fetal bovine serum (FBS) superior	Biochrom GmbH, Berlin, Germany	Cat.#S0615
Hank's balanced salt solution (HBSS)	Sigma Aldrich, St. Louis, Missouri, USA	Cat.#H6648-6x500ML
Hydrochloric acid, 37%	Carl Roth, Karlsruhe, Germany	Cat.#4625.1
L-Glutamin solution	Sigma Aldrich, St. Louis, Missouri, USA	Cat.#G7513-100ml
Live/dead fixable blue dead cell stain kit	Thermo Fisher Scientific, Waltham, Massachusetts, USA	Cat.#L23105
Paraformaldehyde (PFA)	Science Services GmbH, Munich, Germany	Cat.#E15710
Penicillin-streptomycin	Sigma Aldrich, St. Louis, Missouri, USA	Cat.#P4333-100ML

Recombinant human IL-15	PeproTech GmbH, Hamburg, Germany	Cat.#200-15-100
RPMI-1640 medium	Thermo Fisher Scientific, Waltham, Massachusetts, USA	Cat.#21875091
Seahorse XF base medium	Agilent Technologies, Santa Clara, California, USA	Cat.#102353-100
Seahorse XF calibrant solution	Agilent Technologies, Santa Clara, California, USA	Cat.#100840-000
Sodium azide (NaN_3)	Sigma Aldrich, St. Louis, Missouri, USA	Cat.#71289-5G
Trypan blue solution, 0.4%	Sigma Aldrich, St. Louis, Missouri, USA	Cat.#T8154-100ml

2.1.5 Equipment

Equipment	Manufacturer
BD FACSAria Fusion	BD Biosciences, Franklin Lakes, New Jersey, USA
BD LSRFortessa	BD Biosciences, Franklin Lakes, New Jersey, USA
Biological safety cabinet KS 12	Thermo Fisher Scientific, Waltham, Massachusetts, USA
Centrifuge Heraeus Fresco 21	Thermo Fisher Scientific, Waltham, Massachusetts, USA
Centrifuge Megastar 1.6R	VWR International, Radnor, Pennsylvania, USA
Centrifuge Rotanta 46 RC	Hettich, Kirchlengern, Germany
CO_2-Incubator Heracell 240	Thermo Fisher Scientific, Waltham, Massachusetts, USA
CO_2-Incubator Heracell 240i	Thermo Fisher Scientific, Waltham, Massachusetts, USA
Eppendorf Research Plus Pipette	Eppendorf, Hamburg, Germany
Multichannel pipetter, 8-channels, 25 µl	Thermo Fisher Scientific, Waltham, Massachusetts, USA
Multichannel pipetter, 12-channels, 300 µl	Thermo Fisher Scientific, Waltham, Massachusetts, USA
Nanodrop 100 spectrophotometer	Thermo Fisher Scientific, Waltham, Massachusetts, USA
pH-Meter pH526	WTW, Xylem Analytics; Weilheim, Germany
Pipet Boy	INTEGRA Biosciences AG, Zizers, Switzerland
Seahorse XFe96 analyzer	Agilent Technologies, Santa Clara, California, USA
Stratacooler	Agilent Technologies, Santa Clara, California, USA
TC20 Automated cell counter	Bio-Rad Laboratories, Inc., Hercules, California, USA
The big easy EasySep magnet	Stemcell Technologies, Vancouver, Kanada

2.1.6 Plasticware

Product	Source	Catalogue Number
Cell culture micro plate, 96-well, u-bottom	Greiner Holding, Kremsmünster, Austria	Cat.#650180
Counting slides	Bio-Rad Laboratories, Inc., Hercules, California, USA	Cat.#145.0011
CryoPure cryo tubes	Sarstedt, Nümbrecht/Rommelsdorf, Germany	Cat.#72.380.992
Falcon 14mL round bottom polystyrene test tube (FACS tube)	Corning Life Sciences, Tewksbury, Massachusetts, USA	Cat.#352057
Falcon 5mL round bottom polystyrene test tube (FACS tube)	Corning Life Sciences, Tewksbury, Massachusetts, USA	Cat.#352054
Falcon polystyrene test tube with cell strainer snap cap (FACS tube)	Corning Life Sciences, Tewksbury, Massachusetts, USA	Cat.#352235
Falcon tubes 15 ml	Greiner Holding, Kremsmünster, Austria	Cat.#188271
Falcon tubes 50 ml	Greiner Holding, Kremsmünster, Austria	Cat.#227261
Filter tip 10 µl	Sarstedt, Nümbrecht/Rommelsdorf, Germany	Cat.#70.1130.210
Filter tip 100 µl	Sarstedt, Nümbrecht/Rommelsdorf, Germany	Cat.#70.760.212
Filter tip 1000 µl	Sarstedt, Nümbrecht/Rommelsdorf, Germany	Cat.#70.762.211
Filter tips ClipTip 200 µl	VWR International, Radnor, Pennsylvania, USA	Cat.#732-1622
Filter tips ClipTip 300 µl	VWR International, Radnor, Pennsylvania, USA	Cat.#732-1624
Micro tube 1.5 ml SafeSeal	Sarstedt, Nümbrecht/Rommelsdorf, Germany	Cat.#72.706.400
Pipetting reservoirs	VWR International, Radnor, Pennsylvania, USA	Cat.#89094-680
Seahorse XFe96 FluxPak	Agilent Technologies, Santa Clara, California, USA	Cat.#102416-100
Serological pipettes 10 ml	Sarstedt, Nümbrecht/Rommelsdorf, Germany	Cat.#86.1254.001
Serological pipettes 25 ml	Sarstedt, Nümbrecht/Rommelsdorf, Germany	Cat.#86.1685.001
Serological pipettes 5 ml	Sarstedt, Nümbrecht/Rommelsdorf, Germany	Cat.#86.1253.001
T175 Cell culture flasks	Sarstedt, Nümbrecht/Rommelsdorf, Germany	Cat.#83.3912.002
T25 Cell culture flasks	Sarstedt, Nümbrecht/Rommelsdorf, Germany	Cat.#83.3910.002
T75 Cell culture flasks	Sarstedt, Nümbrecht/Rommelsdorf, Germany	Cat.#83.3911.002

2.1.7 Preparation kits

Preparation kit name	Source	Catalogue Number
DNeasy blood & tissue kit	Qiagen, Hilden, Germany	Cat.#69506
EasySep human NK-cell enrichment kit	Stemcell Technologies, Vancouver, Kanada	Cat.#19055

Seahorse XF glycolysis stress test kit	Agilent Technologies, Santa Clara, California, USA	Cat.#103020-100

2.1.8 Software

Software	Source
BD FACS Diva Software; version 7.0	BD Biosciences, Franklin Lakes,New Jersey, USA
FlowJo, version 10.4.2	Tree Star, Ashland, Oregon, USA
Graph Pad Prism, version 7.04	GraphPad Software Inc., La Jolla, California, USA
Mendeley Desktop, version 1.19.1	Mendeley Ltd., London, United Kingdom
Microsoft Office Professional Plus 2010, version 14.0.7212.500	Microsoft, Redmond, Washington, USA
Wave, version 2.3.0.19	Agilent Technologies, Santa Clara, California, USA

2.2 Methods

2.2.1 Workflow and sample processing

Figure 14 illustrates the workflow, showing how the samples were prepared and experimental data was achieved. On the first day, peripheral blood was processed via density gradient centrifugation to obtain peripheral blood mononuclear cells (PBMCs) (**see point 2.2.3**). PBMC samples from each study individual were cryopreserved serving for subsequent HLA-genotyping analysis (**see point 2.2.6**). In order to receive primary human NK-cells for functional and metabolic analysis, NK cells were enriched from PBMCs through immunomagnetic negative selection (**see point 2.2.7**). The next day, NK cells were co-cultured with the HLA class I deficient target cell lines 721.221 and K-562 in a degranulation assay (**see point 2.2.8**). After the stimulation with target cells, flow cytometric analysis was performed to analyze the expression of the inhibitory NK-cell receptors KIR2DL1, KIR2DL2/L3, KIR3DL1 and NKG2A and to investigate NK-cell function via the expression of the degranulation marker CD107a (**see point 2.3.9**). The expression profile of self-inhibitory receptors and subsequent assessment of NK-cell function allowed to discriminate between educated and uneducated NK cells (**see point 2.3.11**). To assess the glycolytic profile, expression of the glucose transporter Glut1 was examined via flow cytometry (**see point 2.3.9**). In order to measure differences in the glycolytic profile of educated and uneducated NK cells subsets, enriched primary NK cells were sorted in educated and uneducated NK-cell subsets based on the expression of self-inhibitory receptors (**see point 2.2.11**). On the third day, a Seahorse assay was performed with sorted educated and uneducated NK cells to assess their glycoclyic activity in a Glycolytic Stress Test (**see point 2.2.13**).

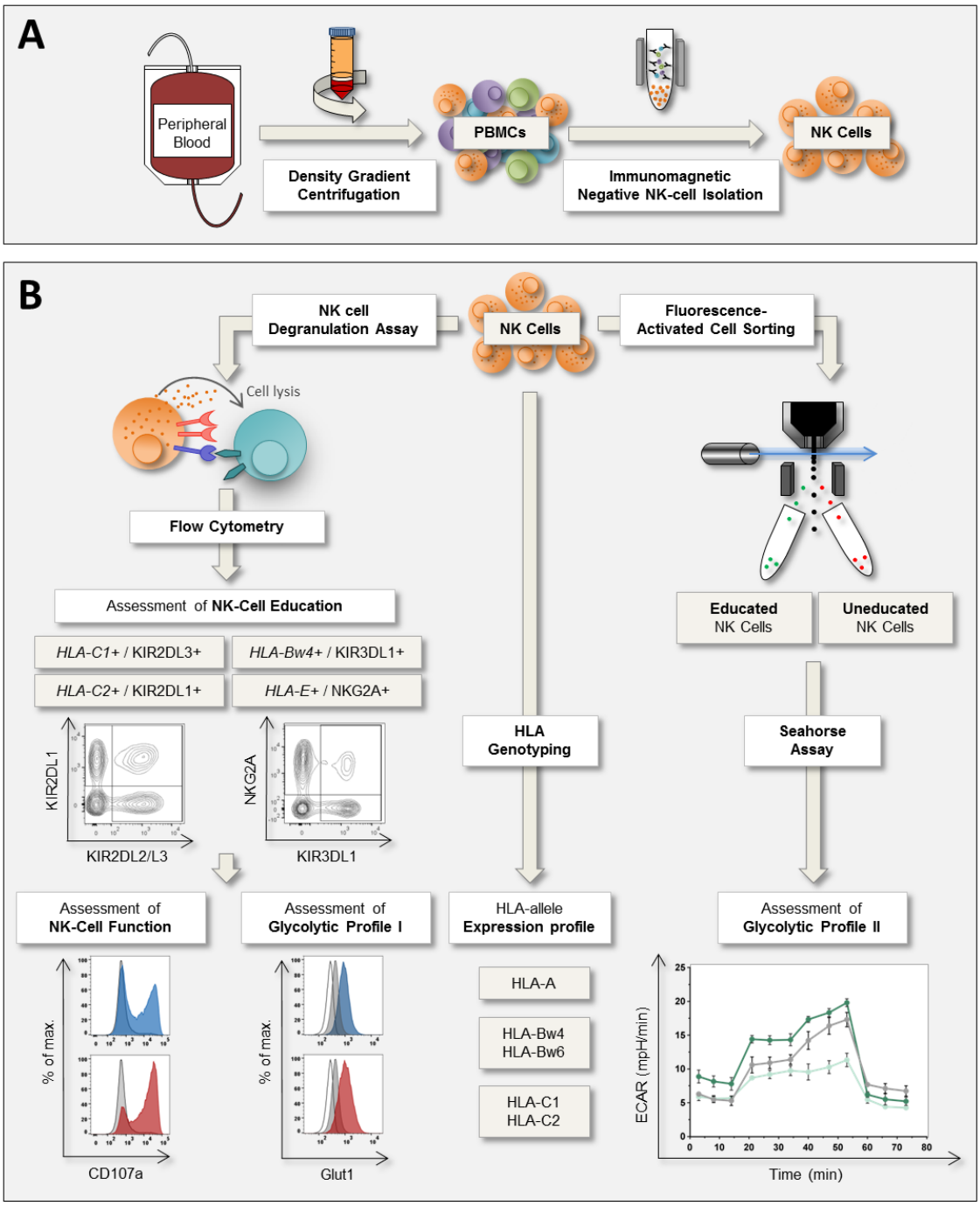

Figure 14: Experimental setup for the assessment of NK-cell function and the glycoclytic profile

Schematic representation of the performed experiments. **(A)** Primary human NK cells were enriched from peripheral blood. **(B)** Isolated NK cells were examined via flow cytometry for the expression of the inhibitory NK-cell receptors KIR2DL1, KIR2DL2/L3, KIR3DL1 and NKG2A and subsequently investigated for NK-cell function (CD107a expression) as well as the expression of the glucose transpoter Glut1. Fluorescence-activated cell sorting allowed separation of NK cells in educated and uneducated subsets, which were further analyzed for their glycolytic profile in a Seahorse Assay. All samples were genotyped for the expression of HLA-alleles.

2.2.2 Cell culture

All working steps were performed under sterile conditions using a biological safety cabinet.

Cell lines

The HLA class I devoid cell lines 721.221 (88) and K-562 (89) were used as target cells to assess NK-cell function. The cells were cultivated in RPMI-1640 Medium supplemented with 10% heat-inactivated FBS, 10 units/ml penicillin and 1 mg/ml streptomycin. The cells were cultured in T75 cell culture flasks and split every two to three days by a split-ratio of 1:4, when cells had reached a density of approximately 4×10^5 cells/ml. After 20 passages the cells were discarded and fresh cells were thawed for further experiments.

Cryopreservation of cell samples

Cryopreservation was performed for longtime storage of cells. Therefore, the cells were counted by the use of a TC20 automated cell counter. The volume of a cell suspension was calculated for 10 to maximal 50×10^6 cells, transferred into a 15 ml falcon and adjusted to 10 ml with DPBS. The cells were then centrifuged at room temperature for 5 min at 500 RCF and maximum ACC and DECEL. The cell pellet was resuspended in 1 ml freezing solution (FBS supplemented with 10% DMSO) and immediately transferred into a cryotube, which was subsequently placed in a pre-cooled stratacooler. The stratacooler was stored at -80 °C and incubated overnight. The following day, the samples were transferred into the liquid nitrogen (LN) tank at -160 °C.

Cell thawing

Frozen vials were thawed in a water bath at 37 °C until a small pellet of ice remained. Then, 1 ml pre-warmed cell culture medium (RPMI-1640 medium, supplemented with 10% FBS) was added to each vial to thaw the residual ice pellet. The cell suspension was transferred into a 15 ml falcon tube containing 9 ml cell culture medium and immediately centrifuged at room temperature for 5 min at 500 relative centrifugal force (RCF) and maximum acceleration (ACC) and deceleration (DECEL). After the centrifugation step, the supernatant was discarded and the pellet was resuspended in cell culture medium in a concentration of 2×10^5 cells/ml and transferred to a T75 cell culture flask. The cells were stored in the incubator at 37°C and 5% CO_2.

2.2.3 Peripheral blood sample acquisition

Peripheral blood samples were obtained from a total of 45 randomly selected healthy blood donors recruited at the Institute for Transfusion Medicine, University medical center Hamburg-Eppendorf, Hamburg, Germany. For this study, only residual amounts of anonymous peripheral blood samples were used which were routinely taken from healthy blood donors and would have been discarded otherwise. All blood donors gave their general written consent to use their blood samples for scientific studies in an anonymized form. The anonymous use of this material is in compliance with a vote by the ethics committee of the German medical association. After the blood was drawn from the donors at the clinics, it was forwarded to the clinical laboratories, where it was further processed within the same day. The whole blood samples were fractionated through centrifugation resulting in three discriminable layers: plasma, erythrocytes and the buffy coat. The three layers were separated from each other and stored for further use. The isolated buffy coat layer is the layer that was obtained for this study and used for the following experiments.

2.2.4 PBMC isolation via density gradient centrifugation

The isolation of the PBMCs (Peripheral Blood Mononuclear Cells) was performed in order to separate the residual plasma and erythrocytes from the buffy coat (90). This method allows to separate the blood components according to their differences in size, density and aggregation behavior. The separation takes place by layering of blood on a separation solution (biocoll) and the subsequent centrifugation. Buffy coat donations contain approximately 60 ml whole blood, enriched in thrombocytes, monocytes, lymphocytes and granulocytes. The blood sample was equally distributed to three 50 ml falcon tubes (20 ml blood per falcon) and each tube was mixed with 15 ml pre-warmed HBSS (Hanks' balanced salt solution). Afterwards each of the blood-HBSS mixtures were carefully layered on room tempered 15 ml biocoll separation solution in a new 50 ml falcon tube. The samples were then centrifuged at room temperature for 20 min at 950 RCF, with the lowest level of ACC and DECEL turned off. After the centrifugation, the samples showed three different layers. **Figure 15** illustrates the layers that are formed after centrifugation. The upper yellow layer consists of fresh plasma, the lower red layer contains the erythrocytes and the middle layer which separates the plasma from the erythrocytes is made of the buffy coat.

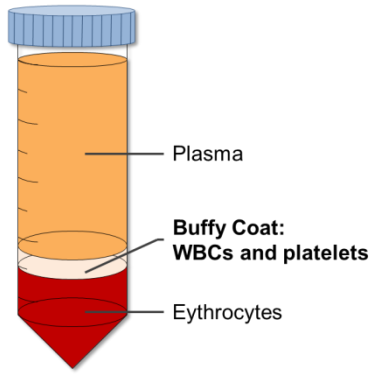

Figure 15: Blood components after centrifugation

After the density gradient centrifugation of whole blood that was layered on top of a separation solution, three different layers are detectable. The upper layer consists of blood plasma, which is a yellow-colored liquid component of the blood that mainly consists of water containing dissolved proteins, coagulation factors, glucose, electrolytes and hormones. The lower red colored layer contains the erythrocytes. The middle layer that separates the plasma from the erythrocytes is the buffy coat, which contains the white blood cells (WBCs) and platelets.

The buffy coat contains the thrombocytes, monocytes, lymphocytes and granulocytes. Therefore, this layer was carefully extracted from the other layers with a pipette dropper and transferred into a new 15 ml falcon tube. The samples were centrifuged at room temperature for 15 min at 500 RCF and maximum ACC and DECEL, in order to wash the cells and separate them from the biocoll-containing surrounding solution. After the centrifugation, the supernatant was discarded, equal pellets were pooled and re-suspended in 10 ml pre-warmed HBSS. The samples were centrifuged at room temperature for 13 min at 300 RCF and maximum ACC and DECEL, to separate the lymphocytes from thrombocytes. Subsequently, the supernatant was discarded and the pellet was re-suspended in 50 ml pre-warmed cell culture medium. Then, the cells were counted and transferred into cell culture flasks in a concentration of 3×10^6 cells/ml cell culture medium supplemented with 5 ng/ml IL-15 and stored in the incubator at 37 °C and 5% CO_2 for further experiments.

2.2.5 DNA isolation

Extraction of genomic DNA from isolated PBMCs was performed using DNA Blood Mini Kit from Qiagen (91). First, the samples were lysed using proteinkinase K and the lysate was loaded onto the DNeasy Mini Spin column. DNA adsorbs to the DNeasy membrane in the presence of high concentrations of chaotropic salt, which remove water from hydrated molecules in solution. Buffer conditions enable specific adsorption of DNA to the silica membrane and removal of contaminants and enzyme inhibitors. Thereby, the DNA was selectively bound to the DNeasy membrane as contaminants passed through. By repeated centrifugation and washing with special buffers, remaining contaminants and enzyme inhibitors were removed. In a final step the purified DNA was eluted in water and the concentration of genomic DNA was measured via a

Nanodrop 100 spectrophotometer. The DNA showed A260/A280 ratios of 1.0–1.9, and absorbance scans showed a symmetric peak at 260 nm.

After the PBMCs were isolated from the buffy coat, 5×10^5 PBMCs of each sample were frozen as a cell pellet at -20 °C. These samples were stored for subsequent genotyping analysis. The frozen samples were thawed and immediately mixed with 20 µl proteinkinase K. Then the samples were adjusted to 220 µl adding DPBS, 200 µl buffer AL was added and the samples were vortexed. The samples were incubated at 56 °C for 10 min. After the incubation, 200 µl ethanol 96% was added to each sample and all samples were vortexed thoroughly. The mixture was transferred into a DNeasy Mini spin column that was placed in a 2 ml collection tube. The samples were centrifuged at 6000 RCF for 1 min. After the centrifugation the collection tube containing the flow through was discarded. The spin column was then placed in a new 2 ml collection tube and 500 µl buffer AW1 was added to each sample. The samples were centrifuged at 6000 RCF for 1 min and after that, the collection tube and the flow through was discarded. The spin column was then placed again in a new 2 ml collection tube and 500 µl buffer AW2 was added to each sample. The samples were centrifuged at 20.000 RCF for 3 min and thereafter the collection tube and the flow through were discarded again. The spin column was placed in a 1.5 ml Eppendorf tube. The DNA was eluted by adding 50 µl Aqua ad iniectabilia. The samples were incubated for 10 min at room temperature. Then the samples were centrifuged for 1 min at 6000 RCF. The eluate contained the genomic DNA and the DNA concentration was subsequently measured at the Nanodrop 100 spectrophotometer.

2.2.6 HLA-genotyping

HLA class I genotyping was partly performed either by the HLA laboratory at the University medical center Hamburg-Eppendorf, Hamburg, Germany or by the DKMS Laboratories in Dresden, Germany. **Table 1** shows the HLA class I haplotypes for HLA-A, -B –C for each study subject. *Bw4*$^+$ individuals were defined by carriage of HLA-B alleles with a *Bw4*$^+$ epitope or the HLA-A alleles A*24:02 and A*23:01 (92,93). *Bw6*$^+$ individuals lack the above stated alleles. The HLA-A and –B alleles that carried the *Bw4*$^+$ epitope are highlighted in red.

Table 1: HLA genotype analysis

Number	Sample ID	HLA-A		HLA-B		Bw4/6^{+}	HLA-C		HLA-C Haplotype C1/C2	Seahorse Assay	Glut1 Assay	CD107a Assay
		A1	A2	B1	B2		C1	C2				
1	180322_BC_A	01:01	02:01	15:01	44:02	4	03:04	05:01	1/2	+	+	+
2	180322_BC_C	01:01	23:01	37:01	44:03	4	04:01	06:02	2/2		+	+
3	180322_BC_D	02:06	03:01	15:01	18:01	6	03:03	12:03	1/1		+	+
4	180316_BC_A	03:01	25:01	35:01	44:02	4	04:01	07:04	1/2	+	+	+
5	180316_BC_B	03:01	03:01	07:04	56:01	6	01:02	07:02	1/1		+	+
6	180316_BC_C	01:01	36:01	08:01	15:03	6	04:01	07:01	1/2		+	+
7	180316_BC_D	68:01	03:01	27:05	07:02	4	07:02	02:02	1/2		+	+
8	180308_BC_A	01:02	29:02	27:05	49:01	4	02:02	07:01	1/2		+	+
9	180308_BC_B	02:01	29:02	44:02	44:03	4	05:01	16:01	1/2		+	+
10	180308_BC_C	01:01	24:02	08:01	40:02	4	02:02	07:01	1/2		+	+
11	180308_BC_D	01:01	25:01	39:01	57:01	4	06:02	12:03	1/2	+	+	+
12	180201_BC_A	02:01	31:01	15:01	51:01	4	03:04	15:02	1/2	+	+	+
13	180201_BC_B	02:01	03:02	35:03	44:02	4	04:01	12:03	1/2	+	+	+
14	180201_BC_C	02:01	03:01	35:01	57:01	4	04:01	06:02	2/2		+	+
15	180201_BC_D	01:01	24:02	07:02	55:01	4	03:03	07:02	1/1	+	+	+
16	180110_BC_A	02:01	11:01	08:01	44:02	4	05:01	07:01	1/2		+	+
17	180110_BC_B	02:01	30:01	13:02	18:01	4	06:02	07:01	1/2		+	+
18	180110_BC_C	01:01	02:01	07:02	52:01	4	07:02	12:02	1/1		+	+
19	180110_BC_D	01:01	01:01	07:02	44:03	4	07:02	16:01	1/1		+	+
20	171129_BC_A	01:01	23:01	37:01	44:03	4	04:01	06:02	2/2	+	+	+
21	171129_BC_B	26:01	29:01	07:05	55:01	6	03:03	15:05	1/2		+	+
22	171129_BC_C	02:01	02:01	51:01	51:01	4	14:02	16:02	1/2		+	+
23	171129_BC_D	03:01	23:01	35:01	41:01	4	04:01	17:01	2/2		+	+
24	171109_BC_B	02:01	29:02	35:01	44:02	4	03:04	05:01	1/2		+	+
25	171109_BC_C	02:01	30:01	15:01	35:01	6	03:04	04:01	1/2		+	+
26	171109_BC_D	01:01	32:01	40:02	57:01	4	02:02	06:02	2/2		+	+
27	171026_BC_B	02:01	33:01	14:02	15:01	6	03:03	08:02	1/1		+	+
28	171026_BC_C	01:01	68:01	08:01	35:01	6	04:01	07:01	1/2		+	+
29	171026_BC_D	01:01	31:01	08:01	35:01	6	04:01	07:01	1/2		+	+
30	171011_BC_A	02:01	11:01	08:01	44:02	4	05:01	07:01	1/2	+		+
31	171011_BC_B	02:05	03:01	07:02	50:01	6	06:02	07:02	1/2			+
32	171011_BC_C	01:01	03:01	07:05	08:01	6	07:01	15:05	1/2			+
33	171011_BC_D	02:01	24:02	44:02	44:05	4	02:02	05:01	2/2			+
34	170816_BC_C	02:01	24:02	15:01	44:05	4	02:02	03:03	1/2	+		+
35	170816_BC_D	02:01	03:01	35:0	45:01	6	04:01	06:02	2/2			+
36	170810_BC_C	01:01	24:02	44:02	57:01	4	05:01	06:02	2/2	+		+
37	170810_BC_E	02:01	24:02	15:01	27:05	4	02:02	03:03	1/2	+		+
38	170727_BC_B	03:01	25:01	35:01	44:02	4	04:01	07:04	1/2	+		+
39	170727_BC_C	03:01	68:01	40:01	45:01	6	03:04	16:01	1/1			+
40	170727_BC_D	02:06	32:01	35:01	37:01	4	03:03	06:02	1/2	+		+
41	170713_BC_D	32:01	68:01	39:01	44:02	4	07:02	07:04	1/1	+		+
42	170706_BC_B	02:01	03:01	15:01	40:01	6	03:04	03:04	1/1	+		+
43	170706_BC_C	03:01	24:02	08:01	57:01	4	06:02	07:01	1/2	+		+
44	170629_BC_C	01:01	02:01	08:01	58:01	4	03:02	07:01	1/1	+		+
45	170629_BC_D	02:01	26:01	15:01	38:01	4	03:03	12:03	1/1	+		+
Total										**18**	**29**	**45**

2.2.7 Immunomagnetic negative NK-cell isolation

In order to enrich NK cells, the EasySep Human NK cell Isolation Kit from Stemcell was used (94). This method allows to isolate a certain cell population from heterogeneous cell mixtures. There are two types of separation: positive isolation and negative isolation. Within the positive isolation method, the desired cell population is selectively labeled with a specific antibody first. This is followed by a second labeling procedure with a secondary antibody which is conjugated to magnetic particles. The cells of interest are thereboy magnetically labeled and can then be separated from the un-labeled cells by using a strong magnet. The desired cells will attach to the magnet, whereas the unwanted cells can be found in the eluate. In the reverse case, which is the negative isolation, the separation is carried out by the marking the unwanted cells that are hold back by the magnetic field. The cells of interest can be found in the eluate. In the negative isolation process the desired cells are un-labeled and untouched, which is a major advantage of the negative isolation process towards the positive isolation.

According to the protocol, up to 400×10^6 PBMCs that were previously isolated via density-gradient centrifugation, were mixed with 8 ml pre-cooled NK cell isolation buffer (DPBS supplemented with 2% FBS and 1 mM EDTA) in a 14 ml polystyrene falcon. Next, the cell suspension was well mixed with 100 µl enrichment cocktail, which contains the magnetically labeled antibodies that bind the unwanted cells. The mixture was then incubated at room temperature for 10 min. After that 200 µl of the magnetic beads were added, while the solution was mixed thoroughly. The sample was incubated at room temperature for 5 min, so that the magnetic beads could bind the antibodies. Additional 2 ml NK cell buffer were added to the solution afterwards and the tube was inserted into the magnet, where the cells stayed for 3 min. Following, the magnet with the installed polystyrene tube that contained the cells was tilted and the cell suspension was poured into a new 15 ml falcon tube. The cell suspension was then centrifuged at room temperature for 7 min at 500 RCF and maximum ACC and DECEL, in order to separate the cells from the surrounding solution. After the centrifugation the supernatant was discarded, equal pellets were pooled and re-suspended in cell culture medium in a concentration of 3×10^6 cells/ml. The cell culture medium was enriched with 5 ng/ml IL-15 and the cells were stored in the incubator at 37 °C and 5% CO_2 overnight for further experiments.

2.2.8 NK-cell degranulation as determinant for NK-cell function

The cytoplasm of NK cells is filled with high concentrations of preformed granules that contain cytolytic proteins, such as perforin and granzyme. Upon activation through target cells, NK cells transport these granules to the cell surface, where their membrane fuses with the cellular membrane. Thereby, the cytolytic proteins are released into the immunological synapse. As a consequence, target cells which are in close contact with degranulating NK cells, can be killed through the contact with perforin and granzymes. CD107a is found within the membrane of cytolytic granules. Once the membrane of cytolytic granules fuses with the cell membrane, CD107a gets transferred onto the cell surface (95,96). In this way, CD107a expression on the cell surface can function as a marker to quantify the levels of cytotoxic NK cell degranulation.

In this assay 721.221 (88) and K-562 (89) cell lines, served as target cells for NK cells. Freshly isolated human NK cells were incubated with 5 ng/ml IL-15 at 37 °C and 5% CO_2 overnight and subsequently co-cultured for 4 h with either 721.221 or K-562 cells in an effector to target ratio of 1:2. Therefore 1×10^5 NK cells were distributed in duplicates with either 2×10^5 721.221 or 2×10^5 K-562 cells respectively, in 200 µl cell culture medium in one well of a 96-well plate. NK cells that were not exposed to any target cell line served as a negative control. All cultures were immediately mixed with CD107a antibody in a dilution of 1:100 (2 µl per 200 µl cell suspension) and incubated for 1 h at 37 °C and 5% CO_2 in the incubator. After that time, BD GolgiStop, a protein transport inhibitor containing Monensin was distributed to all samples. This inhibitor blocks intracellular protein transport processes and prevents the acidification of endocytic vesicles (97). Thereby the degradation of reinternalized CD107a proteins from the surface is reduced and allows for surface staining of this marker after stimulation. In the following the samples were incubated for 3 h at 37 °C and 5% CO_2 in the incubator. After the incubation time the cells were centrifuged at room temperature for 5 min at 400 RCF and maximum ACC and DECEL, in order to separate the cells from the surrounding solution. In a further step these cells were stained with respective antibodies flow cytometric analysis.

2.3.9 Flow cytometric measurements

Flow cytometry

Flow cytometry is a technique to investigate the characteristics of cellular subsets (Murphy & Weaver, 2017). Thereby, cells can be quantified and studied for their size and granularity as well as for the expression of distinct molecules. These molecules can be detected by using monoclonal antibodies that specifically target and bind to unique antigens present on the surface of the cell or intracellularly. Individual cells that have been labeled with fluorescent antibodies are passing in a fine fluidic stream through a laser beam. As each cell passes through the laser beam it scatters the laser light and each fluorescent dye, which is attached to the cell by antibody-binding, will be excited and fluoresce. Highly sensitive photomultiplier tubes (PMT) detect the scattered light, that can give information about the size and the granularity of the cell. Additionally, the emitted light from the fluorophore indicates whether a distinct antibody is bound to a specific target on the cell and hence about the expression of distinct molecules. By the use of multiple antibodies with different dyes multiparametric analysis is possible. The generated data is transferred to a computer and can be analyzed via the FlowJo software. The data from multiparametric analysis is then displayed in a two-dimensional scatter diagram, where the fluorescence intensity of one dye-labeled antibody is plotted against a second one. By discriminating between cells that exhibit a specific fluorescent signal and cells that lack the signal, sub-populations that are characterized by a distinct expression profile can be defined. This work was performed with a BD LSR Fortessa equipped with 5 lasers (see **Table 2**) that can detect up to 18 different fluorochromes simultaneously.

Table 2: Lasers of the BD LSR Fortessa flow cytometer

Laser	**UV**	**Violet**	**Blue**	**Yellow-green**	**Red**
Wavelength	355 nm	405 nm	488 nm	561 nm	633 nm

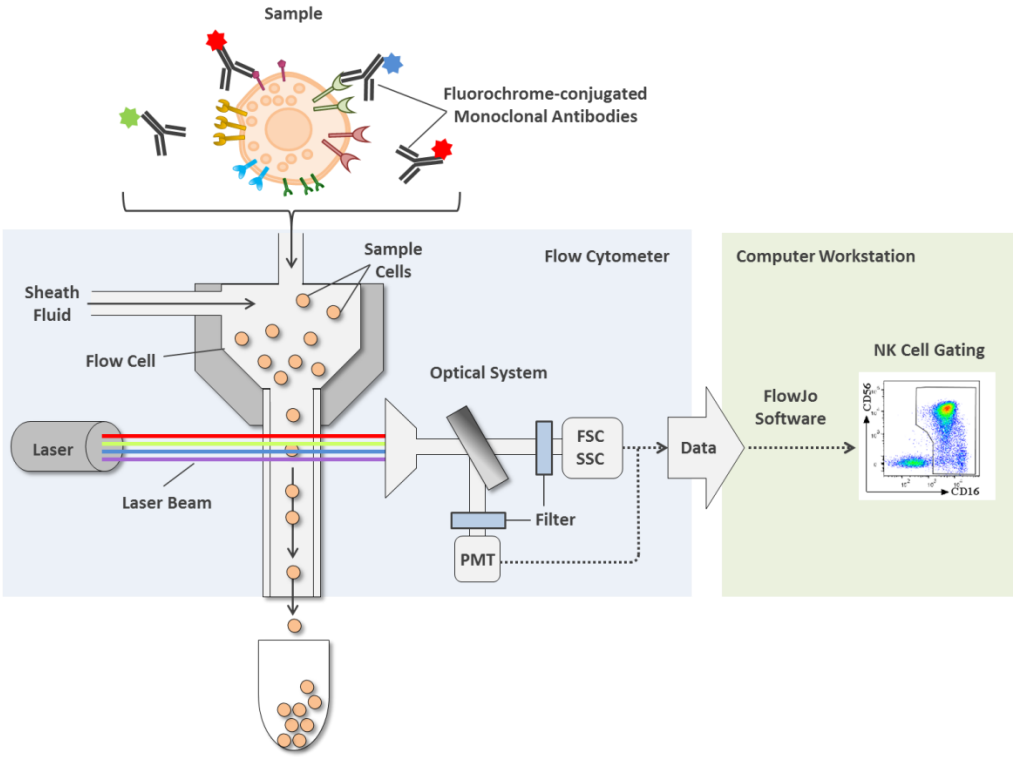

Figure 16: Principle of flow cytometry

Schematic representation of flow cytometry. Flow cytometry is a technique that allows to investigate the physical and chemical characteristics of cells. Therefore, cells are suspended in a sheath fluid, flowing along a stream through a flow cell that is irradiated by a laser beam. As the cells pass through the laser beam, they scatter the light. By capturing the forward scatter (FSC) and the side scatter (SSC) light by optical detectors, the size and granularity of the cells can be determined. In addition, cells that are labeled with fluorochrome-conjugated antibodies emit light as the they pass through the laser beam. The emitted light is detected by a photomultiplier tube (PMT) which in turn is amplifying the detected signal. The data that is generated can furthermore be analysed at the computer via the FlowJo software. By creating gates for characteristic features, the software allows to gain information about the size, granularity and antigen profile of an individual cell within the investigated cell population. During multiparametric analysis flow cytometers can analyse at multiple fluorochromes simultaneously, in addition to the FSC and SSC (figure adapted from (98)).

Live/dead staining

In order to discriminate live and dead cells during flow cytometric analysis, NK cells were stainied with a fluorescent dye from the live/dead fixable blue dead cell stain kit. Live cells react with the reactive dye only on the cell surface leading to weak fluorescent cells. On the other hand, cells with damaged cell membranes react with the dye throughout the membrane, yielding in brightly stained cells. NK cells that have been stimulated with target cells in a degranulation assay (see **2.2.8**) were resuspended

in 200 µl DPBS and centrifuged at room temperature for 5 min at 400 RCF and maximum ACC and DECEL. The supernatant was carefully discarded and the cells were resuspended in 100 µl staining buffer (DPBS supplemented with 2% FBS). In order to prepare a working solution of the live/dead fluorescent reactive dye, 50 µl DMSO was added to one vial of the live/dead fixable blue dead cell stain kit. Next, the live/dead fluorescent reagent was added to the cells in a concentration of 1 µl working solution to 1 ml cell suspension. The cell suspension was mixed gently and the samples were incubated for 10 min at room temperature in the dark. After that time, the surface staining antibodies were added and the samples were incubated for additional 20 min. Thereby the total incubation time with the live/dead fluorescent reactive dye was 30 min.

Surface antibody staining

In order to identify NK cells and the expression of NK cell receptors (KIRs), a staining was performed with mononuclear fluorescent-conjugated antibodies. The used antibodies target specific molecules on the surface of the investigated cells. Each cell type can be identified by the expression of distinct markers, known as cluster of differentiation (CD). NK cells are defined by the presence of the molecular markers, CD56 and CD16 and the absence of CD3, CD14 and CD19 (99). CD56 is a glycoprotein expressed on the surface of NK cells and other lymphoid cells. CD16 is also known as FcγRIII, which is a Fc receptor involved in antibody-dependent cellular cytotoxicity (ADCC) (17). CD16 is expressed on the surface of NK cells, but also on neutrophils, monocytes and macrophages. Furthermore, NK cells lack the expression of CD3, which is a T cell co-receptor (100). Besides they do not express CD14 which is found on macrophages, neutrophils and dendritic cells (101). Finally, CD19 is an adaptor protein which is expressed by B cells (102). First, a mastermix was prepared with the following antibodies as it is shown in **Table 3**. The antibody mastermix was calculated for one sample. Each antibody volume was multiplied with the amount of samples in the assay and the calculated volumes of all antibodies were transferred into the same tube and mixed gently. Then, each sample was mixed with 17,5 µl antibody mastermix and incubated at room temperature for 20 min in the dark. After that time 100 µl DPBS was added to each sample and the cells were centrifuged at room temperature for 5 min at 400 RCF and maximum ACC and DECEL.

Table 3: Antibodies used for surface staining

Target	Fluorochrome	Clone	Dilution	Volume [µl] added to 100 µl cell suspension
CD56	BUV395	NCAM16.2	1:100	1
CD16	BV785	3G8	1:100	1
KIR3DL1	BV421	DX9	1:50	2
CD3	PerCP-Cy 5.5	UCHT1	1:50	2
CD14	PerCP-Cy 5.5	HCD14	1:50	2
CD19	PerCP-Cy 5.5	HIB19	1:200	0.5
NKG2A	Pe-Cy7	Z199	1:50	2
KIR2DL2/L3	PE	DX27	1:50	2
KIR2DL1	APC	143211	1:20	5
			Total	17,5 µl

Glut1 staining

Glut1 (solute carrier family 2, facilitated glucose transporter member 1-SLC2A1-) is the major glucose transporter and is ubiquitously expressed on most cell types (103). As an important transporter for glucose metabolism this receptor was investigated in this project. Glut1 serves as a receptor for the human T cell leukemia virus (HTLV) to gain entry into target cells (104). As the HTLV Env receptor binding domain (RBD) binds Glut1 naturally, the commercially available fusion protein of HTLV Env RBD and an eGFP Tag allows immunofluorescent staining of Glut1. NK cells alone and NK cells that have previously been stimulated with target cells in a degranulation assay were resuspended in 50 µl labeling buffer (cell culture medium supplemented with 0.09% sodium azide (NaN_3) and 1 mM EDTA). Then, 2.5 µl of Glut1.RBD.GFP was added to the cells and the samples were incubated for 30 min at 37 °C and 5% CO_2 in the incubator. Thereafter, 100 µl DPBS were added to each well and the plate was centrifuged at 400×g for 5 min at 4 °C and maximum ACC and DECEL. The supernatant was carefully taken up and discarded. The cell pellet was resuspended in 100 µl acquisition buffer (DPBS, 2% FBS, 0.09% NaN_3, 1 mM EDTA and 1% paraformaldehyde (PFA)) and transferred into a polystyrene round-bottomed FACS tube. The samples were measured at the flow cytometer.

Flow cytometric analysis

The cells were measured at the BD LSRFortessa. First, the machine was started and the cytometer settings (filter settings, **Table 4**) were examined and adjusted. A CS&T was performed with BD FACSDiva CS&T beads in order to standardize the cytometer performance. After the CS&T was completed successfully, a tube with water was installed and the sample was acquired for 10 min to clean the fluidic systems before performing actual measurements. The following measurements were multicolor assays. Therefore fluorescence compensation was performed in order to ensure that the fluorescent signal that was detected during the measurement derived from the investigated fluorochrome itself. This process allows to mathematically subtract signals derived from other fluorochromes spilling over into the respective channel by the BD FACSDiva software. The compensation was performed with compensation beads that have been stained with the respective antibodies before. Then the samples were measured successively. After the measurements the fluidic system of the machine was cleaned by installing a tube with cleaning solution, rinse solution and water, which was acquired for 5 min each at the highest flow rate. The data was further analyzed via the FlowJo 10.4.2 software.

Table 4: LSR Fortessa laser and filter configurations

Detector array	Laser	Laser	Parameter	PMT position	BP-filter	LP-filter	Fluorochrome
Trigon	355 nm	UV	1	A	450/50	420 LP	BUV737
			2	B	380/14		BUV395
Octagon	405 nm	violet	3	A	780/60	735 LP	BV785
			4	B	710/40	670 LP	BV711
			5	C	675/50	635 LP	BV650
			6	D	610/20	600 LP	BV605
			7	E	586/15	570 LP	BV570
			8	F	525/50	505 LP	BV510
			9	G	450/50		BV421
Octagon	488 nm	blue	10	A	710/40	685 LP	PerCP-Cy5.5
			11	B	530/30	505 LP	FITC
				C	488/10		SSC
Octagon	561 nm	yellow-green	12	A	780/60	750 LP	Pe-Cy7
			13	B	670/30	635 LP	Pe-Cy5
			14	C	610/20	600 LP	PE-Texas Red
			15	D	586/15		PE
Trigon	633 nm	red	16	A	780/60	750 LP	APC-Cy7
			17	B	730/45	690 LP	Alexa Fluor 700
			18	C	670/14		APC

2.3.10 Analysis of flow cytometric data

Hierarchical gating strategy

Flow Cytometry Standard (FCS) data files were analyzed via the FlowJo 10.4.2 software. The gating strategy depicts how NK-cell subsets were identified according to the detection of specific expression markers (**Figure 17**).

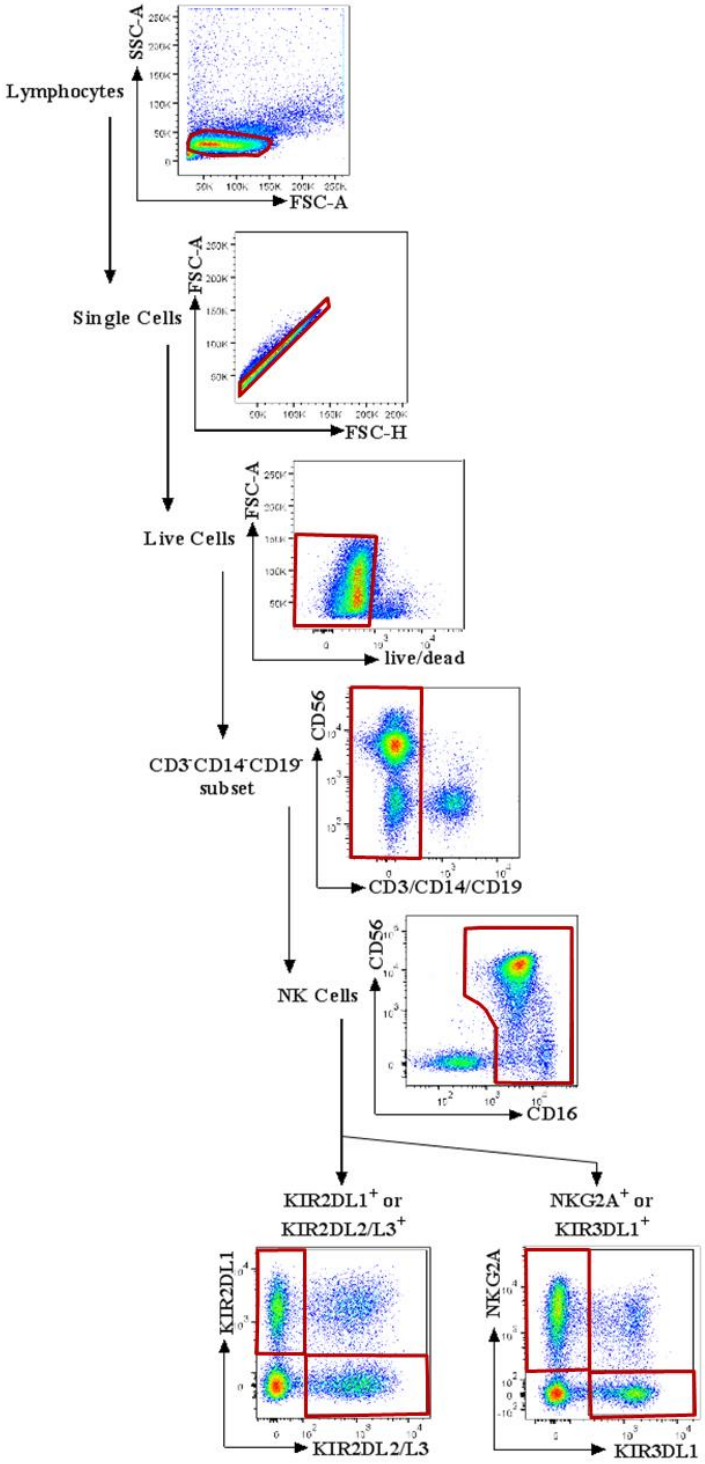

Figure 17: NK-cell gating strategy

Schematic representation of the gating strategy that was used to identify NK cells and NK-cell subsets that expressed the inhibitory receptors KIR2DL1, KIR2DL2/L3, KIR3DL1 and NKG2A. The data is displayed in a two-dimensional scatter diagram, where the fluorescence intensity of one expression marker is plotted against a second one. Each dot represents one cell. The cell density is represented by a color code. Blue dots show low density, whereas red dots illustrate a high cell density. The gate that defines the selected population is highlighted with by a red colored frame. Lymphocytes were gated using forward and side scatter (FSC-A/SSC-A). The lymphocyte cell population was then sub-analyzed by area and height of the forward scatter (FSC-A/FSC-H) defining single cells. Next, dead cells were excluded by the use of the viability dye live/dead fixable blue. Subsequently, the live cell gate was further analyzed to exclude B cells, T cells and Monocytes and Macrophages respectively. Thus, NK cells were identified by the exclusion of $CD3^+$, $CD14^+$, and $CD19^+$ cells and the expression of either CD56 or CD16. Finally, NK-cell subsets were sub-gated for the expression of the inhibitory receptors KIR2DL1, KIR2DL2/L3, KIR3DL1 and NKG2A.

Determination of NK-cell subsets: CD107a/Glut1 NK-cell subsets

The NK-cell population that was identified via the previously described gating strategy allowed to examine the expression of CD107a and Glut1 on stimulated and unstimulated NK-cells. By using the FlowJo application software, NK cells were further gated into the following sub-populations: $CD107a^+/CD107a^-$ and $Glut1^+/Glut1^-$ NK-cell subsets. These sub-populations were further analyzed for the frequency of $CD107a^+$ NK cells as well as the median fluorescence intensity of Glut1. The frequency of $CD107a^+$ NK cells that was measured in stimulated NK-cell subsets was normalized to the frequency measured in unstimulated cells (105). The following formula was used:

$$\text{Frequency normalized } = \frac{(\text{frequency stim.} - \text{frequency unstim.})}{(100 - \text{frequency unstim.})} \times 100$$

Furthermore, the median fluorescence intensity (MFI) of Glut1 that was measured in stimulated and unstimulated NK cells subsets was normalized to the fluorescence minus one (FMO) control. The FMO control is a sample which contains all flurochromes, except the one that is being measured (Glut1). The MFI of the samles that have been stimulated with target cells were transformed to the Relative Fluorescence Intensity (RFI) via the following formula:

$$\text{RFI} = \frac{\text{MFI sample}}{\text{MFI FMO Ctrl.}} - 1$$

The obtained data was analyzed and visualized by using Graph Pad Prism 7.04.

2.3.11 Determination of NK-cell subsets: single positive inhbitory receptors subsets

Boolean Gating is a gating method in FlowJo, which can be applied to define sub-populations. An algorithm allowing for automatic generation identified 16 possible combinations of NK-cell subsets that were generated from the 4 inhibitory NK cell receptors that were analyzed in this study: KIR2DL1, KIR2DL2/L3, KIR3DL1 and NKG2A. **Table 5** lists all subsets that were created via boolean gating. NK-cell subsets that were further investigated in this study are highlighted in orange. These subsets were either single positive (SP) for one specific inhibitory receptor or lacked all of the investigated receptors (R-).

Table 5: NK-cell subsets determined by boolean gating

Inhibitory Receptor	NK-cell subsets															
								SP				SP		SP	SP	R-
KIR2DL1	+	+	+	+	+	+	+	+	-	-	-	-	-	-	-	-
KIR2DL2/L3	+	+	+	+	-	-	-	-	+	+	+	+	-	-	-	-
KIR3DL1	+	+	-	-	+	+	-	-	+	+	-	-	+	+	-	-
NKG2A	+	-	+	-	+	-	+	-	+	-	+	-	+	-	+	-

2.2.12 NK-cell subset enrichment via fluorescence-activated cell sorting

Fluorescence-activated cell sorting (FACS) is based on the principle of flow cytometry (see point **2.3.9**) with the addition that live cells can be isolated from a heterogeneous cell population. This technique allows further analysis of cellular sub-populations. In order to receive two distinct NK-cell populations (educated and uneducated NK cells) for subsequent metabolic analyses, FACS was performed with a BD FACS Aria Fusion machine. In a first step, the samples were labeled with fluorescence-conjugated antibodies. These cells were taken up into the machine where they flow along a stream into the flow cell. The flow cell is irradiated by different laser beams. As the cells pass through one of the laser beams, they scatter the laser light. The scattered light can then captured by optical detectors, which give information about size and granularity of the cell. Furthermore, the fluorophores on fluorescent- labeled cells get excited by the laser beam and hence emit light. Photomultiplier tubes (PMTs) can detect the scattering of light and the information is transformed into a electronic signal. The cells that have passed the laser beam are subsequently forced through a small nozzle (nozzles can have sizes of 70, 85, 100, and 130 µm depending on the cell size), creating a very fine stream of sheath fluid that contains the antibody labeled cells. Based on the information the computer has received from the fluorescent measurement an electric charge is created, which is then passed from the nozzle through the liquid stream. At the precise time, when the streams breaks up into single droplets, the instrument applies a positive or negative charge to the droplet based on the characteristics of the cell. Ideally one droplet contains one single cell. Due to an electrostatic deflection system the charged droplet will be distributed in one of the collection tubes, which allows sorting of single cells according the characteristic surface molecules (**Figure 18**).

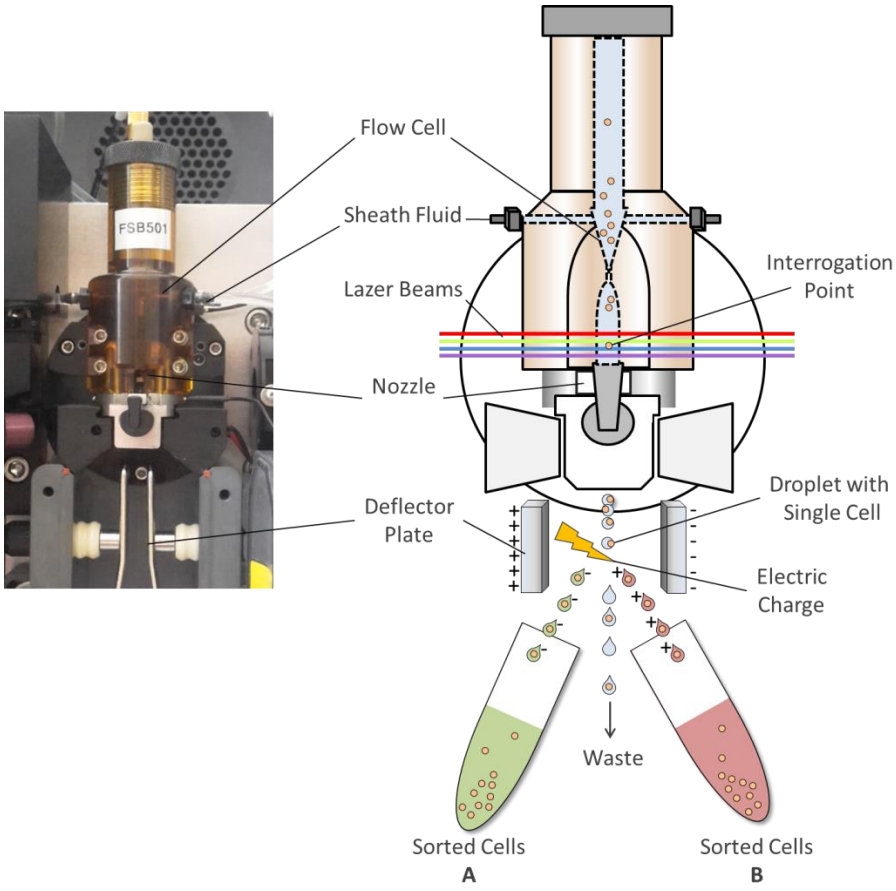

Figure 18: Principle of fluorescence-activated cell sorting

Schematic overview of fluorescence-activated cell sorting. Fluorescence-activated cell sorting is a technique where live cells from a heterogenous cell population can be separated into homogenous sub-populations based on fluorescent labeling of subset-specific markers. The technique is built on the principle of flow cytometry (see point **2.3.9**), where the cells that are flowing along a stream are irradiated by a laser beam. As the cells pass through the laser beam, they scatter the laser light at the interrogation point. The scattered light is then captured by optical detectors and gives information about size and granularity of the cell. Furthermore, the fluorophores on fluorescent- labeled cells get excited by the laser beam and hence emit light that can be detected by a photomultiplier tube (PMT). The generated signals are passed to a computer and are used to create an electric charge, which is then passed from the nozzle through the liquid stream. At the precise time, when the streams breaks up into single droplets, the instrument applies a charge to the droplet based on the characteristics of the cell. An electrostatic deflection system facilitates distribution of the charged droplets into different collecting tubes (figure adapted from (106)).

FACS machine setup

First, the machine was set up for cell sorting by performing a fluidic startup using the BD FACS Diva software v.8.0.1. Initially, the fluidic startup required to manually connect the sheath tank with the machine to allow an automated cleaning process which cleaned the fluidic system including the flow cell. Then a 70 micron nozzle was installed into the flow cell. After the fluidic startup was finished, the stream was turned on. To standardize the cytometer performance a cytometer setup and tracking (CS&T) procedure was performed with BD FACSDiva CS&T beads. As soon as the stream was stable, the sweet spot (automated clog detection and sort tube protection) system was selected. Further quality controls required the performance of an auto drop delay procedure with BD FACS Accudrop beads. This procedure was conducted to ensure precise cell sorting, whereby the droplet that contains the cell of interest is sorted into the correct tube. Then the optical filter system of the machine was examined and equipped with the required filters used in this setting (an overview of the filters is shown in **Table 6**).

Table 6: BD FACS Aria Fusion laser and filter configurations

Detector array	Laser	Laser	Parameter	PMT position	BP-filter	LP-filter	Fluorochrome
Trigon	355 nm	UV	1	A	740/40	685 LP	BUV737
			2	B	380/14		BUV395
Octagon	488 nm	blue	3	A	695/40	655 LP	PerCP-Cy5.5
			4	B	530/30	505 LP	eGFP / FITC
			5	C	488/10		SSC
Octagon	405 nm	violet	6	A	780/60	750 LP	BV785
			7	B	710/50	690 LP	BV711
			8	C	660/20	630 LP	BV650
			9	D	610/20	595 LP	BV605
			10	E	525/50	505 LP	BV510
			11	F	450/50		BV421
Octagon	561 nm	yellow-green	12	A	780/60	735 LP	Pe-Cy7
			13	B	710/50	685 LP	Pe-Cy5.5
			14	C	670/14	630 LP	Pe-Cy5
			15	D	610/20	600 LP	PE-Texas Red
			16	E	582/15		PE
Octagon	640 nm	red	17	A	780/60	755 LP	APC-Cy7
			18	B	730/45	690 LP	Alexa Fluor 700
			19	C	670/30		APC

Finally, the control settings (nozzle size, filter settings and pressure) were examined on the BD FACS Diva control panel and selected for the appropriate configurations. To ensure that the fluorescent signal that was measured during the recording process is derived from the fluorochrome of interest, fluorescence compensation was performed with compensation beads. This process enables the BD FACSDiva software to mathematically subtract signals derived from other fluorochromes spilling over into the respective channel. The compensation was performed with compensation beads that have been stained with the respective antibodies before.

Cell sorting

Fluorescence- labeled enriched NK cells were taken up in sorting buffer (RPMI-1640 Medium without phenol red and supplemented with 5% FBS) in a concentration of 5×10^5 cells/ml. Next, the cells were passed through a cell strainer (snap cap falcon tube with cell strainer) to avoid cell clumps. The cells from different individuals were successively analyzed at the BD FACS Aria Fusion machine. NK cells were identified according to the previously described gating strategy (see **2.3.10**). Then NK cells were further gated into educated and uneducated NK-cell subsets according to the educational profile that was determined for each study subject via preceeding functional assays. The different possible educational profiles resulting from different combinations of the expression of inhibtory receptors and HLA-B or HLA-C alleles are shown in **Table 7**.

Table 7: Combination of educational profiles

	Educational profile					
Inhibitory receptor	**HLA-*C1/C2* heterozygous, HLA-*Bw4+***	**HLA-*C1/C2* heterozygous, HLA-*Bw6+***	**HLA-*C2/2* homozygous, HLA-*Bw4+***	**HLA-*C2/2* homozygous, HLA-*Bw4-***	**HLA-*C1/C1* homozygous, HLA-*Bw4+***	**HLA-*C1/C1* homozygous, HLA-*Bw4-***
KIR2DL1	+	+	+	+	-	-
KIR2DL2/L3	+	+	-	-	+	+
KIR3DL1	+	-	+	-	+	-
NKG2A	+	+	+	+	+	+

2.2.13 Seahorse Assay

The Seahorse assay measures the extracellular acidification rate (ECAR) referring to proton production and glycolysis as well as the oxygen consumption rate (OCR), which gives information about the oxidative phosphorylation (OXPHOS) (107). The assay is performed in a 96-well cell culture plate and a sensor cartridge that represents the lid. First, the cells are seeded into the cell culture plate. Then the sensor cartridge is placed on top of the cell plate and the plate is inserted into the instrument. The sensor cartridge has 96-plastic sleeves in which two fluorophores are embedded (**Figure 19**). The first fluorophor is quenched by oxygen and measures the mitochondrial respiration. The second fluorophor is sensitive to protons and provides information on glycolysis. Quenching refers to any process which decreases the fluorescence intensity of a given substance. Inside the instrument fiber optic bundles simultaneously insert themselves into the sleeves in the sensor cartridge. The fiber optics emit light that excites the embedded fluorophore, and then reads back the change in fluorophore emission due to the change in oxygen and protons. By the use of the drug delivery ports which are located in the sensor cartridge, it is possible to add inhibitors, stimulators or substrates at specified time points. The effects can be measured in real time.

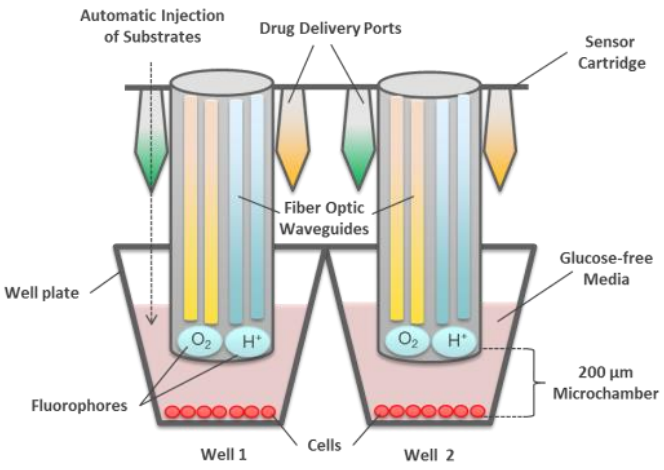

Figure 19: The Seahorse sensor cartridge

Schematic overview of a Seahorse sensor cartridge. The Seahorse sensor cartridge is a specialized cell culture lid that allows to measure the changes in oyxgen and protons in a cell culture medium by a Seahorse machine. The sensor cartridge comprises of 96-plastic sleeves with two different fluorophores that are embedded at the end of each plastic sleeve. One fluorophor is quenched by protons and provides information about glycolysis, the other fluorophore is sensitive to oxygen and measures oxygen consumption referring to mitochondrial OXPHOS. Once the sensor cartridge is placed on top of a cell culture plate, the sleeves are immersed in the cell culture medium whereas the fluorophors are in close proximity to the cells that are located on the bottom of the cell culture plate. The cell culture plate and the sensor cartridge are placed into the Seahorse machine where fiber optic bundles are inserted into all the sleeves of the sensor cartridge. The fiber optics emit light that excite the embedded fluorophores, and can read back the change in fluorophore emission due to the change in oxygen and protons. In addition, 4 drug delivery ports are located next to each sleave, whereby it is possible to add inhibitors, stimulators or substrates to a given time to the cell culture medium. The effects of the added substrates on the changes in protons or oxygen in the media can be measured in real time.

First, the cells are starved in glucose free medium. The first addition is a saturated glucose solution, which enables the cells to rapidly utilize glucose and catabolize it via the glycolytic pathway to pyruvate, producing ATP, NADH, water and protons. Glycolysis causes an expulsion of protons into the surrounding medium leading to an increase in ECAR. The glucose-induced response is detected as the rate of glycolysis under basal conditions. The second addition is oligomycin, which is an ATP synthase inhibitor. Oligomycin inhibits mitochondrial ATP production and shifts the energy production towards glycolysis. This leads to an continious increase in ECAR, defining the maximum glycolytic capacity of the cell. The final addition is 2-Deoxy-D-glucose (2-DG). 2-DG is a glucose analog, which inhibits glycolysis through competetive binding to glucose hexokinase. The decrease in ECAR is a proof that the ECAR measured in the experiment is due to glycolysis (**Figure 20**). The delta between glycolyctic capacity and glycolysis rate defines glycolytic reserve. The ECAR, that was measured prior to glucose addition, is referred to as non-glycolytic acidification, which is caused by processes in the cell other than glycolysis.

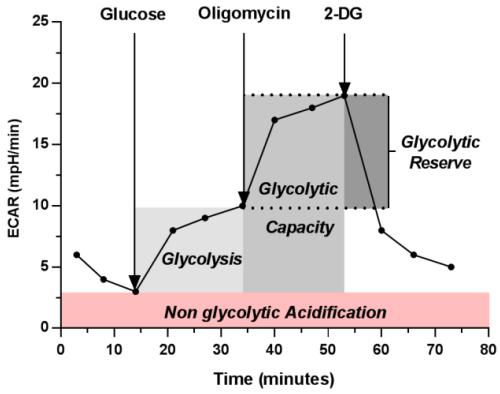

Figure 20: The Seahorse Glycolytic Stress Test

Schematic overview of the Seahorse Glycolytic Stress Test. The Seahorse Glycolytic Stress Test measures the glycolytic function of cells and provides information about several parameters of the glycolytic flux, including glycolysis, glycolytic capacity and glycolytic reserve. During the assay the Seahorse XF analyzer performs sequential measurements of the extracellular acidification rate (ECAR) after the addition of glucose (fueling glycolysis), oligomycin (ATP synthase inhibitor blocking oxidative phosphoryliation (OXPHOS)) and 2-deoxy-D-glucose (2-DG, synthetic glucose analogue inhibiting glycolysis) (figure adapted from (107)).

The Seahorse analyzer implements the addition of specific compounds at different time points allowing the calculation of (I) glycolysis, (II) glycolytic capacity and (II) glycolytic reserve (107): (I) Glycolysis is the process of converting glucose to pyruvate and is measured as ECAR rate that is reached by a given cell population after the addition of saturating amounts of glucose. (II) The glycolytic capacity is defined as the maximum ECAR rate that can be reached following the addition of oligomycin. Oligomycin inhibits oxidative phosphorylation and drives the cell to use glycolysis to its maximum capacity. (III) The glycolytic reserve is considered as the capability to

respond to an energetic demand as well as how close the glycolytic function is to the cell's theoretical maximum.

Seahorse preparations

One day before the Seahorse assay was performed, the XFe96 sensor cartridge needed to be hydrated overnight. Therefore, each well of the utility plate was filled with 200 µl of a Seahorse XF calibrant solution. Then the sensor cartridge was placed back onto the utility plate, submerging the sensors completely in calibrant solution. The plate was further placed into a non-CO_2 incubator and stored at 37 °C overnight.

The day the Seahorse assay was performed, the medium that was needed for the assay was prepared first. In order to prepare the assay medium, 50 µl Seahorse XF base medium was filled into a beaker adding a stirring magnet into the solution and covering the beaker with aluminum foil to avoid contamination. The beaker was then put into a water bath heating the solution to a temperature of 37 °C. Once the solution had reached the temperature, 500 µl of a 200 mM L-Glutamine solution was added so that the final concentration of L-Glutamine was 2 mM. Next the beaker was put on a magnetic stirrer mixing the solution in a steady manner. A pH electrode was installed to measure the pH of the solution. The pH was adjusted to 7.4± 0.1 by using 1 N NaOH and 37% HCl. After the pH was adjusted, the solution was kept at 37 °C until it was further used. Next, the compound solutions were prepared. The Seahorse XF Glycolysis Stress Test Kit that was used in this study contained lyophilized glucose, oligomycin and 2-Deoxy-D-glucose (2-DG) compounds. To generate stock solutions, the compounds were solved in the previously prepared assay medium according to **Table 8**. To ensure that the compounds were completely solved, all stock solutions were vortexed rigorously.

Table 8: Seahorse stock solutions preparation

Compound	Volume of assay medium added [µl]	Final stock solution concentration [mM]
2-DG	3000	500
Glucose	3000	100
Oligomycin	720	100

Next the stock solutions were further prepared to generate working solutions (compare **Table 9**). The 2-DG stock solution was ready to use. The glucose stock solution was mixed with additional 750 µl assay medium. For the oligomycin solution, 270 µl were transferred into a 15 ml falcon tube and mixed with 2730 µl assay medium. All solutions were mixed gently and were stored at room temperature for further use.

Table 9: Seahorse working solutions preparation

Compound	Stock solution Volume [µl]	Volume of Assay medium added [µl]	Volume of working solution added to the port	Final concentration in Seahorse Assay
2-DG	3000	/	25	50 mM
Glucose	3000	750	25	10 mM
Oligomycin	270	2730	25	1.0 µM

Seahorse Glycolysis Stress Test

After all preparation steps were completed, NK cells were counted. The total cell number that was counted for each NK-cell subset determined the cell number that was used in the Seahorse Assay. Provided that the cell numbers were high enough, each sample set was performed in triplicates. The volume for each cell suspension was transferred into falcon tubes and filled up with DPBS to wash the samples. The cells were centrifuged at room temperature for 7 min at 350 RCF and maximum ACC and DECEL. The cell pellets were then re-suspended in 600 µl pre-warmed assay medium (=glucose free medium). Each well of the Seahorse assay cell culture plate needed to be filled with 175 µl cell suspension. Due to pipetting errors the volume for one well was calculated for 200 µl cell suspension according to the calculation example shown in **Table 10**.

Table 10: Calculation scheme for cell counts in Seahorse assay

	Total cell number per well		
	1×10^6 cells	**5×10^5 cells**	**2×10^5 cells**
Total cell number in triplicate	3×10^6 cells/ sample	$1{,}5\times10^6$ cells/ sample	6×10^5 cells/ sample
Total amount of medium in triplicate	3×200 µl	3×200 µl	3×200 µl
Total amount of cells in triplicate	5714 cells/µl × 600 µl **$3{,}43\times10^6$ cells/ sample**	2857 cells/µl × 600 µl **$1{,}71\times10^6$ cells/sample**	1142 cells/µl × 600 µl **$6{,}9\times10^5$ cells/sample**

Data acquisition and analysis

The Seahorse XFe96 analyzer is operated by the Wave software. Before the experiment was started, the instrument protocol needed to be adjusted via the control panel of the software. Next, the machine needed to be calibrated. For this step, the sensor cartridge that was hydrated overnight was loaded with each of the compounds (glucose, oligomycin, 2-DG). Therefore, 25 µl of each solution were transferred into the respective drug delivery port of the hydrated sensor cartridge according to the scheme shown in **Table 11**.

Table 11: Loading scheme for the Seahorse sensor cartridge

Port **A**: Glucose
Port **B**: Oligomycin
Port **C**: 2-DG
Port **D**: empty

A	**B**
C	**D**

The loaded sensor cartridge was then placed into the Seahorse XFe96 analyzer and the calibration was started. During the time the machine was calibrated, the samples were loaded on a Seahorse cell culture microplate. For each sample 175 µl cell suspension were transferred into a well of the cell culture plate in triplicates. For background calculations, the well at each corner of the cell culture plate was filled with 175 µl assay medium. Residual wells were filled with 175 µl PBS each. After the cell culture plate was loaded completely it was stored at 37 °C for 30 min in a non-CO_2 incubator. Afterwards the plate was centrifuged for 7 min at 350 RCF and maximum ACC and DECEL, in order to place the cells at the bottom of the cell culture plate. Next, the cell culture plate was installed in the Seahorse XFe96 analyzer and the assay was started. The data was further analyzed via the WAVE software. The data was further processsed by calculating the values for glycolysis, glycolytic capacity and glycolytic reserve according to **Table 12**.

Table 12: Calculating parameters of glycolytic flux

Parameter	Rate measurement equation
Glycolysis	(Maximum rate measurement before oligomycin addition) – (last rate measurement before glucose addition)
Glycolytic capacity	(Maximum rate measurement after oligomycin addition) – (last rate measurement before glucose addition)
Glycolytic reserve	Glycolytic Capacity - Glycolysis

3 Results

3.1 CD107a expression as a marker for NK-cell function

NK-cell degranulation and subsequent lysis of target cells has been shown to directly correlate with surface expression of CD107a, which makes CD107a an established marker to measure NK-cell function (97). Enriched primary human NK cells were incubated for 6 h in the presence or absence of the HLA class I devoid target cell lines 721.221 and K-562. **Figure 21** demonstrates the flow cytometric analysis of CD107a on bulk NK cells. Despite the absence of target cells, surface expression of CD107a was detectable in unstimulated NK cells (no target, 11%) due to unspecifc and spontaneous degranulation. Nevertheless, surface expression of CD107a increased from 11% in unstimulated NK cells up to 49% $CD107a^+$ NK cells after exposure to 721.221 cells and up to 58% $CD107a^+$ NK cells after stimulation with K-562 cells.

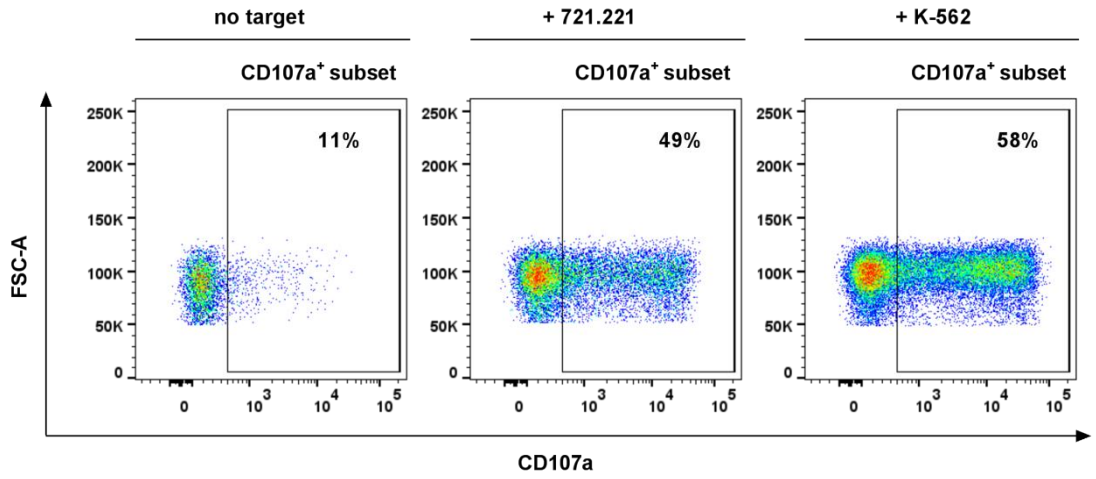

Figure 21: Flow cytometric assessment of CD107a as a marker for NK-cell function

Flow cytometric assessment of NK-cell function after exposure to various target cells. The figure shows data from one subject. Enriched primary human NK cells were co-cultured for 6 h either in the absence (left panel) or presence of 721.221 cells (middle panel) or K-562 cells (right panel). All samples were stained for the degranulation marker CD107a and the obtained flow cytometric data was subsequently analyzed via FlowJo software. Numbers indicate the frequency of $CD107a^+$ NK cells in each subset.

3.2 Quantification of NK-cell degranulation over time

Using established protocols, CD107a expression is usually measured after 6 h incubation with target cells (97). In order to streamline the assessment of NK-cell function together with consecutive experiments, the experimental workflow needed to be optimised. With the intention to define the shortest time of target cell stimulation that

allows for the measurement of NK-cell function, CD107a expression was assessed over time. Therefore, NK cells were stimulated over a time period of 6 h and analyzed for expression levels of CD107a after each hour. **Figure 22** shows the CD107a expression on bulk NK cells following exposure to various target cell lines. K-562 stimulated NK cells displayed a detectable population of $CD107a^+$ cells (9%) at an incubation time of 0 h, measured directly after the co-culture was set up, while the 721.221 stimulated NK cells showed only a marginal subset of $CD107a^+$ cells (2%) at the same time point. The overall percentage of $CD107a^+$ cells increased over time reaching 37% after 6 h stimulation with 721.221 cells and 55% with K-562 cells.

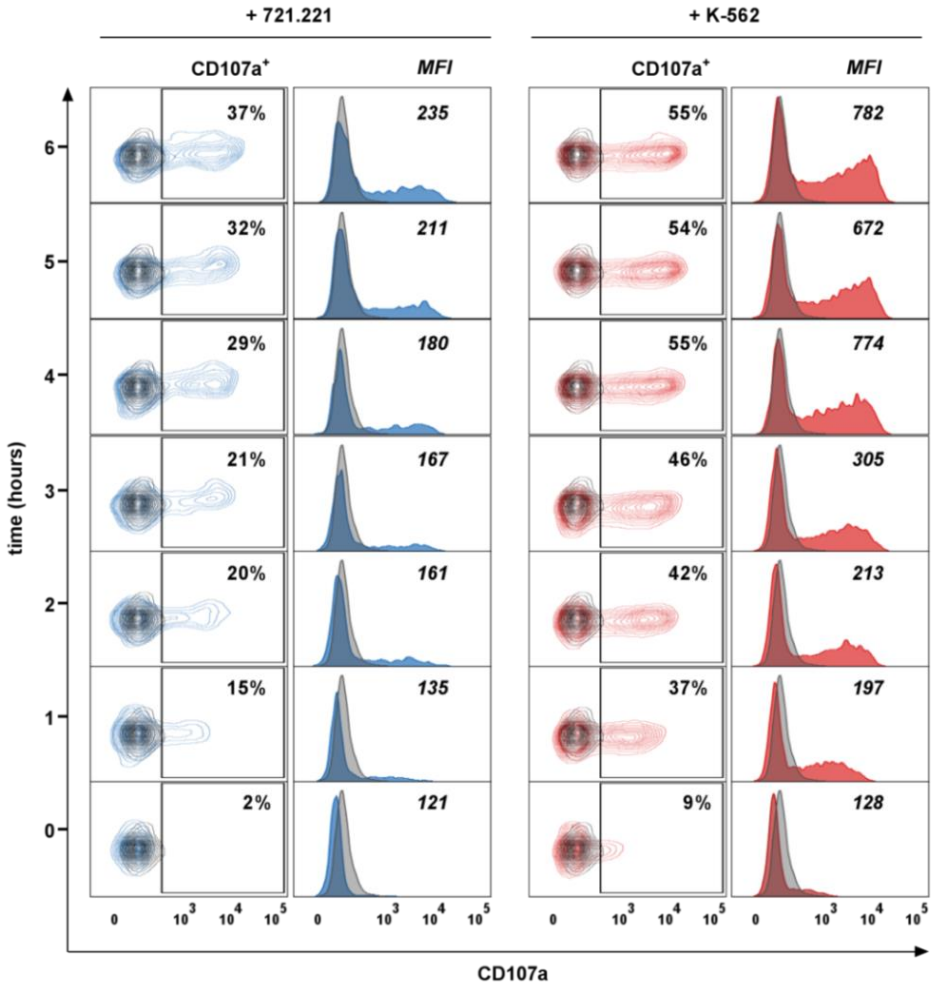

Figure 22: Measurement of CD107a as marker for NK-cell degranulation over time

Flow cytometric assessment of CD107a expression on bulk NK cells over time. Enriched primary human NK cells were co-cultured over a time period from 1 to 6 h in the presence or absence (grey) of 721.221 (blue) or K-562 cells (red). All samples were stained for the degranulation marker CD107a. The figure shows data from one subject. Each panel is divided into a contour plot on the left side and a histogram on the right side. Numbers stated within the contour plot indicate the percentage of $CD107a^+$ NK cells, whereas numbers stated within the histogram indicate the median fluorescence intensity (MFI) of CD107a.

The progression of CD107a expression on NK cells upon stimulation with distinct target cells over time is shown in **Figure 23**. Noticeably, the exposure to K-562 cells led to a stronger NK-cell response rate compared to 721.221 cells. The frequency of $CD107a^+$ NK cells increased rapidly in the first 4 h of co-incubation with both tested target cell lines and climaxed at 4 h incubation with K-562 cells, whereas the incubation with 721.221 cells reached its maximum frequency of $CD107a^+$ NK cells after 6 h. However, the 4 h time point allowed for the discrimination of degranulating and non-degranulating NK cells upon incubation with both tested target cell lines. Therefore, all functional data shown hereafter was obtained by degranulation experiments with an incubation time of 4 h.

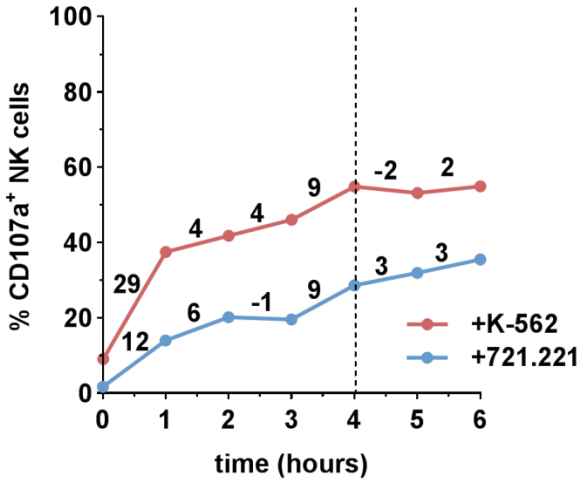

Figure 23: CD107a expression on bulk NK cells over time

Percentage of $CD107^+$ NK cells measured over time. The figure shows data from one subject. Enriched primary human NK cells were co-cultured over a time period from 1 to 6 h in the presence of 721.221 (blue) or K-562 cells (red). All samples were stained for the degranulation marker CD107a. The numbers above the graph indicate the delta between two measurement points.

In the following, the degranulation assay was performed with NK cells from 45 individual subjects to allow for subsequent determination of the educational profile and the measurement of the associated glycolytic function within educated and uneducated NK cells. **Figure 24** shows the percentage of $CD107a^+$ cells that was measured in unstimulated and stimulated bulk NK cells. In general, NK cells exhibited an increased frequency of $CD107a^+$ cells in the presence of 721.221 cells ($p<0.0001$) or K-562 cells ($p<0.0001$) compared to unstimulated NK cells. Noteworthy, the co-incubation with K-562 cells induced an overall significantly stronger NK-cell response compared to 721.221 cells ($p=0.0001$).

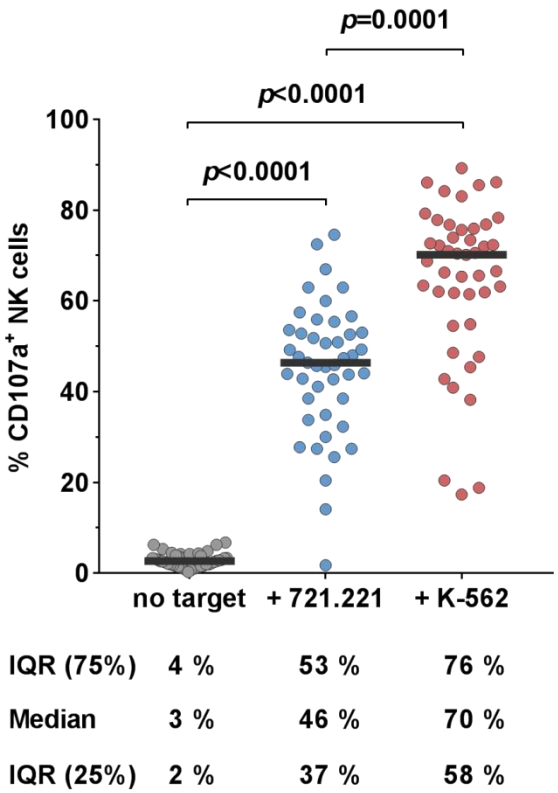

Figure 24: Frequency of CD107a$^+$ bulk NK cells after stimulation with target cell lines

Flow cytometric assessment of NK-cell function on bulk NK cells after exposure to various target cell lines. Enriched primary human NK cells from 45 study subjects were co-cultured for 4 h either in the absence (grey) or in the presence of 721.221 cells (blue) or K-562 cells (red). All samples were stained for the degranulation marker CD107a. The figure shows the proportion of CD107a+ bulk NK cells in each condition. All values have been normalized to unstimulated NK cells. Statistical analysis: Friedmann test, Dunn's multiple comparisons test. Black bars represent the median. The interquartile range (IQR) 75%= 75% Percentile, IQR 25% = 25 % Percentile and Median for each subset are stated below.

3.3 NK-cell function in educated and uneducated NK-cell subsets

Subsequently, target cell-stimulated bulk NK cells were stratified into educated and uneducated NK-cell subsets and analyzed for CD107a expression. Through the use of a boolean gating strategy, which is a gating method in FlowJo, bulk NK cells were separated into NK-cell subsets that were either single positive for one or negative for all of the tested inhibitory killer cell immunoglobulin-like receptors (iKIRs) and NKG2A (see **Table 14** and **2.3.11**). The measured response rates of these NK-cell subsets in combination with the HLA expression profile of that particular individual allowed to determine, which of the iKIR contributed to mediate NK-cell education in that individual. Once the response rate in a single iKIR expressing NK-cell subset exceeded

the response rate of an NK-cell subset that lacked all of the tested iKIRs, this particular iKIR expressing NK-cell subset was defined as educated. In addition, HLA genotyping analysis showed if the cognate HLA class I molecule that serves as ligand for the specific iKIR was expressed by the individual and might therefore contribute to NK-cell education. All NK-cell subsets that showed higher response rates compared to iKIR negative NK cells were defined as educated, whereas all NK-cell subsets that showed lower or equal response rates than the iKIR negative subsets, plus the iKIR negative subset itself, were defined as uneducated NK cells. **Figure 25** illustrates the response rate as frequency of CD107a+ cells in educated and uneducated NK cells upon exposure to target cell lines. The data revealed that educated NK cells expressed a significantly higher percentage of $CD107a^+$ NK cells than uneducated NK cells upon stimulation with both tested target cell lines.

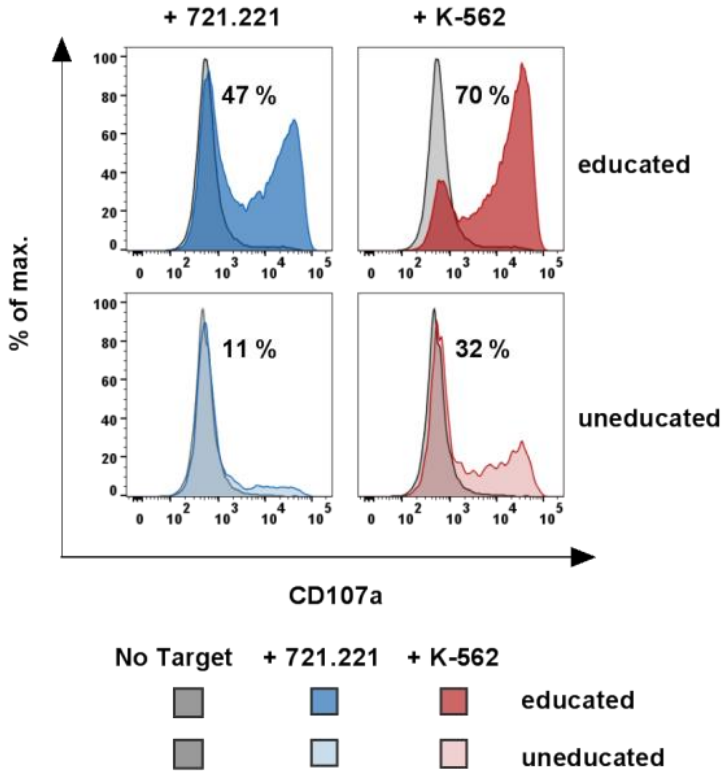

Figure 25: CD107a as distinguishing feature of educated and uneducated NK cells

Flow cytometric assessment of NK-cell function on educated and uneducated NK cells after exposure to various target cells. The figure shows data from one subject. Enriched primary human NK cells were co-cultured for 4 h either in the absence (grey, no target) or in the presence of 721.221 cells (blue) or K-562 cells (red). All samples were stained for the degranulation marker CD107a and and the obtained flow cytometric data was subsequently analyzed via FlowJo software. The numbers indicate the percentages of $CD107a^+$ NK cells after stimulation with target cells.

The data from all 45 study subjects are shown in **Figure 26**. Overall, educated NK cells exhibited an increased frequency of $CD107a^+$ cells in the presence of 721.221 cells ($p<0.00001$) or K-562 cells ($p<0.000001$) compared to uneducated NK cells.

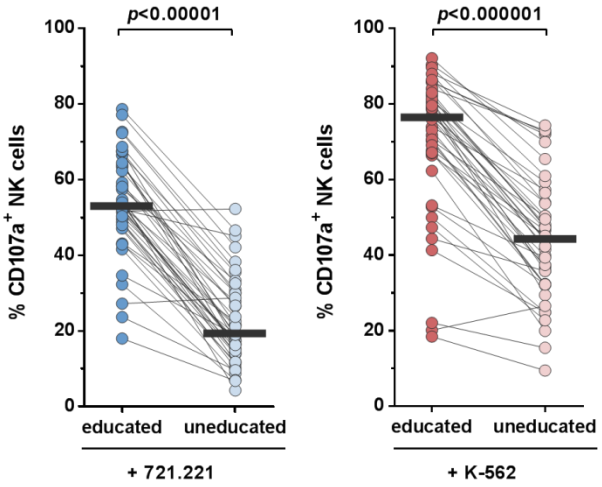

Figure 26: Frequency of $CD107a^+$ NK cells in educated and uneducated NK-cell subsets

Flow cytometric assessment of NK-cell function on educated and uneducated NK cells after exposure to various target cell lines. Enriched primary human NK cells from healthy individuals (n = 45) were co-cultured for 4 h in the presence of 721.221 cells (blue) or K-562 cells (red). All samples were stained for the degranulation marker CD107a and the obtained flow cytometric data was subsequently analyzed via FlowJo software. The education status was determined based on the expression of self-iKIRs. The figure shows the proportion of $CD107a^+$ NK cells on educated and uneducated NK cells. All values have been normalized to unstimulated NK cells. Statistical analysis: Wilcoxon matched-pairs signed-rank test with subsequent Bonferroni correction. Black bars represent the median.

These data demonstrate that CD107a is significantly upregulated on the surface of NK cells following activation within both tested target cell lines 721.221 and K-562. Moreover the results demonstrate, that the expression of self-iKIRs was associated with an increased functional competence in educated NK cells. The distinct surface expression of CD107a allowed for the discrimination of educated and uneducated NK-cell populations in the same individual for subsequent metabolic assessments.

3.4 Interplay of inhibitory NK-cell receptors with distinct HLA alles

Inhibitory KIRs (iKIRs) are major receptors that shape the functional responses of human NK cells by the interaction with their cognate HLA class I ligands, whereas each KIR exhibits a different specificity for different HLA-molecules. Due to polymorphisms within the α1-helix of HLA class I molecules, distinct epitopes can be defined that are recognized by specific KIRs (108) (see **Table 13**). The HLA-*Bw4* epitope is bound by KIR3DL1, while HLA-*C1* serves as a ligand for KIR2DL2/L3 and HLA-*C2* is recognized by KIR2DL1. Whereas a minority of HLA-B molecules encode for the *Bw4* epitope, all HLA-C molecules express either the *C1* or *C2* epitope (109).

Table 13: The specific recognition of HLA class I molecules by KIRs

KIR	Ligand
KIR3DL1	HLA-*Bw4*
KIR2DL2/L3	HLA-*C1*
KIR2DL1	HLA-*C2*

The following investigations in this section were sub-analyses from the flow cytometric data obtained in functional experiments from chapter 3.2. Boolean gating allowed for sub-division of the samples beyond bulk NK cells into subsets that were either single positive for each investigated iKIR or negative for all investigated iKIR and NKG2A (see **Table 14** and **2.3.11**). In addition, HLA genotyping allowed for determination of the expression of HLA epitopes in each individual (see **2.2.6**). According to the HLA-expression profile of each individual, the data was sorted by the different HLA allele variants that were expressed in each indiviual. Hereafter, the investigated receptors KIR2DL1, KIR3DL1 and KIR2DL2/L3 are referred to as 2DL1, 3DL1 and 2DL2/L3 respectively.

Table 14: NK-cell subsets

Inhibitory receptor	NK-cell subset				
	2DL1 single positive	2DL2/L3 single positive	3DL1 single positive	NKG2A single positive	Receptor negative
2DL1	+	-	-	-	-
2DL2/L3	-	+	-	-	-
3DL1	-	-	+	-	-
NKG2A	-	-	-	+	-

3.4.1 2DL1 mediates increased NK-cell response rates in HLA-*C2*$^+$ individuals

Expression frequency of CD107a in individuals with different HLA-C group haplotypes (*C1/1*, *C1/2* and *C2/2*) was analyzed in 2DL1$^+$ and 2DL1$^-$ NK-cell subsets after stimulation with target cell lines. 2DL1$^+$ NK cells were tested negative for 2DL2/L3, 3DL1 and NKG2A, whereas 2DL1$^-$ NK-cells lacked all tested inhibitory receptors. **Figure 27** shows the frequency of CD107a$^+$ NK cells after stimulation with 721.221 or K-562 cells.

Significant differences in the response rates of NK cells were observed intra-individually between 2DL1$^+$ and 2DL1$^-$ NK cell subsets as well as among individuals expressing different HLA-C group alleles (*C1* and/or *C2*). First, receptor bearing (2DL1$^+$) NK-cell subsets were compared to receptor lacking (2DL1$^-$) NK-cell subsets. Data revealed that stimulation with target cell lines led to significant stronger response rates within 2DL1$^+$ NK-cell subsets compared to 2DL1$^-$ NK-cell subsets in individuals that expressed *C2* group alleles serving as ligand for 2DL1. On the other hand, *C1/1* individuals that lacked *C2* group alleles, exhibited differences in the frequency of CD107a between 2DL1$^+$ and 2DL1$^-$ NK-cell subsets also upon exposure to 721.221 cells (p=0.005). The observed differences, however, were very small compared to individuals expressing *C2* group alleles. An exposure to K-562 cells however, showed no difference in *C1/1* individuals between 2DL1$^+$ and 2DL1$^-$ NK-cell subsets (p=0.6). Next, the subsets of 2DL1$^+$ NK cells were compared between individuals expressing different HLA-C group alleles. Individuals which expressed *C2* group alleles exhibited significantly increased response rates in 2DL1$^+$ NK-cell subsets after target cell stimulation compared to individuals that lacked the *C2* group allele (+721.221 p<0.0001 and +K-562 p=0.0009). Conversely, the response rates among *C2* positive individuals showed no difference between 2DL1$^+$ NK-cell subsets upon stimulation with both tested target cell lines (+721.221 p=0.6 and +K-562 p>0.9).

Overall, this data shows that the presence of HLA-*C2* group alleles lead to increased NK-cell function on NK cells expressing the iKIR 2DL1, compared to NK cells that lacked the receptor. Furthermore, the response rates between *C2/2* homozygous and *C1/2* heterozygous individuals did not differ from each other, implicating that the expression of one single *C2* group allele in *C1/2* heterozygous individuals is sufficient to induce education in 2DL1$^+$ NK-cell subsets.

+721.221

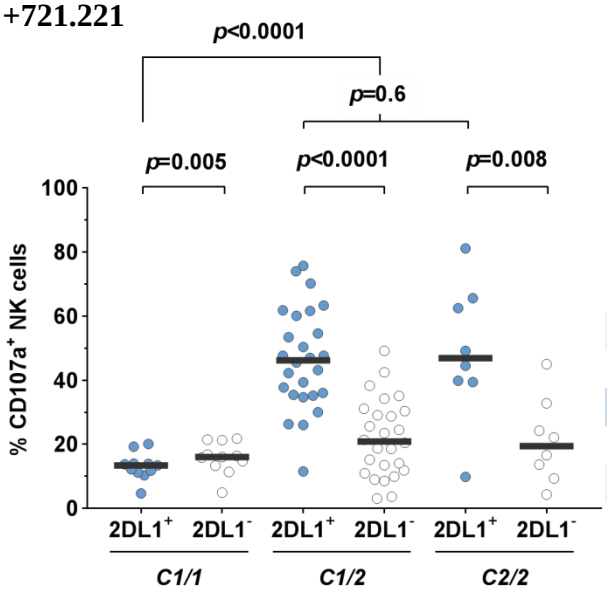

+721.221	C1/1		C1/2		C2/2	
	2DL1+	2DL1-	2DL1+	2DL1-	2DL1+	2DL1-
Max.	20	22	76	49	81	45
Perc. (75%)	14	21	61	31	65	31
Median	**13**	**16**	**46**	**21**	**47**	**19**
Perc. (25%)	11	13	35	12	40	10
Min.	5	5	12	3	10	4

+K-562

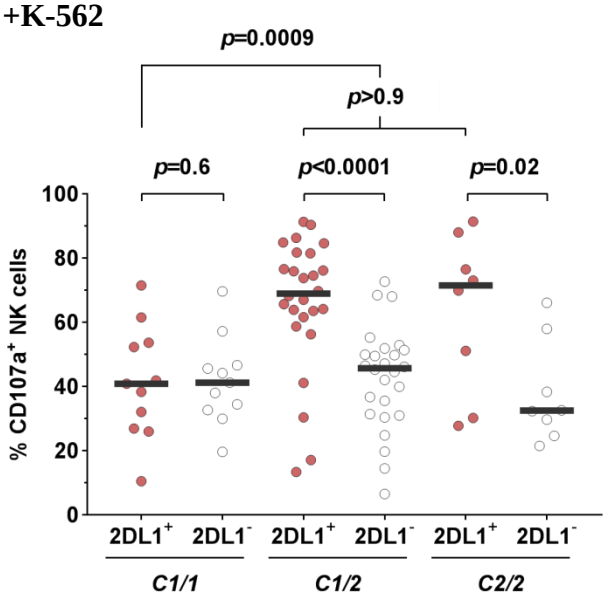

+K-562	C1/1		C1/2		C2/2	
	2DL1+	2DL1-	2DL1+	2DL1-	2DL1+	2DL1-
Max.	72	70	91	73	91	66
Perc. (75%)	54	47	82	52	85	53
Median	**41**	**41**	**69**	**46**	**72**	**32**
Perc. (25%)	27	33	61	31	35	26
Min.	11	20	13	7	28	22

Figure 27: Frequency of CD107a$^+$ NK cells in 2DL1$^+$ and 2DL1$^-$ NK-cell subsets among study subjects expressing various HLA-C group alleles

Flow cytometric assessment of NK-cell function on 2DL1 single positive (**2DL1$^+$**2DL2/L2$^-$3DL1$^-$NKG2A$^-$) (colored) and 2DL1 negative (**2DL1$^-$**2DL2/L2$^-$3DL1$^-$NKG2A$^-$) (white) NK cells in HLA-*C1/1* homozygous individuals (n = 11), HLA-*C1/C2* heterozygous individuals (n =26) and HLA-*C2/2* homozygous individuals (n = 8) after exposure to various target cell lines. Enriched primary human NK cells from 45 study subjects were co-cultured for 4 h either in the presence of 721.221 cells (upper panel) or K-562 cells (lower panel). All samples were stained for the degranulation marker CD107a. The figure shows the proportion of CD107a$^+$ NK cells. All values have been normalized to unstimulated NK cells. Statistical analysis: For paired samples Wilcoxon matched-pairs signed-rank test was used, for idependent samples the Mann-Whitney Test was performed. Black bars represent the median. Min. = minimal frequency of CD107a$^+$ NK cells; Max. = maximal frequency of CD107a$^+$ NK cells, interquartile range (IQR) 75%= 75% Percentile, IQR 25% = 25 % Percentile and Median are stated in a table on the right side of each condition.

3.4.2 2DL2/L3 mediates increased NK-cell response rates in HLA-C1$^+$ individuals

The impact of 2DL2/L3 expression on NK-cell function was investigated next. Conversely to 2DL1, which specifically binds to HLA-C group 2 alleles, 2DL2/L3 recognizes HLA-C group 1 alleles. **Figure 28** shows the frequency of CD107a$^+$ NK cells after stimulation with 721.221 or K-562 cells in individuals with different HLA-C group haplotypes (*C1/1*, *C1/2* and *C2/2*). 2DL2/L3$^+$ NK cells were tested negative for 2DL1, 3DL1 and NKG2A, whereas 2DL2/L3$^-$ NK-cells lacked all tested inhibitory receptors.

Receptor bearing (2DL2/L3$^+$) NK cells that were exposed to both tested target cell lines displayed significantly higher frequencies of CD107a$^+$ NK cells than receptor negative (2DL2/L3$^-$) NK cells in *C1* positive study subjects. Conversely, *C2/2* homozygous individuals missing the *C1* group allele displayed no difference in the response rate of 2DL1$^+$ and 2DL1$^-$ NK-cell subsets after target cell stimulation with 721.221 cells (p=0.5) or K-562 cells (p=0.6). Furthermore, the frequency of CD107a$^+$ NK cells in 2DL2/L3$^+$ NK cell subsets was compared among individuals expressing different HLA-C group alleles. The response rates of 2DL2/L3$^+$ NK-cell subsets were similar compared among individuals that are either heterozygous (*C1/2*) or homozygous (*C1/1*) for the *C1* group allele (+721.221 p=0.7 and +K-562 p=0.9), but differed when compared to individuals that lacked the *C1* group allele (+721.221 p=0.008 and +K-562 p=0.009).

Taken together, NK cells expressing the iKIRs 2DL2/L3 exhibit an increased NK-cell function in individuals that express the HLA-*C1* group allele compared to individuals that lack the stated allele. Additionally, the expression of one single *C1* group allele in *C1/2* heterozygous individuals is sufficient to induce education in 2DL2/L3$^+$ NK-cell subsets.

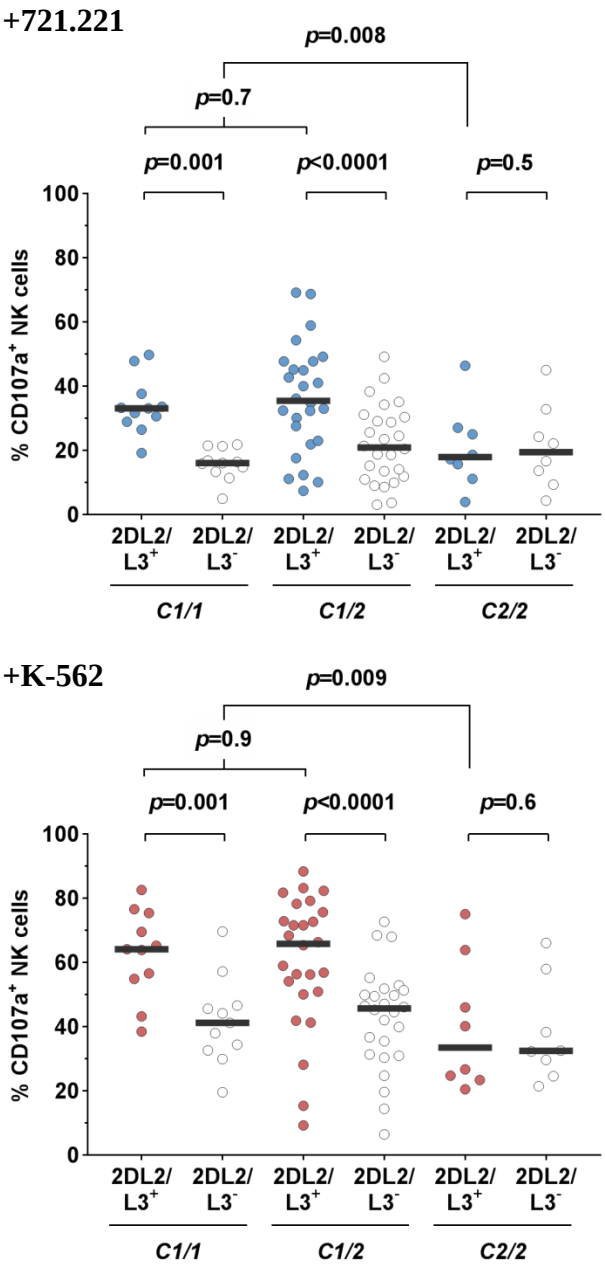

+721.221	C1/1		C1/2		C2/2	
	2DL2/ L3+	2DL2/ L3-	2DL2/ L3+	2DL2/ L3-	2DL2/ L3+	2DL2/ L3-
Max.	50	22	69	49	46	45
Perc. (75%)	38	21	48	31	27	31
Median	**33**	**16**	**36**	**21**	**18**	**19**
Perc. (25%)	29	13	23	12	12	10
Min.	19	5	7	3	4	4

+K-562	C1/1		C1/2		C2/2	
	2DL2/ L3+	2DL2/ L3-	2DL2/ L3+	2DL2/ L3-	2DL2/ L3+	2DL2/ L3-
Max.	83	70	88	73	75	66
Perc. (75%)	75	47	76	52	59	53
Median	**64**	**41**	**66**	**46**	**34**	**32**
Perc. (25%)	55	33	51	31	24	26
Min.	39	20	9	7	21	22

Figure 28: Frequency of CD107a$^+$ NK cells in 2DL2/L3$^+$ and 2DL2/L3$^-$ NK-cell subsets among study subjects with various HLA-C allele expression

Flow cytometric assessment of NK-cell function on 2DL2/L3 single positive (2DL1$^-$**2DL2/L2**$^+$3DL1$^-$NKG2A$^-$) (colored) and 2DL2/L3 negative (2DL1$^-$**2DL2/L2**$^-$3DL1$^-$NKG2A$^-$) (white) NK cells in HLA-C1/1 homozygous individuals (n = 11), HLA-C1/2 heterozygous individuals (n =26) and HLA-C2/2 homozygous individuals (n = 8) after exposure to various target cell lines. Enriched primary human NK cells from 45 study subjects were co-cultured for 4 h either in the presence of 721.221 cells (upper panel) or K-562 cells (lower panel). All samples were stained for the degranulation marker CD107a and the obtained flow cytometric data was subsequently analyzed via FlowJo software. The figure shows the proportion of CD107a$^+$ NK cells. All values have been normalized to unstimulated NK cells. Statistical analysis: paired analysis: Wilcoxon matched-pairs signed-rank test, unpaired analysis: Mann-Whitney Test. Black bars represent the median. Min. = minimal frequency of CD107a$^+$ NK cells; Max. = maximal frequency of CD107a$^+$ NK cells, interquartile range (IQR) 75%= 75% Percentile, IQR 25% = 25 % Percentile and Median are stated in a table on the right side of each condition.

3.4.3 3DL1$^+$ and 3DL1$^-$ NK cells exhibit different response rates in Bw4+ and Bw6+ individuals

HLA-B alleles can be divided by the expression of the serological epitopes *Bw4* and *Bw6*, whereas only the *Bw4* epitope is recognized by the iKIR 3DL1 (60,61). Of note, the study subjects that were classified positive for *Bw4* were either homozygous (*Bw4/Bw4*) or heterozygous for *Bw4 (Bw4/Bw6)*, whereas the study subjects that were classified negative for *Bw4* lacked the stated allele *(Bw6/Bw6)*. 3DL1$^+$ NK cells were tested negative for 2DL1, 2DL2/L3 and NKG2A, whereas 3DL1$^-$ NK-cells lacked all tested inhibitory receptors.

Figure 29 shows the expression of CD107a upon target cell stimulation in *Bw4*$^+$ and *Bw4*$^-$ individuals in 3DL1 receptor-bearing and 3DL1 receptor-lacking NK cell subsets. Upon exposure to both tested target cell lines, the 3DL1$^+$ NK cell subsets displayed significantly higher percentages of CD107a$^+$ NK cells in *Bw4*$^+$ and *Bw4*$^-$ individuals compared to NK-cell subsets that did not express 3DL1. The response rates of 3DL1$^+$ NK cell subsets did not differ between *Bw4*$^+$ and *Bw4*$^-$ individuals upon target cell stimulation (+721.221 p=0.07 and +K-562 p=0.2). Of note, when comparing the medians between 3DL1$^+$ and 3DL1$^-$ NK-cell subsets, there is a major difference among *Bw4*$^+$ and *Bw4*$^-$ individuals detectable. The delta median between 3DL1$^+$ and 3DL1$^-$ NK cells is significantly higher in *Bw4*$^+$ individuals compared to *Bw4*$^-$ individuals after stimulation with 721.221 cells (*Bw4*$^-$: 24; 21 and *Bw4*$^+$ 39; 18) and K-562 cells (*Bw4*$^-$: 54; 46 and *Bw4*$^+$ 66;38).

In summary, this data demonstrated that 3DL1$^+$ NK cells exhibited higher frequencies of CD107a$^+$ NK cells than 3DL1$^+$ NK cells upon stimulation with both tested target cell lines in individuals that expressed the *Bw4* epitope compared to individuals that lacked the *Bw4* epitope. These differences, however, were not significant.

+721.221

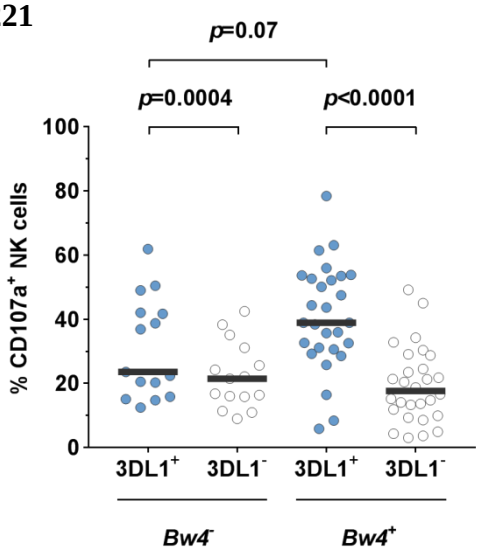

+721.221	Bw4⁻		Bw4⁺	
	3DL1⁺	3DL1⁻	3DL1⁺	3DL1⁻
Max.	62	43	78	49
Perc. (75%)	42	31	53	28
Median	24	21	39	18
Perc. (25%)	16	16	31	10
Min.	13	9	6	3

+K-562

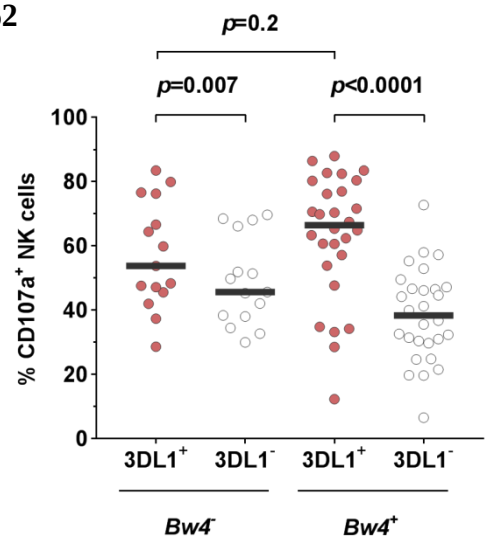

+K-562	Bw4⁻		Bw4⁺	
	3DL1⁺	3DL1⁻	3DL1⁺	3DL1⁻
Max.	84	70	88	73
Perc. (75%)	76	66	79	47
Median	54	46	66	38
Perc. (25%)	46	38	55	30
Min.	29	30	12	7

Figure 29: Frequency of CD107a$^+$ NK cells in 3DL1$^+$ and 3DL1$^-$ NK-cell subsets in Bw4$^+$ and Bw4$^-$ study subjects

Flow cytometric assessment of NK-cell function on 3DL1 single positive (2DL1$^-$2DL2/L2$^-$**3DL1**$^+$NKG2A$^-$) (colored) and 3DL1 negative (2DL1$^-$2DL2/L2$^-$**3DL1**$^-$NKG2A$^-$) (white) NK cells in HLA-Bw4$^-$ individuals (n = 15) and HLA-Bw4$^+$ individuals (n = 28) after exposure to various target cell lines. Enriched primary human NK cells from 43 study subjects were co-cultured for 4 h either in the presence of 721.221 cells (left panel) or K-562 cells (right panel). All samples were stained for the degranulation marker CD107a and the obtained flow cytometric data was subsequently analyzed via FlowJo software. The figure shows the proportion of CD107a$^+$ NK cells. All values have been normalized to unstimulated NK cells.Statistical analysis: paired analysis: Wilcoxon matched-pairs signed-rank test, unpaired analysis: Mann-Whitney Test. Black bars represent the median. Min. = minimal frequency of CD107a$^+$ NK cells; Max. = maximal frequency of CD107a$^+$ NK cells, interquartile range (IQR) 75%= 75% Percentile, IQR 25% = 25 % Percentile and Median are stated in a table on the right side of each condition.

3.4.4 NKG2A$^+$ NK cells exhibit increased response rates compared to NKGA2$^-$ NK cells

The non-classical HLA class I molecule HLA-E serves as a ligand for the iKIR NKG2A on human NK cells. As shown in **Figure 30**, NKG2A$^+$ NK cells exhibited significantly increased expression of CD107a after stimulation with both tested target cell lines compared to NKG2A$^-$ NK cells (p<0.0001). NKG2A$^+$ NK cells were tested negative for 2DL1, 2DL2/L3 and 3DL1, whereas NKG2A$^-$ NK-cells lacked all tested inhibitory receptors.

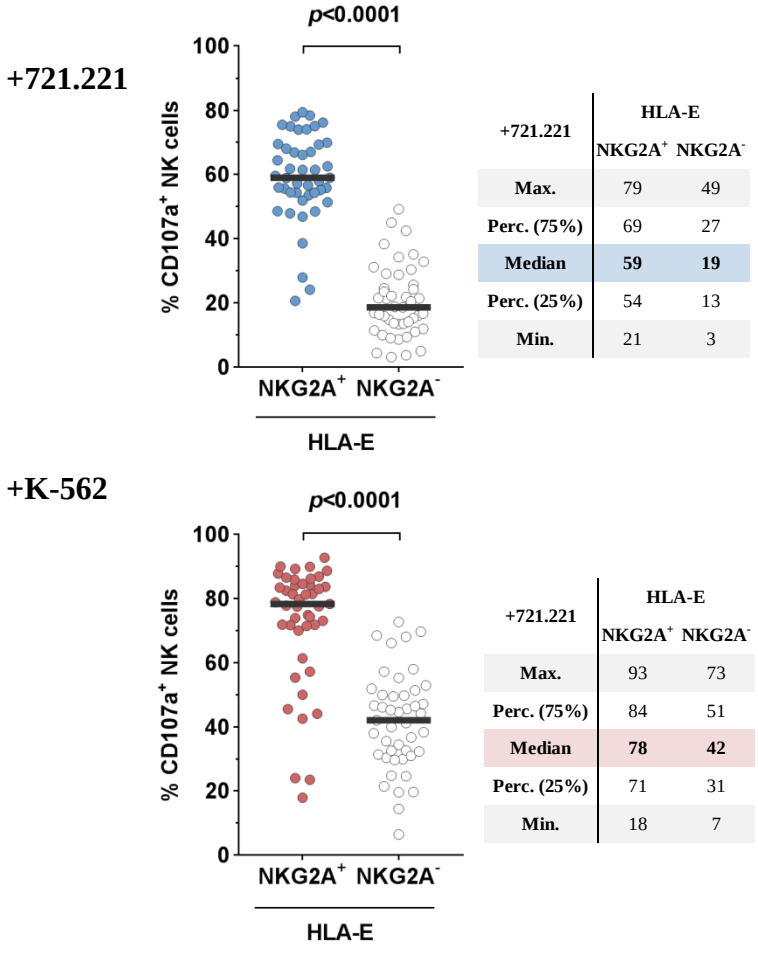

+721.221	HLA-E	
	NKG2A$^+$	NKG2A$^-$
Max.	79	49
Perc. (75%)	69	27
Median	**59**	**19**
Perc. (25%)	54	13
Min.	21	3

+721.221	HLA-E	
	NKG2A$^+$	NKG2A$^-$
Max.	93	73
Perc. (75%)	84	51
Median	**78**	**42**
Perc. (25%)	71	31
Min.	18	7

Figure 30: Frequency of CD107a$^+$ NK cells in NKG2A$^+$ and NKG2A$^-$ NK-cell subsets

Flow cytometric assessment of NK-cell function on NKG2A single positive (colored) and 2DL1-2DL2/L2-3DL1-NKG2A negative NK cells (white) after exposure to various target cell lines. Enriched primary human NK cells from 45 study subjects were co-cultured for 4 h either in the presence of 721.221 cells (left panel) or K-562 cells (right panel). All samples were stained for the degranulation marker CD107a and the obtained flow cytometric data was subsequently analyzed via FlowJo software. The figure shows the proportion of CD107a$^+$ NK cells. All values have been normalized to unstimulated NK cells. Statistical analysis: Wilcoxon matched-pairs signed-rank test. Black bars represent the median. Min. = minimal frequency of CD107a$^+$ NK cells; Max. = maximal frequency of CD107a$^+$ NK cells, interquartile range (IQR) 75%= 75% Percentile, IQR 25% = 25 % Percentile and Median are stated in a table on the right side of each condition.

3.5 Glut1 expression in educated and uneducated NK-cell subsets

Recent studies have provided evidence that the expression of the glucose transporter Glut1 can influence effector functions in lymphocytes (85,110). To date, there is not much knowledge about the role of Glut1 in NK-cell function. As demonstrated in this thesis, educated and uneducated NK cells display functional differences. To elucidate whether these subsets also differ in the expression levels of Glut1, flow cytometric analysis was performed with educated and uneducated NK cells in the presence or absence of HLA class I devoid target cell lines.

3.5.1 Target cell stimulated NK cells upregulate Glut1

The expression of the glucose transporter Glut1 was examined on bulk NK cells upon target cell stimulation, to elucidate whether NK-cell activation has an effect on Glut1 expression levels. **Figure 31** displays the expression levels of Glut1 on target cell stimulated and unstimulated NK cell subsets. Exposure to either tested target cell lines caused an increase in Glut1 surface expression compared to unstimulated NK cells.

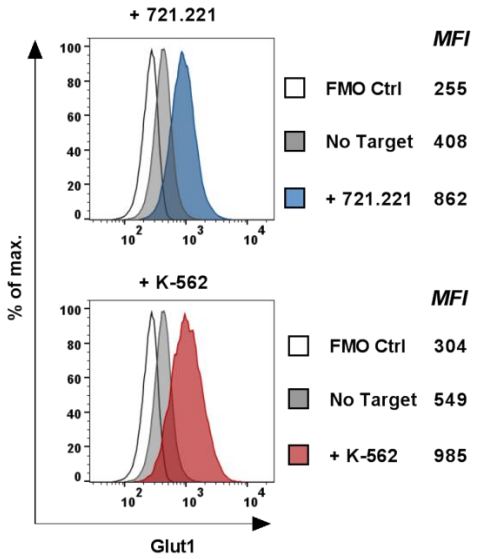

Figure 31: Flow cytometric assessment of Glut1 as metabolic marker for glucose transport on NK cells

Flow cytometric assessment of Glut1 expression on bulk NK cells after exposure to various target cells. The figure shows data from one subject. Enriched primary human NK cells were co-cultured for 4 h either in the absence (grey, no target) or in the presence of 721.221 cells (blue) or K-562 cells (red). All samples were stained for the degranulation marker Glut1 with exeption of the FMO control (black outline) and the obtained flow cytometric data was subsequently analyzed via FlowJo software.

Moreover, the Glut1 expression of bulk NK cels after exposure to target cells from 29 individual subjects is shown in **Figure 32**. Bulk NK cells significantly upregulated Glut1 in the presence of 721.221 cells (p=0.005) or K-562 cells (p<0.00001) compared to unstimulated NK cells (no target). The co-incubation with K-562 cells induced a significantly strong Glut1 expression compared to 721.221 cells (p=0.005).

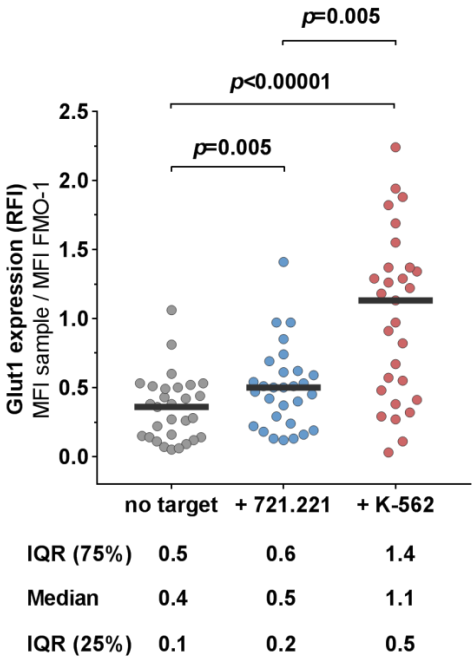

Figure 32: Assessment of Glut1 expression on bulk NK cells upon stimulation with target cells

Flow cytometric assessment of Glut1 expression on bulk NK cells after exposure to various target cell lines. Enriched primary human NK cells from 29 study subjects were co-cultured for 4 h either in the absence (grey, no target) or in the presence of 721.221 cells (blue) or K-562 cells (red). All samples were stained for Glut1 and the obtained flow cytometric data was subsequently analyzed via FlowJo software. The figure shows the Relative Fluorescence Intensity (RFI) of Glut1 on bulk NK cells in each subset. Statistical analysis: Friedmann test, Dunn's multiple comparisons test. Black bars represent the median.

To reassess if the pronounced Glut1 expression in response to K-562 cells was due to increased activation previously observed by higher CD107a expression upon the same stimulus, bulk NK cells were stratisfied into CD107a$^-$ and CD107a$^+$ NK cells and analyzed for the expression levels of Glut1 (**Figure 33**). The data revealed that CD107a$^+$ NK cells expressed higher levels of Glut1 than CD107a$^-$ NK cells (p<0.00001).

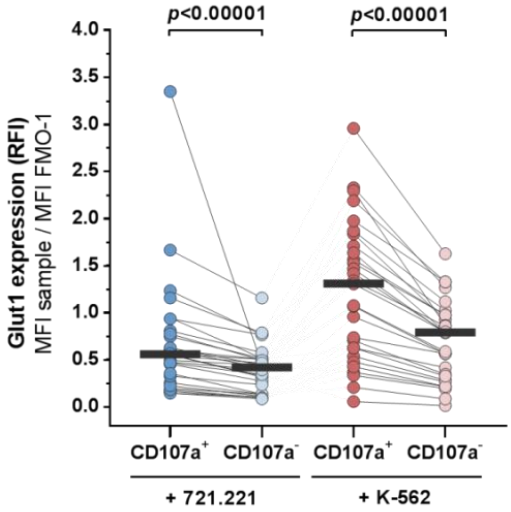

Figure 33: Glut1 expression levels on CD107a$^+$ and CD107a$^-$ NK-cell subsets

Flow cytometric assessment of Glut1 expression on a subset of CD107a$^-$ and CD107a$^+$ NK cells after exposure to various target cells. Enriched primary human NK cells from 45 study subjects were co-cultured for 4 h either in the absence (grey, no target) or in the presence of 721.221 cells (blue) or K-562 cells (red). All samples were stained for Glut1 and the obtained flow cytometric data was subsequently analyzed via FlowJo software. The figure shows the Relative Fluorescence Intensity (RFI) on CD107a$^-$ and CD107a$^+$ NK cells in each subset. Statistical analysis: Wilcoxon matched-pairs signed-rank test with subsequent Bonferroni correction. Black bars represent the median.

3.5.2 Educated NK cells show higer Glut1 levels compared to uneducated NK cells

Next, target cell stimulated bulk NK cells were stratified into educated and uneducated NK-cell subsets based on the expression of iKIR and cognate HLA class I molecules (see **3.4**) and analyzed for Glut1 expression. **Figure 34** demonstrates the Glut1 expression levels in educated and uneducated NK cells before and after target cell stimulation. Educated NK cells exhibited a significantly higher levels of Glut1 than uneducated NK cells upon stimulation with 721.221 cells (p=0.0001) or K-562 cells (p=0.00001). Of note, elevated surface expression levels of Glut1 were already detectable on educated NK cells prior to activation (no target, p<0.00001).

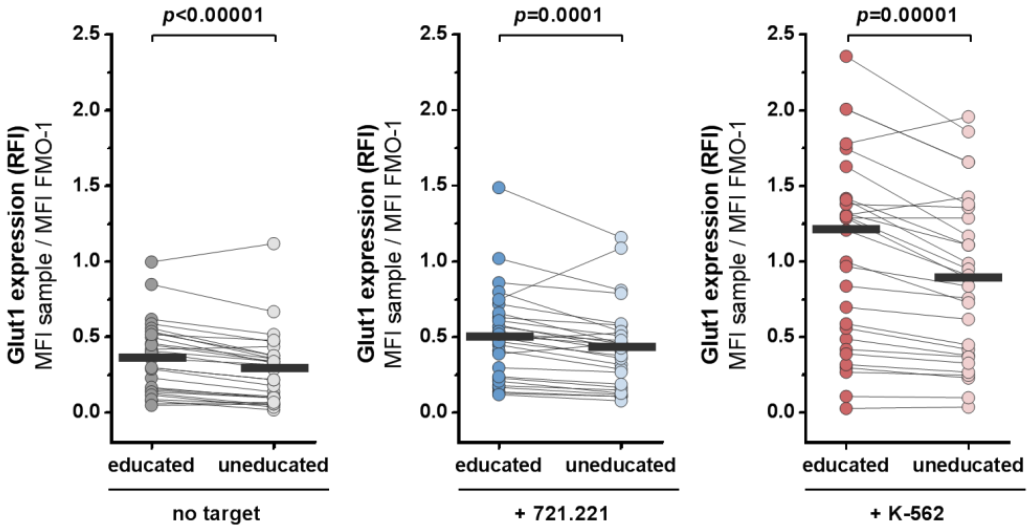

Figure 34: Glut1 expression profile of educated and uneducated NK cells upon stimulation with target cells

Flow cytometric assessment of Glut1 on educated and uneducated NK cells after exposure to various target cell lines. Enriched primary human NK cells from 29 study subjects were co-cultured for 4 h in the presence of 721.221 cells (blue) or K-562 cells (red). All samples were stained for Glut1 and the obtained flow cytometric data was subsequently analyzed via FlowJo software. The education status was determined based on the expression of self-iKIRs. The figure shows the Relative Fluorescence Intensity (RFI) of Glut1 NK cells on educated and uneducated NK cells. Statistical analysis: Wilcoxon matched-pairs signed-rank test with subsequent Bonferroni correction. Black bars represent the median.

Further analysis was performed to find out whether Glut1 expression in educated and uneducated NK-cell subsets differs between degranulating and non-degranulating NK cells. **Figure 35** displays the Glut1 expression levels of educated and uneducated NK-cell subsets stratified into $CD107a^+$ and $CD107^-$ NK cells. Aligned with the previously obtained data, levels of Glut1 were significantly increased in degranulating NK cells compared to non-degranulating NK cells in both educated and uneducated

NK cells (p<0.00001) upon stimulation with both tested target cell lines. Of note, when NK cells were exposed to K-562 cells, CD107a$^+$ NK cells upregulated Glut1 to a higher extent in educated NK cells compared to uneducated NK cells (**Figure 35**, p=0.02). Conversely, NK cells that were exposed to 721.221 cells did not differ in Glut1 expression between the subsets of CD107a$^+$ educated and uneducated NK cells (p=0.5).

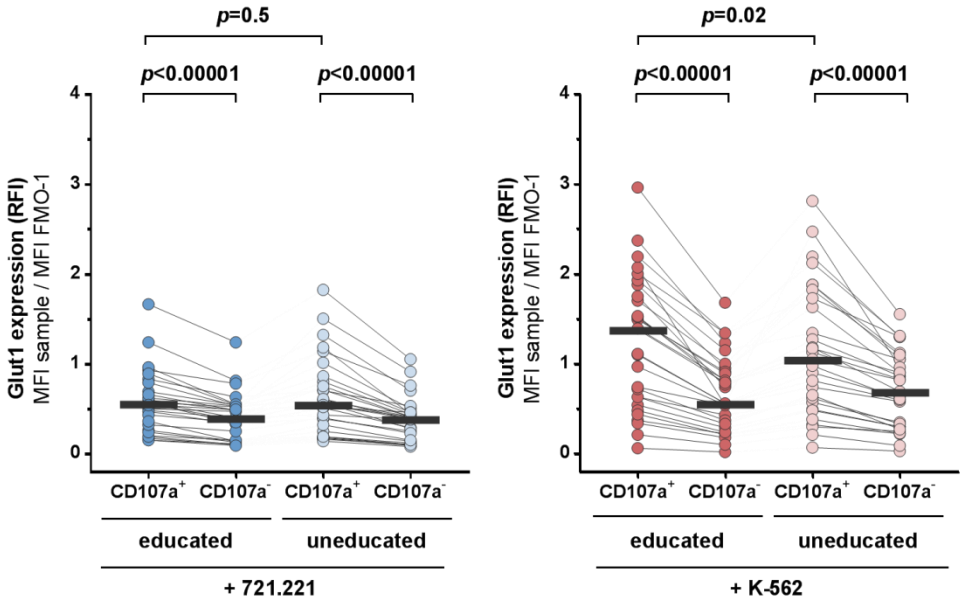

Figure 35: Glut1 expression levels of degranulating and non-degranulating educated and uneducated NK cells

Flow cytometric assessment of Glut1 on educated and uneducated NK cells after exposure to various target cell lines. Enriched primary human NK cells from 29 study subjects were co-cultured for 4 h in the presence of 721.221 cells (blue) or K-562 cells (red). All samples were stained for Glut1 and the obtained flow cytometric data was subsequently analyzed via FlowJo software.. The figure shows the Relative Fluorescence Intensity (RFI) of Glut1 on degranulating (CD107a$^+$) and non-degranulating (CD107a$^-$) NK cells in the subset of educated and uneducated NK cells. Statistical analysis: Wilcoxon matched-pairs signed-rank test with subsequent Bonferroni correction. Black bars represent the median.

Taken together, it was demonstrated that Glut1 expression levels increased on bulk NK cells upon target cell stimulation. Furthermore, educated NK cells showed elevated Glut1 expression levels compared to uneducated NK cells. This observation was made after stimulation with target cells lines and of particular note also in the absence of stimulation.

3.6 Glycolytic profile of educated and uneducated NK cells

Glycolytic metabolism is a key factor for lymphocyte function. The Seahorse XF analyzer determines the glycolytic function by measuring the extracellular acidification rate (ECAR) referring to proton production and glycolysis.

3.6.1 Educated NK cells exhibit increased ECAR rates

To elucidate potential differences in the metabolic profile of educated and uneducated NK cells, a Seahorse XF Glycolytic Stress Test was performed with FACS-sorted NK cell subsets. **Figure 36** shows the ECAR values measured for bulk, educated and uneducated NK cells. Educated NK cells exhibited overall higher ECAR values compared to uneducated NK cells. Bulk NK cells showed ECAR values that are situated between educated and uneducated NK cells. All subsets showed an increase in ECAR after the addition of glucose, indicating of an increased glucose turnover through the glycolysis pathway. The additon of oligomycin inhibits mitochondrial OXPHOS, allowing for measurement of the cells' maximum glycoclytic capacity. All subsets showed increased values of ECAR, showing that all subsets are capable of increasing the glycolytic activity beyond the basal glycolytic rate. Abrogation of glycolysis by adding 2-DG led to a rapid decrease within the measured ECAR rates. The decrease seen in ECAR indicates that the ECAR measured during the assay resulted from glycolytic activity.

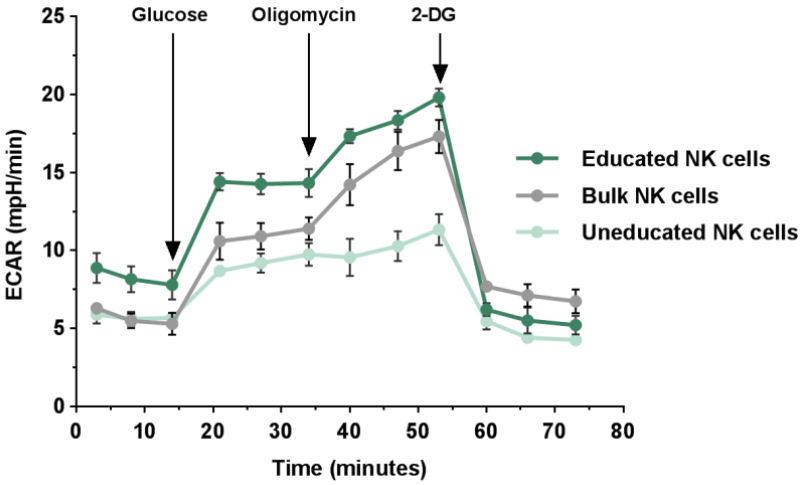

Figure 36: ECAR analysis of educated and uneducated NK cells in a Seahorse Glycolytic Stress Test

FACS-sorted educated (dark green) uneducated (light green) and bulk (grey) NK cells were analyzed in a Glycolytic Stress Test usting the Seahorse XF extracellular flux analyzer. The figure shows data from one subject. The data is shown as the mean of three replicates. Error bars indicate the standard deviation.

3.6.2 Educated NK cells show increased glycolytic rates

The measured ECAR values were further analyzed by calculating the parameters for glycolytic flux. The rates for glycolysis, glycolytic capacity and glycolytic reserve are depicted in **Figure 37**. The data showed that educated NK cells exhibited significantly higher ECAR values compared to uneducated NK cells (glycolysis p=0.002). When OXPHOS was interrupted, educated and uneducated NK cells showed no significant differences in glycolytic capacity (p=0.08). In addition, the glycolytic reserve did not differ between educated and uneducated NK cells (p=0.5). Taken together, the results show that when OXPHOS is interrupted, educated and uneducated NK-cell subsets exhibited similar glycolytic capacity and reserve, whereas educated NK cells were able to utilize glucose significantly better (increased glycolysis) than uneducated NK cells.

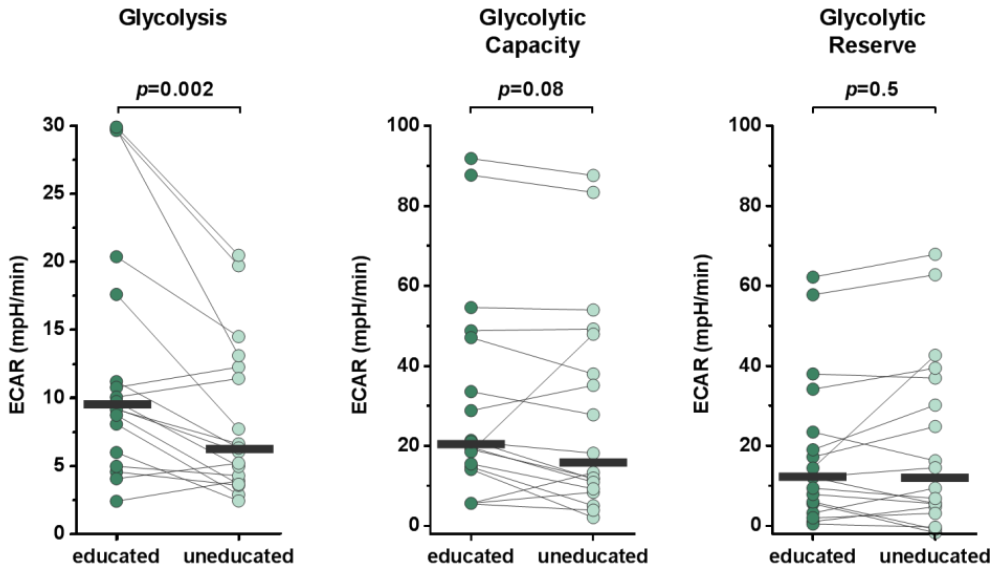

Figure 37: Glycolytic activity of educated and uneducated NK cells

FACS-sorted educated (dark green) and uneducated (light green) NK cells of were analyzed in a Glycolytic Stress Test usting the Seahorse XF extracellular flux analyzer. The figures shows the representative data from 18 subjects. Comparison of glycolysis (left panel), glycolytic capacity (middle panel) and glycolytic reserve (right panel) between educated and uneducated NK cells. Statistical analysis: Wilcoxon matched-pairs signed-rank test with subsequent Bonferroni corection. Black bars represent the median.

4 Discussion

NK cells must be tolerant towards healthy tissue and need to be able to recognize and attack infected or malignant cells at the same time. To avoid imbalance and malfunction, it is essential that the activity of NK cells is tightly regulated. NK-cell function is regulated by signals derived from surface receptors. Upon engagement with their cognate ligand, these receptors transfer either inhibitory or activating signals into the cell. Inhibitory receptors bind to HLA class I molecules that are expressed by all nucleated cells of the host. The engagement of these receptors with self-HLA class I molecules mediates tolerance and tunes the reactivity of an individual NK cell in a process called education. Educated NK cells display an increased reactivity towards target cells compared to uneducated NK cells. Several models of NK-cell education describe how NK-cells achieve functional competence, but the molecular mechanisms underlying NK-cell education are not well understood to date. Recent studies in the field of immunometabolism have revealed that the cellular metabolism is able to shape immune cell effector functions (77). These observations led to the hypothesis that NK-cell metabolism might play a role in NK-cell education as well. Hence, this study aimed to investigate the metabolism of primary human NK cells in the setting of NK-cell education.

NK cells play an important role in innate immunity against tumors and viral infections. Upon activation, NK cells exert effector functions that can lead to the death of the target cell. CD107a is a marker for degranulation in NK cells and cytotoxic T cells and its expression can give information about the cytotoxic activity of a cell (97). This study showed that enriched primary human NK cells which were co-cultured with the HLA class I deficient target cell lines 721.221 and K-562, exhibited increased levels of CD107a compared to unstimulated NK cells. Interestingly, the frequency of $CD107a^{+}$ NK cells was significantly higher in K-562 stimulated compared to 721.221 stimulated NK cells. In contrast, a study by Lisovsky *et al.* described that 721.221 cells induced a higher activation and responsiveness of bulk and specific NK-cell subsets than K-562 cells (111). The lack of cell surface HLA class I molecules on target cells, abrogates negative signaling through inhibitory NK-cell receptors, whereas subsequent engagement of activating NK-cell receptors by stimulating ligands on the surface of the target cells leads to NK-cell activation and the implementation of effector functions. It has been described that the activating NK-cell receptor NKG2D initiates a signaling

cascade triggering cytotoxicity upon ligand binding (112,113). The ligands for this activating receptor, however, are found to a higher extent on K-562 cells, whereas some are completely absent on 721.221 cells (112). Differences in the ligand repertoire expressed by the tested target cell lines might explain variations within the NK-cell response after stimulation with distinct cell lines.

Despite the differences in the intensity of the response rates that have been detected in-between the tested target cell lines, both cell lines induced an increase of $CD107a^+$ NK cells in educated and uneducated NK–cell subsets. These results show that the stimulation with the tested target cell lines was irrespective of the education status of the cell. Nevertheless, educated NK cells significantly exceeded the response rates of uneducated NK cells after target cell stimulation. Of note, a subset of NK cells was identified in this study that lacked the expression of all inhibitory receptors that were investigated in this work. In contrary to the assumption that these cells are hyperfunctioning, uneducated NK cells are hyporesponsive towards HLA class I-deficient target cells (65,114). NK cells from either MHC[3] class I-deficient mice or Ly49[4] receptor-deficient mice failed to reject targets that lacked the expression of MHC class I and responded poorly to many other stimuli (114,115). Even though uneducated NK cells underperform in cytotoxicity and pro-inflammatory cytokine secretion compared to educated NK cells, they are still capable of becoming activated (116). While educated NK cells play a major role in the control of HLA class I-deficient tumors (117), uneducated NK cells have been shown to benefit from the lack of self-specific inhibitory receptors in the control of tumors that still express HLA class I (118). Under the circumstances, that uneducated NK cells encounter robust activating signals through Fc receptors, they eliminated HLA class I-expressing tumor cells, whereas educated NK cells did not (118). These results indicate that uneducated NK cells play a role in tumor eradication but outweigh the functions of educated NK cells only in a certain context.

[3] HLA class I molecules are the human pendant to *major histocompatibility complex (MHC)* class I molecules, that are found in all modern species of jawed vertebrates (1).

[4] *Ly49* are MHC class I–specific receptors on mouse NK cells and represent the mouse functional equivalents of the human killer-cell Ig-like receptor family (115).

NK-cells that express inhibitory receptors, however, can get educated upon receptor engagement of their inhibitory receptors with polymorphic HLA-A,-B and –C molecules on the surface of host cells (65). Each iKIR exhibits specificity for distinct HLA molecules (see **1.4.2**) (54). Provided that an NK cell has been educated, it will exert an increased cytotoxic response upon target cell stimulation compared to an uneducated NK cell (42). The experimental data obtained in this study validated this phenomenon: NK cells that expressed self-HLA class I-specific iKIRs were responsive to activating stimuli while those lacking such receptors were hyporesponsive. Noteworthy, the response rates of educated NK cells were similar in individuals that were either homozygous or heterozygous for the allele that encoded the cognate HLA class I ligand. This implicates that the possession of one single allele, which encodes for a specific HLA class I molecule, was sufficient to mediate education in NK cells that expressed the matching iKIR in this setting (119). In this study, individuals, which possessed the HLA-*C2* group alleles developed educated $2DL1^+$ NK cells, HLA-*C1* positive individuals displayed educated $2DL2/L3^+$ NK cells and the possession of an HLA-*Bw4* epitope resulted in educated $3DL1^+$ NK cells.

Surprisingly, data indicated that *Bw6/6* homozygous individuals that lacked the *Bw4* epitope on *HLA-B* alleles exhibited significantly increased response rates after stimulation in $3DL1^+$ NK cells compared to $3DL1^-$ NK cells. In addition, the response rates of $3DL1^+$ NK cells between $Bw4^+$ *and Bw6/6* homozygous individuals did not show significant differences, although it has been described that the *Bw6* epitope does not serve as a ligand for $3DL1^+$ (94). The *Bw4* and *Bw6* epitopes can be distinguished as they display an amino acid substitution at residue 83, which has been described to influence the molecular microarchitecture of the epitope and thus leads to functional differences regarding 3DL1 engagement (120). Importantly, *Bw4* epitopes that can bind to 3DL1 are also found in a subset of *HLA-A* alleles (92,93). The study by Stern *et al.* identified three *HLA-A* alleles (*HLA-A*2301, A*2402 or A*3201*) which carry the *Bw4* epitope (93). Target cells which expressed these HLA class I molecules were protected from lysis by $KIR3DL1^+$ NK cells. All individuals that were investigated in this study were genotyped for *HLA-A, -B, -C* alleles. The genotyping analysis revealed that among individuals which lacked the *Bw4* epitope within the *HLA-B* gene, two were tested positive for *HLA-A*2402* and one individual was found to be positive for the *HLA-A*3201* allele (see **2.2.6**). Functional data revealed that $3DL1^+$ NK cells in these

individuals indeed exhibited a functional superiority compared to 3DL1$^-$ NK cells. For that reason, these individuals were numbered among *Bw4*$^+$ NK-cell subsets. These examples demonstrate the possibility of the existence of other *Bw4*-containing *HLA-A* alleles that have not been characterized yet, which can also mediate NK-cell education upon binding to iKIRs on NK cells. Nonetheless, the education of NK cells is neither static nor binary. The reactivity of an educated NK cell is determined by the number of self-HLA class I inhibitory receptors expressed by an NK cell and the affinity towards their ligand (69,119). Furthermore, studies have shown that NK-cell reactivity can increase in the presence of a novel cognate ligand (99-101) and also decrease upon loss of the cognate ligand (122,124). In summary, recent data support the concept that NK cells are highly susceptible to the environmental HLA, which is manifested by an ongoing tuning process in an individual NK cell ensuring tolerance of that particular cell towards healthy "self" cells.

NK cell education, however, is not exclusively realized by the expression of one or various iKIR that can recognize self-HLA class I molecules. Because NK cells express a wide range of inhibitory receptors in addition to KIRs it is critical to determine whether other inhibitory receptors such as CD94/NKG2A (hereafter referred to as NKG2A) also contribute to the education of NK cells. The data of this study demonstrated that NK cells which lacked the investigated KIRs but expressed NKG2A exhibited significantly increased levels of CD107a$^+$ NK cells after stimulation with both tested target cell lines compared to iKIR$^-$NKG2A$^-$ NK cells. NKG2A is especially important because its ligand HLA-E is ubiquitously expressed among different cell types (125,126). On the other hand, NKG2A is differentially expressed in the course of NK-cell development. At an early stage in NK-cell maturation, a subset of NK cells that are CD56^{bright}, express high levels of NKG2A but lack KIRs. During NK-cell development, CD56^{bright} NK cells differentiate into CD56^{dim} NK cells accompanied by a progressive loss of NKG2A and a gain in KIR (127–129). The role of NKG2A as a mediator for functional capacity has been studied in functional assays with NK-cell subsets that varied in NKG2A and KIR expression. It has been shown that the less mature NKG2A$^+$/3DL1$^-$ NK cells exhibited stronger functional responses over the more mature NKG2A$^-$/3DL1$^+$ NK cells after stimulation with target cell lines in individuals expressing a ligand for 3DL1 (128). Nevertheless, NK cells which co-expressed NKG2A and 3DL1 displayed the highest response rate after stimulation in this setting.

Furthermore, a study by Ivarsson *et al.* demonstrated that HLA class I-specific KIRs on fetal human NK cells are not able to mediate NK-cell education, showing that fetal NK cells which expressed KIRs responded poorly to HLA class I–negative target cells (130). In contrast, NKG2A was able to educate fetal NK cells in the same way as adult peripheral blood NK cells. As the ligand for NKG2A, *HLA-E*, is shared between the mother and the fetus, *HLA-A, -B* and *–C* are semiallogeneic[5], meaning that they partially differ between the mother and the fetus. Therefore, the KIR-induced hyporesponsiveness in fetal NK cells potentially prevents the recognition of maternal allogeneic cells. Despite the fact that fetal NK cells are hyporesponsive towards HLA class I-deficient target cells, it has been reported that these cells are able to kill target cells via ADCC (131). The differential education via NKG2A and KIRs in fetal NK cells might therefore provide a mechanism that sustains fetal-maternal tolerance while preserving protection against pathogens. These observations highlight the important role of NKG2A in the context of NK-cell education.

As part of the innate immune response, NK cells necessitate to react quickly and fulfill their effector functions immediately upon activation. Cellular proliferation and the implementation of effector functions require an enormous supply of biomolecules. For this reason, activated lymphocytes have an increased demand for energy. To meet the metabolic demands, they have been shown to utilize large amounts of glucose in cellular glycolysis (77). Glucose can provide the energy for lymphocytes in various ways, as it is the primary substrate for the generation of ATP. Nevertheless, it can also serve as a carbon source for the synthesis of other macromolecules, such as nucleic acids and phospholipids (132). However, glucose cannot pass the lipid membrane of the cell by simple diffusion. Glucose utilization in the glycolytic pathway is limited by the transport of glucose into the cells, demonstrating the critical role for glucose transporters for the energy supply of a cell. The entry of glucose molecules into the cells is accomplished by a large family of structurally related transport proteins known as facilitated diffusion glucose transporters (Glut) (133). To date, there are 14 different

[5] *Allogeneic* individuals differ at genes in the HLA, whereas *semiallogeneic* individuals are sharing some, but not all genes (1).

glucose transporter isoforms characterized in humans, which are expressed on different cell types (134,135). Glut1 is the most ubiquitously distributed of the transporter isoforms that facilitates an energy-independent transfer of glucose across the membrane (132,136).

Immune cell activation is associated with an upregulation of Glut1 on the cell surface that allows the uptake of available glucose from the surroundings fueling cellular energy production and assembly of biomolecules (81,137,138). Many studies have shown that CD3/CD28 T cell receptor (TCR) stimulation leads to an upregulation of Glut1 on the surface of human T cells (85,86,139–143). Due to the fact that NK cells and cytotoxic CD8 T cells share common features, as they both are able to exert direct cytotoxic responses and produce proinflammatory cytokines upon activation, this study aimed to investigate the expression of Glut1 within the functional different subsets of educated and uneducated NK cells. The data of this study revealed that educated NK cells exhibited higher amounts of Glut1 on their cell surface already prior to stimulation and moreover increased the expression of Glut1 after activation by target cell lines. To date, it was unknown whether educated and uneducated NK cells have a distinct Glut1 receptor profile. The distinct Glut1 expression profile among functionally different NK-cell subsets raises the question of how this transporter is regulated.

Extracellular nutrient availability leads to continuous cell growth and proliferation in unicellular eukaryotes, which can take up extracellular nutrients in a cell-autonomous manner (144). The cells of multicellular organisms are generally surrounded by sufficient amounts of nutrients that can fuel cellular metabolic pathways. However, extracellular availability of nutrients does not automatically lead to cellular growth and proliferation in these cells. In fact, they are tightly regulated to prevent uncontrolled proliferation and to preserve the integrity of an organism (145,146). Tissue-specific growth factors ensure that the cells can only survive in their designated environment. As soon as these cells are missing extracellular survival signals, they undergo atrophy[6] and eventually initiate programmed cell death upon intrinsic cellular pathways (147,148). A study by Rathmell *et al.* postulated that TCR stimulation provided surviving signals that

[6] Atrophy is a form of cell adaptation in response to a lack of nutrients, trophic influences or functional demands which is characterized by decrease in cell size, protein content, cellular ATP and the rate of glycolysis (165).

allowed T cells to utilize available nutrients and furthermore upregulate Glut1 expression (149). They showed that T cells which were cultivated without TCR stimulation displayed undetectable levels of Glut1 *in vitro*. The authors concluded that T cells require extrinsic signals to utilize available nutrients and that TCR stimulation was required to maintain basal Glut1 expression. In addition, it has been shown that Glut1 upregulation was also cytokine-dependent. Glut1 mRNA and Glut1 surface expression were decreased upon cytokine withdrawal in an IL-3-dependent pro-B cell line (150,151). IL-3 is a cytokine, which functions as a growth factor promoting proliferation and differentiation in hematopoietic cells (1). IL-3 and other growth factors induce pathways leading to activation of phosphatidylinositide 3-kinases (PI3Ks) and protein kinase B (PKB), also known as Akt, which have been described multiple times to directly influence cellular metabolism and Glut1 expression in immune cells (85,142,143,152,153). Together with the mammalian target of rapamycin (mTOR), PI3Ks and Akt are the main components of the PI3K/Akt/mTOR signaling cascade that regulates proliferation, survival and cellular metabolism (154). mTOR is an evolutionarily conserved serine/threonine protein kinase that associates with other proteins to form two distinct complexes (mTORC1 and mTORC2). Extracellular signals, such as growth factors, nutrients, energy status and cellular stress activate mTORC1 (155,156). Upon activation, mTORC1 regulates cell growth and protein synthesis, whereas stress conditions such as starvation, reduce mTORC1 signaling that can lead to autophagy (154,157). Donnelly *et al.* demonstrated in mice that mTORC1 activity was required for maintaining glycolysis and moreover for the production of the NK-cell effector molecules IFN-γ and granzyme B (158). Limiting the rate of glycolysis led to an abrogation of IFN-γ and granzyme B production. Interestingly, cytokine-stimulated NK cells that have been treated with the mTORC1 inhibitor rapamycin significantly downregulated Glut1 from the cell surface.

To date, there are only a few studies that have investigated the impact of cytokine stimulation on the expression of Glut1 in human NK cells. Keating *et al.* provided evidence that a subset of NK cells, $CD56^{bright}$ NK cells, which are potent producers of IFN-γ, display high levels of Glut1 compared to their counterpart $CD56^{dim}$ NK cells which express low levels of Glut1 without stimulation (110,129). They demonstrated that $CD56^{dim}$ NK cells, which are considered to be more cytotoxic than $CD56^{bright}$ NK cells, upregulated Glut1 after stimulation with IL-2 or a cytokine combination of

IL-12/15, whereas $CD56^{bright}$ NK cells did not change after cytokine stimulation. However, the regulation of Glut1 is complex, since it is controlled at the level of transcription, translation and transport to the cell surface (159). A recent study from Schafer *et al.* performed RNA sequencing expression analysis for Glut1 in NK cells (160). To receive sufficient cells for their analyses, they co-cultured NK cells over a time period of 14 to 21 days with a K-562-based feeder cell line. This cell line expressed membrane-bound IL-12, which supported NK-cell proliferation. The study showed that the levels of Glut1 RNA in NK cells after cytokine-driven expansion did not differ from freshly isolated, unstimulated NK cells. However, the authors stated that the feeder cell lines, which stimulated NK cells in this setting, were added on day 1, 7 and 14 during the expansion process. A study by Macintyre *et al.* investigated the levels of Glut1 mRNA in naïve and CD3/CD28-stimulated CD4 murine T cells (85). Glut1 mRNA levels were increased after 8 h stimulation and declined already after 24 h stimulation. Thus there is the possibility that the study by Schafer *et al.* did not detect differences in Glut1 mRNA levels between the tested NK-cell subsets due to inadequate stimulation methods. Furthermore, the same group performed fluorescence-activated cell sorting to separate expanded NK cells into educated and uneducated cells and analyzed the protein expression levels of these NK-cell subsets. They observed a strong increase of the glycolytic enzyme pyruvate kinase M2 (PKM2) in educated NK cells compared to their uneducated counterpart (160). PKM2 is an isoform of pyruvate kinase that catalyzes the production of pyruvate in the last step of glycolysis providing energy in form of ATP (see **1.5.1, Figure 10**). Remarkably, it has been described that PKM2 is regulated by the hypoxia-inducible factor 1a (HIF1α) which in turn is controlled by mTOR, indicating a regulation of PKM2 activity through the PI3K/Akt/mTOR signaling pathway (161,162).

In summary, elevated levels of PKM2 as a crucial enzyme for energy production during glycolysis might lead to enhanced glycolytic flux in educated NK cells. As a consequence, educated NK cells might benefit from a better supply with energy and important biomolecules that contribute to the implementation of their effector functions. In order to fuel glycolysis, the cells would require greater amounts of glucose. Consequently, the cells would need to upregulate the levels of Glut1 on the cell surface to meet the increased demands of glucose. This model is supported by the observation in this study, whereas educated NK cells exhibited increased surface expression of

Glut1 compared to uneducated NK cells already before and also after stimulation with target cell lines. To recapitulate, the integration of extracellular activation signals can support the upregulation of Glut1 in various immune cells. The studies of different authors point into the direction that the upregulation of Glut1 is achieved through the activation of the PI3K/Akt/mTOR signaling cascade, regulating proliferation, survival and cellular metabolism. Further studies are now required to investigate if the stimulation of inhibitory and activating NK cell receptors leads to the activation of the PI3K/Akt/mTOR signaling cascade in the context of NK-cell education. One recent study by Marçais *et al.* addressed the role of mTOR in murine NK cells. The authors discovered that the activity of the PI3K/Akt/mTOR pathway was selectively higher in reactive NK cells (163). They showed that the phosphorylation of direct and indirect targets of mTOR correlated with the level of NK-cell responsiveness. Furthermore, NK-cell function was abrogated in mTOR deficient knock-out mice. The authors hypothesized that an unopposed signaling by activating receptors might abrogate mTOR signaling in uneducated NK cells. However, the interaction of inhibitory receptors with their cognate ligand prevents the desensitization and maintains mTOR signaling for optimal NK-cell functions upon activating receptor stimulation. Moreover, this model was supported by their observation that SHP-1, the phosphatase triggered upon inhibitory receptor engagement, was necessary to maintain activity of the mTOR signaling pathway (164).

Here I provided evidence, that the functionally superior subset of educated NK cells exhibited significantly increased surface levels of the glucose transporter Glut1 compared to uneducated NK cells. This difference was detected prior to stimulation and increased significantly after stimulation with target cell lines. Until today, it is unclear which metabolic processes lead to the functional superiority of educated NK cells. Recent studies in immune cells demonstrated an interplay between the cellular metabolism and the effector functions in these cells. The activation of the PI3K/Akt/mTOR pathway has been described to regulate proliferation, survival and cellular metabolism (144). Recent observations in mice provided evidence that this pathway is involved in NK-cell education. The PI3K/Akt/mTOR pathway has been described to promote Glut1 upregulation upon stimulation with extracellular factors. I suggest the model that the upregulation of Glut1 in educated NK cells is promoted by an activation of PI3K/Akt/mTOR pathway. Upon the interaction of inhibitory and

activating receptors with downstream molecules of the PI3K/Akt/mTOR pathway, the educated NK cells can upregulate Glut1 on their cell surface and promote the uptake of Glucose fueling cellular metabolic pathways that contribute to the functional superiority of educated NK cells (**Figure 38**).

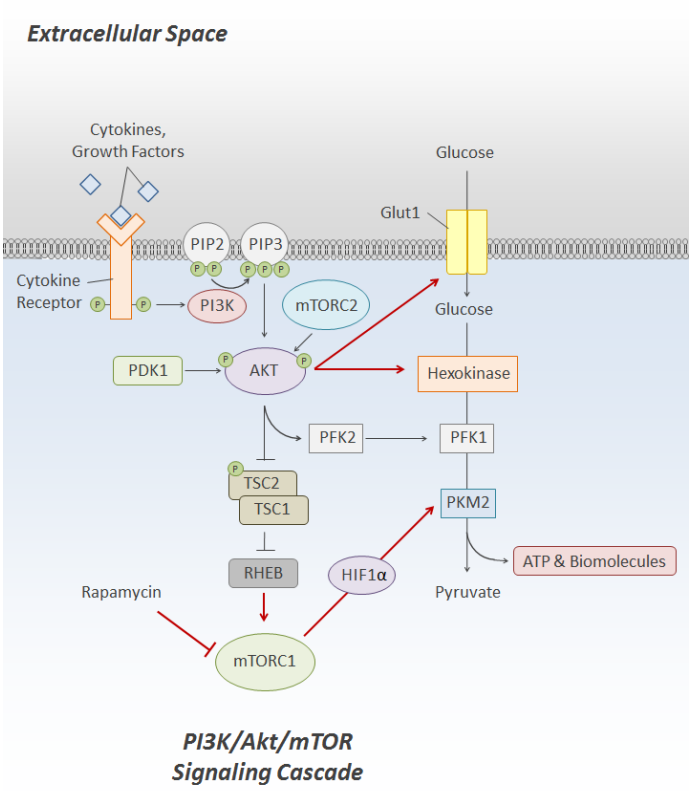

Figure 38: The activation of the PI3K/Akt/mTOR signaling pathway by extracellular signals leads to the upregulation of Glut1 in NK cells

Schematic illustration of signal transduction pathways that might support Glut1 upregulation in NK cells based on findings in other cells. Growth factor or cytokine signaling activates PI 3-kinase (PI3K) and mediates the conversion of membrane-bound phosphatidylinositol (4,5)-bisphosphate (PIP2) to phosphatidylinositol (3,4,5)-trisphosphate (PIP3) (154). PIP3 acts as a secondary messenger that facilitates the recruitment and activation of the PI3K-dependent kinase (PDK1). PDK1 and mammalian target of rapamycin complex 2 (mTORC2) both phosphorylate Akt. Following activation, Akt can phosphorylate various target proteins that have an impact on different downstream pathways promoting proliferation, differentiation, cellular metabolism or apoptosis. Akt enhances the translation and localization of Glut1 to the cell surface and stimulates hexokinase activity supporting increased glycolysis (144,153,165). Another function of Akt is the inhibition of tuberous sclerosis proteins (TSC) 2 upon phosphorylation. Inactive TSC1/2 is not able to bind to RAS homolog enriched in brain (RHEB), leading to the activation of mammalian target of rapamycin complex 1 (mTORC1). mTORC1 is a serine/threonine protein kinase that regulates numerous cellular functions, such as cell growth, protein synthesis and autophagy (154). It has been demonstrated that mTORC1 induces pyruvate kinase M2 (PKM2) activity via hypoxia-inducible factor 1a (HIF1α)-mediated transcription activation (161). PKM2 is an isoenzyme of the glycolytic enzyme pyruvate kinase, which directly supports glycolysis by enhancing the formation of pyruvate in the last step of glycolysis. Recently, a strong upregulation of PKM2 in educated NK cells that sustain glycolysis has been observed (160). Glycolysis provides the cell with energy and biomolecules that can fuel the production of effector molecules, such as cytotoxic mediators and cytokines. Inhibition of mTORC1 by its inhibitor rapamycin abrogates glycolysis and was shown to decrease the ability of cytokine production in NK cells (158). These observations point into the direction that NK cells, which receive different signals upon ligand-engagement with their inhibitory and activating receptors, might use the same pathways to increase Glut1 and upregulate glycolysis for the production of effector molecules.

Cellular metabolism is considered as a complex interplay of various chemical reactions that occur in living organisms to maintain cellular functions. However, recent findings in immune cells demonstrated that cellular metabolism does not only provide energy and substrates for growth and survival but also plays an important role in differentiation and immune responses (166). In order to meet the changing metabolic demands upon activation, immune cells have been shown to actively reprogram their intracellular metabolism from a mitochondrial oxidative phosphorylation (OXPHOS) to enhanced glycolysis (110,158,167). This process is known as metabolic reprogramming (168–172). The first evidence for metabolic reprogramming, however, was not observed in immune cells. Metabolic reprogramming is known as one of the hallmarks for cancer cells, as these cells exhibit increased glycolytic rates compared to normal cells (173,174). This phenomenon is described as the Warburg effect, discovered by Otto Warburg in 1924 (175–177). In normal cells, glycolysis is used to catabolize glucose to pyruvate, which can be later converted to Acetyl-CoA fueling the citric acid cycle in the mitochondria. The citric acid cycle generates the coenzymes NADH and $FADH_2$, providing the electrons for the mitochondrial respiratory chain and subsequent energy production of ATP. Unlike normal cells, which utilize glycolysis only when oxygen supply is limited, cancer cells preferentially use glycolysis even in the abundance of oxygen (173). Interestingly, T cells have been shown to undergo metabolic reprogramming upon activation, which promotes an enhanced glycolytic flux, the upregulation of Glut1 as well as the expression of glycolytic enzymes (76,138,172,178,179). Hence, distinct immune cell subsets exhibit different metabolic demands that are accompanied by the use of different metabolic pathways (178,180). The metabolic mechanisms that lead to the functional differences between educated and uneducated NK cells are not fully understood to date. This study provided evidence that educated NK cells exhibit increased levels of the glucose transporter Glut1, leading to the hypothesis, that metabolic reprogramming is an underlying mechanism for the superior function of educated NK cells. The data of this study revealed that educated NK cells displayed an enhanced glycolytic profile in comparison to uneducated NK cells. The metabolic profile of a cell population can be assessed through metabolic flux assays. In this assay, OXPHOS is determined by the oxidative consumption rate (OCR), whereas glycolysis is defined by the extracellular acidification rate (ECAR) (see **2.2.13**). A study by Keppel *et al.* investigated the basic metabolic profile of murine splenic NK cells (181). Analyzing the OCR and ECAR of freshly isolated NK cells

revealed that NK cells preferentially used OXPHOS at a resting state. Short-term activation with the cytokine combination of IL-12 and IL-18 or antibodies against activating receptors did not induce substantial changes in energy pathway usage. As OXPHOS can be fueled by different pathways, such as glycolysis, fatty acid oxidation or glutaminolysis, the authors performed inhibition experiments elucidating glucose as the main fuel for OXPHOS. Interestingly, the inhibition of glycolysis or OXPHOS did not affect the IFN-γ production in cytokine-stimulated NK cells. In contrast, IFN-γ production was nearly abrogated upon inhibition of glycolysis or OXPHOS in receptor-stimulated NK cells. The authors concluded, that the receptor-stimulated IFN-γ production is dependent on metabolism-driven signaling, whereas cytokine-driven IFN-γ production is not. Of note, long-term culture with high doses of IL-15 restored the IFN-γ production capacity in receptor-stimulated NK cells despite inhibition of the metabolic pathways. IL-15 is a cytokine that is critical for NK-cell differentiation and survival and is known to prime NK cells for the implementation of effector functions (182,183). Aligned with this finding, high doses of IL-15 have been described to activate mTOR, to stimulate glucose uptake, proliferation and cytotoxic effector functions in murine NK cells (158,163,184). Enhanced IL-15 signaling that leads to increased stimulation of mTOR might be an explanation for the recovered IFN-γ production capacity in receptor-stimulated NK cells. Furthermore, a study by Viel *et al.* provided evidence for this hypothesis. Treatment of murine and human NK cells with the mTOR inhibitors rapamycin and transforming growth factor-β (TGF-β), abrogated the IL-15-induced activation of mTOR resulting in reduced metabolic activity and impaired cytotoxicity (185). In comparison to the studies in mice, Schafer *et al.* described that human educated NK cells displayed increased glycolysis, higher glycolytic capacity and a greater glycolytic reserve than uneducated NK cells. OXPHOS levels did not differ between the two functionally different subsets. In contrast to this, Keating *et al.* observed that elevated levels of OXPHOS but not glycolysis were required to support cytotoxicity and IFN-γ production in cytokine-stimulated NK cells. In accordance with observations in mice, they reported a cytokine-driven upregulation of mTORC1 in human NK cells (110). Of note, the stimulation with IL-2 or a combination of IL-12/15 robustly upregulated mTORC1, but only IL-2-induced upregulation was shown to be sensitive to inhibition by rapamycin. This observation suggests that different cytokine stimulations activate distinct downstream signaling pathways that might explain inconsistent observations.

Figure 39

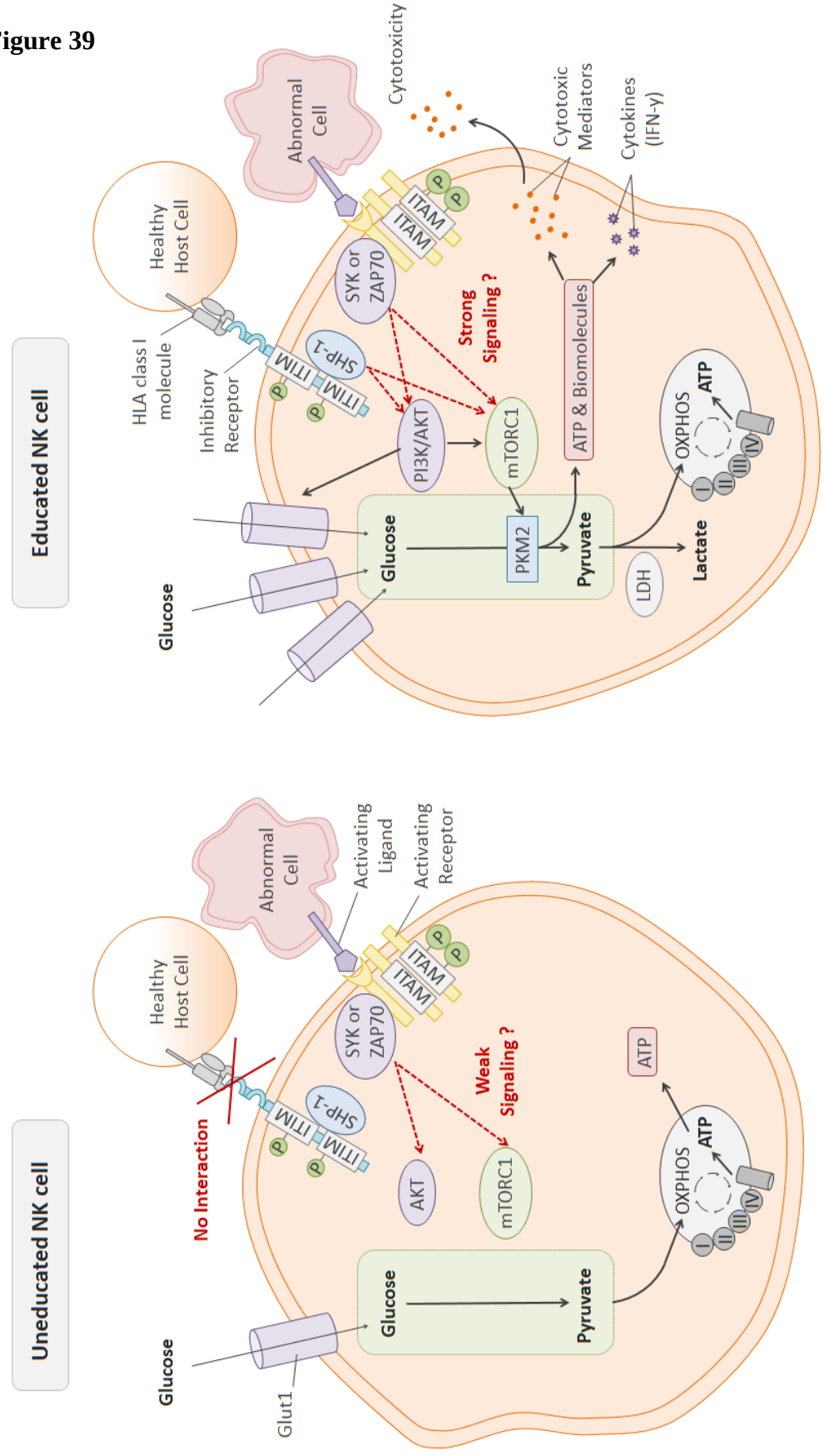
Educated NK cell
Abnormal Cell
Cytotoxicity
Cytotoxic Mediators
Cytokines (IFN-γ)
Healthy Host Cell
ITAM
ITAM
SYK or ZAP70
Strong Signaling ?
HLA class I molecule
Inhibitory Receptor
SHP-1
ITIM
ITIM
PI3K/AKT
mTORC1
ATP & Biomolecules
OXPHOS
ATP
Glucose
Glucose
PKM2
Pyruvate
LDH
Lactate
Uneducated NK cell
Abnormal Cell
Activating Ligand
Activating Receptor
Healthy Host Cell
ITAM
ITAM
SYK or ZAP70
Weak Signaling ?
No Interaction
SHP-1
ITIM
ITIM
AKT
mTORC1
ATP
OXPHOS
ATP
Glucose
Glucose
Pyruvate
Glut1

Figure 39: Educated NK cells possess the exclusive ability to activate the PI3K/Akt/mTOR signaling pathway as a model for the functional differences between educated and uneducated NK cells

Schematic overview of the metabolic pathways that are used upon activation in educated and uneducated NK cells. Uneducated NK cells (left) are characterized by a low surface expression of the glucose transporter Glut1. Therefore only low amounts of glucose are transferred into the cytosol of the cell. Glycolysis catabolizes glucose to pyruvate, which is directly transferred into the mitochondria where it is transformed to Acetyl-CoA fueling OXPHOS. Thereby uneducated NK cells can produce high amounts of ATP for basal cellular activities. Uneducated NK cells either lack the expression of self-inhibitory receptors or express inhibitory receptors that cannot engage with self-HLA class I molecules. Unstimulated inhibitory receptors fail to transfer signals that lead to the activation of the PI3K/Akt/mTOR signaling cascade. In contrast, activating receptors that engage with stimulatory ligands might transfer a signal into the cell, which however might not be sufficient to activate the PI3K/Akt/mTOR signaling cascade. Educated NK cells (right) express self-inhibitory receptors that engage with self-HLA class I molecules. The interaction leads to an activation of SHP-1 and transfers a signal into the cell that leads to an activation of the PI3K/Akt/mTOR signaling cascade. The activation of this pathway leads to an upregulation of Glut1 on the surface of educated NK cells. High amounts of glucose are transported into the cell that fuel glycolysis. Furthermore the activation of mTOR leads to an upregulation of pyruvate kinase M2 (PKM2) increasing the glycolytic flux by enhancing the formation of pyruvate. Furthermore, educated NK cells have increased levels of Lactate dehydrogenase (LDH) promoting the conversion of pyruvate to lactate. Although glycolysis is characterized as an inefficient way for energy production it also generates biosynthetic precursors that are used for the production of cytotoxic effector molecules and cytokines.

Consistent with the data of Schafer *et al.* this study showed that educated NK cells exhibited increased levels glycolysis compared to uneducated NK cells. Conversely, the data of this study did not reveal differences in the glycolytic capacity or the glycolytic reserve of educated and uneducated NK cells. However, these differences might be explained by a distinct experimental setup, as Schafer *et al.* used cytokine-driven expanded NK cells for their experiments in contrast to rested NK cells that were used in this study.

Unraveling the metabolic mechanisms that regulate functional responses in NK cells is difficult, as NK cells can be divided into distinct phenotypical and functional subsets that might use different metabolic pathways. In addition, NK cells are stimulated through various receptors that might activate distinct downstream signaling molecules. The molecular mechanisms underlying the functional differences of educated an uneducated NK cells have not been fully elucidated to date. However, this study provided evidence that a characteristic glycolytic profile might serve as the underlying mechanism for the functional superiority of educated NK cells. Further studies that investigate the downstream signaling molecules of the described metabolic pathways in the context of NK-cell education are necessary to verify this model in human NK cells.

References

1. Murphy K., Weaver C. *Janeway's immunobiology*. 9th ed. New York, NY, 10017, USA: Garland Science, Taylor & Francis Group, LLC (2017). doi:10.1201/9781315533247

2. Vivier E, Raulet D, Moretta A, Caligiuri M. Innate or adaptive immunity? The example of natural killer cells. *Science (80-)* (2011) **331**:44–49. doi:10.1126/science.1198687.Innate

3. Riera Romo M, Pérez-Martínez D, Castillo Ferrer C. Innate immunity in vertebrates: An overview. *Immunology* (2016) **148**:125–139. doi:10.1111/imm.12597

4. Markiewski MM, Lambris JD. The role of complement in inflammatory diseases from behind the scenes into the spotlight. *Am J Pathol* (2007) **171**:715–727. doi:10.2353/ajpath.2007.070166

5. Vivier E, Artis D, Colonna M, Diefenbach A, Di Santo JP, Eberl G, Koyasu S, Locksley RM, McKenzie ANJ, Mebius RE, et al. Innate Lymphoid Cells: 10 Years On. *Cell* (2018) **174**:1054–1066. doi:10.1016/j.cell.2018.07.017

6. Herberman RB, Nunn ME, Lavrin DH. Natural cytotoxic reactivity of mouse lymphoid cells against syngeneic acid allogeneic tumors. I. Distribution of reactivity and specificity. *Int J cancer* (1975) **16**:216–29. Available at: http://www.ncbi.nlm.nih.gov/pubmed/50294

7. Herberman RB, Nunn ME, Holden HT, Lavrin DH. Natural cytotoxic reactivity of mouse lymphoid cells against syngeneic and allogeneic tumors. II. Characterization of effector cells. *Int J cancer* (1975) **16**:230–9. Available at: http://www.ncbi.nlm.nih.gov/pubmed/1080480

8. Kiessling R, Klein E, Wigzell H. "Natural" killer cells in the mouse. I. Cytotoxic cells with specificity for mouse Moloney leukemia cells. Specificity and distribution according to genotype. *Eur J Immunol* (1975) **5**:112–7. doi:10.1002/eji.1830050208

9. Rosenberg EB, Herberman RB, Levine PH, Halterman RH, McCoy JL, Wunderlich JR. Lymphocyte cytotoxicity reactions to leukemia-associated

antigens in identical twins. *Int J cancer* (1972) **9**:648–58. Available at: http://www.ncbi.nlm.nih.gov/pubmed/4513057

10. Paul S, Lal G. The molecular mechanism of natural killer cells function and its importance in cancer immunotherapy. *Front Immunol* (2017) **8**: doi:10.3389/fimmu.2017.01124

11. Yu J, Freud AG, Caligiuri MA. Location and cellular stages of natural killer cell development. *Trends Immunol* (2013) **34**:573–582. doi:10.1016/j.it.2013.07.005

12. Pascal V, Schleinitz N, Brunet C, Ravet S, Bonnet E, Lafarge X, Toussi M, reviron D, Viallard JF, Moreau JF, et al. Comparative analysis of NK cell subset distribution in normal and lymphoproliferative disease of granular lymphocyte conditions. *Eur J Immunol* (2004) **34**:2930–2940. doi:10.1002/eji.200425146

13. Jost S, Altfeld M. Control of Human Viral Infections by Natural Killer Cells. *Annu Rev Immunol* (2013) **31**:163–194. doi:10.1146/annurev-immunol-032712-100001

14. Wu J, Lanier LL. Natural killer cells and cancer. *Adv Ca Res* (2003) **13**:731–6. doi:10.1016/S0065-230X(03)90004-2

15. Zwirner NW, Domaica CI. Cytokine regulation of natural killer cell effector functions. *BioFactors* (2010) **36**:274–288. doi:10.1002/biof.107

16. Vivier E, Raulet DH, Moretta A, Caligiuri MA, Zitvogel L, Lanier LL, Yokoyama WM, Ugolini S. Innate or Adaptive Immunity? The Example of Natural Killer Cells. *Science (80-)* (2011) **331**:44–49. doi:10.1126/science.1198687

17. Le Bouteiller P, Tabiasco J, Polgar B, Kozma N, Giustiniani J, Siewiera J, Berrebi A, Aguerre-Girr M, Bensussan A, Jabrane-Ferrat N. CD160: A unique activating NK cell receptor. *Immunol Lett* (2011) **138**:93–96. doi:10.1016/j.imlet.2011.02.003

18. Biburger M, Lux A, Nimmerjahn F. *How immunoglobulin G antibodies kill target cells: Revisiting an old paradigm*. 1st ed. Elsevier Inc. (2014). doi:10.1016/B978-0-12-800147-9.00003-0

19. Guicciardi ME, Gores GJ. Life and death by death receptors. *FASEB J* (2009) **23**:1625–1637. doi:10.1096/fj.08-111005

20. Orange JS. Human natural killer cell deficiencies and susceptibility to infection. *Microbes Infect* (2002) **4**:1545–1558. doi:10.1016/S1286-4579(02)00038-2

21. Orange JS. Unraveling human natural killer cell deficiency. *J Clin Invest* (2012) **122**:798–801. doi:10.1172/JCI62620.798

22. Nowbakht P, Ionescu MCS, Rohner A, Kalberer CP, Rossy E, Mori L, Cosman D, De Libero G, Wodnar-Filipowicz A. Ligands for natural killer cell-activating receptors are expressed upon the maturation of normal myelomonocytic cells but at low levels in acute myeloid leukemias. *Blood* (2005) **105**:3615–3622. doi:10.1182/blood-2004-07-2585

23. Fogel LA, Yokoyama WM, French AR. Natural killer cells in human autoimmune disorders. *Arthritis Res Ther* (2013) **15**:216. doi:10.1186/ar4232

24. Poggi A, Zocchi MR. NK cell autoreactivity and autoimmune diseases. *Front Immunol* (2014) **5**:1–15. doi:10.3389/fimmu.2014.00027

25. Shifrin N, Raulet DH, Ardolino M. NK cell self tolerance, responsiveness and missing self recognition. *Semin Immunol* (2014) **26**:138–44. doi:10.1016/j.smim.2014.02.007

26. Raulet DH, Vance RE. Self-tolerance of natural killer cells. *Nat Rev Immunol* (2006) **6**:520–531. doi:10.1038/nri1863

27. Petersen JL, Morris CR, Solheim JC. Virus Evasion of MHC Class I Molecule Presentation. *J Immunol* (2003) **171**:4473–4478. doi:10.4049/jimmunol.171.9.4473

28. Vivier E, Ugolini S, Blaise D, Chabannon C, Brossay L. Targeting natural killer cells and natural killer T cells in cancer. *Nat Rev Immunol* (2012) **12**:239–252. doi:10.1038/nri3174

29. Carrillo-Bustamante P, Keşmir C, de Boer RJ. The evolution of natural killer cell receptors. *Immunogenetics* (2015)3–18. doi:10.1007/s00251-015-0869-7

30. Parham P. MHC class I molecules and kirs in human history, health and survival.

Nat Rev Immunol (2005) **5**:201–214. doi:10.1038/nri1570

31. Suto Y, Yabe T, Maenaka K, Tokunaga K, Tadokoro K, Juji T. The human natural killer gene complex (NKC) is located on chromosome 12p13.1-p13.2. *Immunogenetics* (1997) **46**:159–162. doi:10.1007/s002510050256

32. Chang C, Rodríguez A, Carretero M, López-Botet M, Phillips JH, Lanier LL. Molecular characterization of human CD94: A type II membrane glycoprotein related to the C-type lectin superfamily. *Eur J Immunol* (1995) **25**:2433–2437. doi:10.1002/eji.1830250904

33. Hikami K, Tsuchiya N, Yabe T, Tokunaga K. Variations of human killer cell lectin-like receptors: Common occurrence of NKG2-C deletion in the general population. *Genes Immun* (2003) **4**:160–167. doi:10.1038/sj.gene.6363940

34. Romero P, Ortega C, Palma a, Molina IJ, Peña J, Santamaría M. Expression of CD94 and NKG2 molecules on human CD4(+) T cells in response to CD3-mediated stimulation. *J Leukoc Biol* (2001) **70**:219–224. doi:10.1189/jlb.70.2.219

35. Sullivan LC, Clements CS, Beddoe T, Johnson D, Hoare HL, Lin J, Huyton T, Hopkins EJ, Reid HH, Wilce MCJ, et al. The Heterodimeric Assembly of the CD94-NKG2 Receptor Family and Implications for Human Leukocyte Antigen-E Recognition. *Immunity* (2007) **27**:900–911. doi:10.1016/j.immuni.2007.10.013

36. Gunturi A, Berg RE, Forman J. The Role of CD94/NKG2 in Innate and Adaptive Immunity. *Immunol Res* (2004) **30**:029–034. doi:10.1385/IR:30:1:029

37. Lanier LL, Corliss B, Wu J, Phillips JH. Association of DAP12 with activating CD94/NKG2C NK cell receptors. *Immunity* (1998) **8**:693–701. doi:10.1016/S1074-7613(00)80574-9

38. Wada H, Matsumoto N, Maenaka K, Suzuki K, Yamamoto K. The inhibitory NK cell receptor CD94/NKG2A and the activating receptor CD94/NKG2C bind the top of HLA-E through mostly shared but partly distinct sets of HLA-E residues. *Eur J Immunol* (2004) **34**:81–90. doi:10.1002/eji.200324432

39. Kaiser BK, Barahmand-pour F, Paulsene W, Medley S, Geraghty DE, Strong RK. Interactions between NKG2x Immunoreceptors and HLA-E Ligands Display Overlapping Affinities and Thermodynamics. *J Immunol* (2005) **174**:2878–2884.

doi:10.4049/jimmunol.174.5.2878

40. Björkström NK, Béziat V, Cichocki F, Liu LL, Levine J, Larsson S, Koup R a, Anderson SK, Ljunggren H, Malmberg K. CD8 T cells express randomly selected KIRs with distinct specificities compared with NK cells CD8 T cells express randomly selected KIRs with distinct specificities compared with NK cells. *Blood* (2012) **120**:3455–3465. doi:10.1182/blood-2012-03-416867

41. Kelley J, Walter L, Trowsdale J. Comparative genomics of natural killer cell receptor gene clusters. *PLoS Genet* (2005) **1**:0129–0139. doi:10.1371/journal.pgen.0010027

42. Long EO, Sik Kim H, Liu D, Peterson ME, Rajagopalan S. Controlling NK Cell Responses: Integration of Signals for Activation and Inhibition. *Annu Rev Biochem* (2013) **31**:1–36. doi:10.1146/annurev-immunol-020711-075005.Controlling

43. Yokoyama WM, Plougastel BFM. Immune functions encoded by the natural killer gene complex. *Nat Rev Immunol* (2003) **3**:304–316. doi:10.1038/nri1055

44. Howell WM, Carter V, Clark B. The HLA system: Immunobiology, HLA typing, antibody screening and crossmatching techniques. *J Clin Pathol* (2010) **63**:387–390. doi:10.1136/jcp.2009.072371

45. Wieczorek M, Abualrous ET, Sticht J, Álvaro-Benito M, Stolzenberg S, Noé F, Freund C. Major histocompatibility complex (MHC) class I and MHC class II proteins: Conformational plasticity in antigen presentation. *Front Immunol* (2017) **8**:1–16. doi:10.3389/fimmu.2017.00292

46. Thananchai H, Gillespie G, Martin MP, Bashirova A, Yawata N, Yawata M, Easterbrook P, McVicar DW, Maenaka K, Parham P, et al. Cutting Edge: Allele-Specific and Peptide-Dependent Interactions between KIR3DL1 and HLA-A and HLA-B. *J Immunol* (2007) **178**:33–37. doi:10.4049/jimmunol.178.1.33

47. Boyton RJ, Altmann DM. Natural killer cells, killer immunoglobulin-like receptors and human leucocyte antigen class I in disease. *Clin Exp Immunol* (2007) **149**:1–8. doi:10.1111/j.1365-2249.2007.03424.x

48. Cassidy SA, Cheent KS, Khakoo SI. Effects of peptide on NK cell-mediated

MHC I recognition. *Front Immunol* (2014) **5**:1–8. doi:10.3389/fimmu.2014.00133

49. Sim MJW, Malaker SA, Khan A, Stowell JM, Shabanowitz J, Peterson ME, Rajagopalan S, Hunt DF, Altmann DM, Long EO, et al. Canonical and cross-reactive binding of NK cell inhibitory receptors to HLA-C allotypes is dictated by peptides bound to HLA-C. *Front Immunol* (2017) **8**:1–16. doi:10.3389/fimmu.2017.00193

50. Fadda L, Borhis G, Ahmed P, Cheent K, Pageon S V., Cazaly A, Stathopoulos S, Middleton D, Mulder A, Claas FHJ, et al. Peptide antagonism as a mechanism for NK cell activation. *Proc Natl Acad Sci* (2010) **107**:10160–10165. doi:10.1073/pnas.0913745107

51. Hickman HD, Luis AD, Bardet W, Buchli R, Battson CL, Shearer MH, Jackson KW, Kennedy RC, Hildebrand WH. Cutting Edge: Class I Presentation of Host Peptides Following HIV Infection. *J Immunol* (2003) **171**:22–26. doi:10.4049/jimmunol.171.1.22

52. Neefjes J, Jongsma MLM, Paul P, Bakke O. Towards a systems understanding of MHC class I and MHC class II antigen presentation. *Nat Rev Immunol* (2011) **11**:823–836. doi:10.1038/nri3084

53. Borrego F, Kabat J, Kim D-KK, Lieto L, Maasho K, Pena J, Solana R, Coligan JE, Peña J. Structure and function of major histocompatibility complex (MHC) class I specific receptors expressed on human natural killer (NK) cells. *Mol Immunol* (2002) **38**:637–660. doi:10.1016/S0161-5890(01)00107-9

54. Rajalingam R. Human diversity of killer cell immunoglobulin-like receptors and disease. *Korean J Hematol* (2011) **46**:216–28. doi:10.5045/kjh.2011.46.4.216

55. Mandelboim O, Reyburn HT, Sheu EG, Valés-Gómez M, Davis DM, Pazmany L, Strominger JL. The binding site of NK receptors on HLA-C molecules. *Immunity* (1997) **6**:341–350. doi:10.1016/S1074-7613(00)80336-2

56. Colonna M, Borsellino G, Falco M, Ferrara GB, Strominger JL. HLA-C is the inhibitory ligand that determines dominant resistance to lysis by NK1- and NK2-specific natural killer cells. *Proc Natl Acad Sci U S A* (1993) **90**:12000–4.

doi:10.1073/pnas.90.24.12000

57. Rasmussen M, Harndahl M, Stryhn A, Boucherma R, Nielsen LL, Lemonnier FA, Nielsen M, Buus S. Uncovering the Peptide-Binding Specificities of HLA-C: A General Strategy To Determine the Specificity of Any MHC Class I Molecule. *J Immunol* (2014) **193**:4790–4802. doi:10.4049/jimmunol.1401689

58. Biassoni R, Falco M, Cambiaggi A, Costa P, Verdiani S, Pende D, Conte R, Di Donato C, Parham P, Moretta L. Amino acid substitutions can influence the natural killer (NK)-mediated recognition of HLA-C molecules. Role of serine-77 and lysine-80 in the target cell protection from lysis mediated by "group 2" or "group 1" NK clones. *J Exp Med* (1995) **182**:605–9. doi:10.1084/JEM.182.2.605

59. Moesta AK, Norman PJ, Yawata M, Yawata N, Gleimer M, Parham P. Synergistic polymorphism at two positions distal to the ligand-binding site makes KIR2DL2 a stronger receptor for HLA-C than KIR2DL3. *J Immunol* (2008) **180**:3969–79. doi:10.4049/JIMMUNOL.180.6.3969

60. Gumperz JE, Litwin V, Phillips JH, Lanier LL, Parham P. The Bw4 public epitope of HLA-B molecules confers reactivity with natural killer cell clones that express NKB1, a putative HLA receptor. *J Exp Med* (1995) **181**:1133–44. doi:10.1084/jem.181.3.1133

61. O'Connor GM, Vivian JP, Widjaja JM, Bridgeman JS, Gostick E, Lafont BAP, Anderson SK, Price DA, Brooks AG, Rossjohn J, et al. Mutational and Structural Analysis of KIR3DL1 Reveals a Lineage-Defining Allotypic Dimorphism That Impacts Both HLA and Peptide Sensitivity. *J Immunol* (2014) **192**:2875–2884. doi:10.4049/jimmunol.1303142

62. Raulet DH, Held W, Correa I, Dorfman JR, Wu MF, Corral L. Specificity, tolerance and developmental regulation of natural killer cells defined by expression of class I-specific Ly49 receptors. *Immunol Rev* (1997) **155**:41–52. doi:10.1111/j.1600-065X.1997.tb00938.x

63. Fernandez NC, Treiner E, Vance RE, Jamieson a M, Lemieux S, Raulet DH. A subset of natural killer cells achieve self-tolerance without expressing inhibitory receptors specific for self MHC molecules. *Blood* (2005) **105**:4416–4424. doi:10.1182/blood-2004-08-3156

64. Cooley S, Xiao F, Pitt M, Gleason M, Mccullar V, Mcqueen KL, Guethlein L a, Parham P. A subpopulation of human peripheral blood NK cells that lacks inhibitory receptors for self MHC is developmentally immature. *Blood* (2007) **110**:578–587. doi:10.1182/blood-2006-07-036228

65. Anfossi N, André P, Guia S, Falk CS, Roetynck S, Stewart CA, Breso V, Frassati C, Reviron D, Middleton D, et al. Human NK Cell Education by Inhibitory Receptors for MHC Class I. *Immunity* (2006) **25**:331–342. doi:10.1016/j.immuni.2006.06.013

66. Boudreau JE, Hsu KC. Natural Killer Cell Education and the Response to Infection and Cancer Therapy: Stay Tuned. *Trends Immunol* (2018) **39**:222–239. doi:10.1016/j.it.2017.12.001

67. Brodin P, Kärre K, Höglund P. NK cell education: not an on-off switch but a tunable rheostat. *Trends Immunol* (2009) **30**:143–149. doi:10.1016/j.it.2009.01.006

68. Boudreau JE, Hsu KC. Natural killer cell education in human health and disease. *Curr Opin Immunol* (2018) **50**:102–111. doi:10.1016/j.coi.2017.11.003

69. Brodin P, Lakshmikanth T, Johansson S, Karre K, Hoglund P. The strength of inhibitory input during education quantitatively tunes the functional responsiveness of individual natural killer cells. *Blood* (2009) **113**:2434–2441. doi:10.1182/blood-2008-05-156836

70. Schartl M., Gessler M., von Eckardstein A. *Biochemie und Molekularbiologie des Menschen*. 1st ed. München, Germany: Elsevier GmbH (2009).

71. Berg J. M., Tymoczko J. L., Gatto jr. G. J., Stryer L. *Biochemie*. 8th ed. Heidelberg, Germany: Springer-Verlag GmbH Deutschland (2018). doi:10.1007/978-3-662-54620-8

72. Dashty M. A quick look at biochemistry: Carbohydrate metabolism. *Clin Biochem* (2013) **46**:1339–1352. doi:10.1016/j.clinbiochem.2013.04.027

73. Bender T, Martinou JC. The mitochondrial pyruvate carrier in health and disease: To carry or not to carry? *Biochim Biophys Acta - Mol Cell Res* (2016) **1863**:2436–2442. doi:10.1016/j.bbamcr.2016.01.017

74. Toyoda Y, Saitoh S. Adaptive regulation of glucose transport, glycolysis and respiration for cell proliferation. *Biomol Concepts* (2015) **6**:423–430. doi:10.1515/bmc-2015-0018

75. Finlay DK. Metabolic regulation of natural killer cells. *Biochem Soc Trans* (2015) **43**:758–62. doi:10.1042/BST20150116

76. Puleston DJ, Villa M, Pearce EL. Ancillary Activity: Beyond Core Metabolism in Immune Cells. *Cell Metab* (2017) **26**:131–141. doi:https://doi.org/10.1016/j.cmet.2017.06.019

77. Pearce EL, Pearce EJ. Metabolic pathways in immune cell activation and quiescence. *Immunity* (2013) **38**:633–43. doi:10.1016/j.immuni.2013.04.005

78. Pearce EJ, Pearce EL. Immunometabolism in 2017: Driving immunity: All roads lead to metabolism. *Nat Rev Immunol* (2018) **18**:81–82. doi:10.1038/nri.2017.139

79. Buck MD, O'Sullivan D, Pearce EL, Sullivan DO, Pearce EL, O'Sullivan D, Pearce EL. T cell metabolism drives immunity. *J Exp Med* (2015) **212**:1345–1360. doi:10.1084/jem.20151159

80. Almeida L, Lochner M, Berod L, Sparwasser T. Metabolic pathways in T cell activation and lineage differentiation. *Semin Immunol* (2016) **28**:514–524. doi:10.1016/j.smim.2016.10.009

81. MacIver NJ, Michalek RD, Rathmell JC. Metabolic Regulation of T Lymphocytes. *Annu Rev Immunol* (2013) **31**:259–283. doi:10.1146/annurev-immunol-032712-095956

82. Wahl DR, Byersdorfer CA, Ferrara JLM, Opipari AW, Glick GD. Distinct metabolic programs in activated T cells: opportunities for selective immunomodulation. *Immunol Rev* (2012) **249**:104–15. doi:10.1111/j.1600-065X.2012.01148.x

83. Kelly AP, Finlay DK, Hinton HJ, Clarke RG, Fiorini E, Radtke F, Cantrell DA. Notch-induced T cell development requires phosphoinositide-dependent kinase 1. *EMBO J* (2007) **26**:3441–3450. doi:10.1038/sj.emboj.7601761

84. Cretenet G, Clerc I, Matias M, Loisel S, Craveiro M, Oburoglu L, Kinet S,

Mongellaz C, Dardalhon V, Taylor N. Cell surface Glut1 levels distinguish human CD4 and CD8 T lymphocyte subsets with distinct effector functions. *Sci Rep* (2016) **6**:24129. doi:10.1038/srep24129

85. Macintyre AN, Gerriets VA, Nichols AG, Michalek RD, Rudolph MC, Deoliveira D, Anderson SM, Abel ED, Chen BJ, Hale LP, et al. The glucose transporter Glut1 is selectively essential for CD4 T cell activation and effector function. *Cell Metab* (2014) **20**:61–72. doi:10.1016/j.cmet.2014.05.004

86. Frauwirth KA, Thompson CB. Regulation of T Lymphocyte Metabolism. *J Immunol* (2004) **172**:4661–4665. doi:10.4049/jimmunol.172.8.4661

87. Nath MD, Ruscetti FW, Petrow-sadowski C, Jones KS. Regulation of the cell-surface expression of an HTLV-I binding protein in human T cells during immune activation. (2003) **101**:3085–3092. doi:10.1182/blood-2002-07-2277.Supported

88. Shimizu Y, DeMars R. Production of human cells expressing individual transferred HLA-A,-B,-C genes using an HLA-A,-B,-C null human cell line. *J Immunol* (1989) **142**:3320–8. Available at: http://www.ncbi.nlm.nih.gov/pubmed/2785140

89. Lozzio CB, Lozzio BB. Human chronic myelogenous leukemia cell-line with positive Philadelphia chromosome. *Blood* (1975) **45**:321–34. Available at: http://www.ncbi.nlm.nih.gov/pubmed/163658

90. Ulmer AJ, Scholz W, Ernst M, Brandt E, Flad HD. Isolation and Subfractionation of Human Peripheral Blood Mononuclear Cells (PBMC) by Density Gradient Centrifugation on Percoll. *Immunobiology* (1984) **166**:238–250. doi:10.1016/S0171-2985(84)80042-X

91. Qiagen. Qiagen - DNeasy Blood & Tissue Handbook - Cat.#69506. (2006)

92. Foley BA, De Santis D, Van Beelen E, Lathbury LJ, Christiansen FT, Witt CS. The reactivity of Bw4+ HLA-B and HLA-A alleles with kir3dll: Implications for patient and donor suitability for haploidentical stem cell transplantations. *Blood* (2008) **112**:435–443. doi:10.1182/blood-2008-01-132902

93. Stern M, Ruggeri L, Capanni M, Mancusi A, Velardi A. Human leukocyte

antigens A23, A24, and A32 but not A25 are ligands for KIR3DL1. *Blood* (2008) **112**:708–710. doi:10.1182/blood-2008-02-137521

94. Saunders PM, Pymm P, Pietra G, Hughes VA, Hitchen C, O'Connor GM, Loiacono F, Widjaja J, Price DA, Falco M, et al. Killer cell immunoglobulin-like receptor 3DL1 polymorphism defines distinct hierarchies of HLA class I recognition. *J Exp Med* (2016) **213**:791–807. doi:10.1084/jem.20152023

95. Zaritskaya L, Shurin MR, Sayers TJ, Malyguine AM. New flow cytometric assays for monitoring cell-mediated cytotoxicity. *Expert Rev Vaccines* (2010) **9**:601–616. doi:10.1586/erv.10.49

96. Hines MR, Nichols KE. Go with the flow: Perforin and CD107a in HLH. *Blood* (2017) **129**:2954–2955. doi:10.1182/blood-2017-04-773192

97. Alter G, Malenfant JM, Altfeld M. CD107a as a functional marker for the identification of natural killer cell activity. *J Immunol Methods* (2004) **294**:15–22. doi:10.1016/j.jim.2004.08.008

98. Barnett D, Walker B, Landay A, Denny TN. CD4 immunophenotyping in HIV infection. *Nat Rev Microbiol* (2008) **6**:7–15. doi:10.1038/nrmicro1998

99. Luetke-Eversloh M, Killig M, Romagnani C. Signatures of human NK cell development and terminal differentiation. *Front Immunol* (2013) **4**:1–6. doi:10.3389/fimmu.2013.00499

100. Boldt A, Borte S, Fricke S, Kentouche K, Emmrich F, Borte M, Kahlenberg F, Sack U. Eight-color immunophenotyping of T-, B-, and NK-cell subpopulations for characterization of chronic immunodeficiencies. *Cytom Part B - Clin Cytom* (2014) **86**:191–206. doi:10.1002/cyto.b.21162

101. Yang J, Zhang L, Yu C, Yang XF, Wang H. Monocyte and macrophage differentiation: Circulation inflammatory monocyte as biomarker for inflammatory diseases. *Biomark Res* (2014) **2**:1–9. doi:10.1186/2050-7771-2-1

102. Wang K, Wei G, Liu D. CD19: a biomarker for B cell development, lymphoma diagnosis and therapy. *Exp Hematol Oncol* (2012) **1**:36. doi:10.1186/2162-3619-1-36

103. Fu Y. Facilitative glucose transporter gene expression in human lymphocytes, monocytes, and macrophages: a role for GLUT isoforms 1, 3, and 5 in the immune response and foam cell formation. *Blood Cells, Mol Dis* (2004) **32**:182–190. doi:10.1016/j.bcmd.2003.09.002

104. Manel N, Kim FJ, Kinet S, Taylor N, Sitbon M, Battini JL. The Ubiquitous Glucose Transporter GLUT-1 Is a Receptor for HTLV. *Cell* (2003) **115**:449–459. doi:10.1016/S0092-8674(03)00881-X

105. Körner C, Granoff ME, Amero MA, Sirignano MN, Vaidya SA, Jost S, Allen TM, Rosenberg ES, Altfeld M. Increased frequency and function of KIR2DL1-3+NK cells in primary HIV-1 infection are determined by HLA-C group haplotypes. *Eur J Immunol* (2014) **44**:2938–2948. doi:10.1002/eji.201444751

106. Hu P, Zhang W, Xin H, Deng G. Single Cell Isolation and Analysis. *Front Cell Dev Biol* (2016) **4**:1–12. doi:10.3389/fcell.2016.00116

107. Agilent. Agilent Technologies - Seahorse XFp Glycolysis Stress Test Kit User Guide - Cat.#103017-100.

108. Saunders PM, Vivian JP, O'Connor GM, Sullivan LC, Pymm P, Rossjohn J, Brooks AG. A bird's eye view of NK cell receptor interactions with their MHC class I ligands. *Immunol Rev* (2015) **267**:148–166. doi:10.1111/imr.12319

109. Hilton HG, Parham P. Missing or altered self: human NK cell receptors that recognize HLA-C. *Immunogenetics* (2017) **69**:567–579. doi:10.1007/s00251-017-1001-y

110. Keating SE, Zaiatz-Bittencourt V, Loftus RM, Keane C, Brennan K, Finlay DK, Gardiner CM. Metabolic Reprogramming Supports IFN-γ Production by CD56bright NK Cells. *J Immunol* (2016) **196**:2552–60. doi:10.4049/jimmunol.1501783

111. Lisovsky I, Isitman G, Bruneau J, Bernard NF. Functional analysis of NK cell subsets activated by 721.221 and K562 HLA-null cells. *J Leukoc Biol* (2015) **97**:761–767. doi:10.1189/jlb.4AB1014-499R

112. Pende D, Rivera P, Marcenaro S, Chang CC, Biassoni R, Conte R, Kubin M, Cosman D, Ferrone S, Moretta L, et al. Major histocompatibility complex class I-

related chain A and UL16-binding protein expression on tumor cell lines of different histotypes: analysis of tumor susceptibility to NKG2D-dependent natural killer cell cytotoxicity. *Cancer Res* (2002) **62**:6178–6186. doi:10.1016/s0952-7915(97)80155-0

113. Chen X, Trivedi PP, Ge B, Krzewski K, Strominger JL. Many NK cell receptors activate ERK2 and JNK1 to trigger microtubule organizing center and granule polarization and cytotoxicity. *Proc Natl Acad Sci* (2007) **104**:6329–6334. doi:10.1073/pnas.0611655104

114. Kim S, Poursine-Laurent J, Truscott SM, Lybarger L, Song Y-J, Yang L, French AR, Sunwoo JB, Lemieux S, Hansen TH, et al. Licensing of natural killer cells by host major histocompatibility complex class I molecules. *Nature* (2005) **436**:709–13. doi:10.1038/nature03847

115. Bélanger S, Tu MM, Rahim MMA, Mahmoud AB, Patel R, Tai LH, Troke AD, Wilhelm BT, Landry JR, Zhu Q, et al. Impaired natural killer cell self-education and "missing-self" responses in Ly49-deficient mice. *Blood* (2012) **120**:592–602. doi:10.1182/blood-2012-02-408732

116. Thomas LM. Current perspectives on natural killer cell education and tolerance : emerging roles for inhibitory receptors. *ImmunoTargets Ther* (2015) **4**:45–53. doi:10.2147/ITT.S61498

117. Stern P, Gidlund M, Örn A, Wigzell H. Natural killer cells mediate lysis of embryonal carcinoma cells lacking MHC. *Nature* (1980) **285**:341–342. doi:10.1038/285341a0

118. Tarek N, Luduec JB Le, Gallagher MM, Zheng J, Venstrom JM, Chamberlain E, Modak S, Heller G, Dupont B, Cheung NK V., et al. Unlicensed NK cells target neuroblastoma following anti-GD2 antibody treatment. *J Clin Invest* (2012) **122**:3260–3270. doi:10.1172/JCI62749

119. Sim MJW, Stowell J, Sergeant R, Altmann DM, Long EO, Boyton RJ. KIR2DL3 and KIR2DL1 show similar impact on licensing of human NK cells. *Eur J Immunol* (2016) **46**:185–191. doi:10.1002/eji.201545757

120. Saunders PM, Vivian JP, Baschuk N, Beddoe T, Widjaja J, O'Connor GM,

Hitchen C, Pymm P, Andrews DM, Gras S, et al. The Interaction of KIR3DL1*001 with HLA Class I Molecules Is Dependent upon Molecular Microarchitecture within the Bw4 Epitope. *J Immunol* (2015) **194**:781–789. doi:10.4049/jimmunol.1402542

121. Elliott JM, Wahle JA, Yokoyama WM. MHC class I–deficient natural killer cells acquire a licensed phenotype after transfer into an MHC class I–sufficient environment. *J Exp Med* (2010) **207**:2073–2079. doi:10.1084/jem.20100986

122. Joncker NT, Shifrin N, Delebecque F, Raulet DH. Mature natural killer cells reset their responsiveness when exposed to an altered MHC environment. *J Exp Med* (2010) **207**:2065–2072. doi:10.1084/jem.20100570

123. Boudreau JE, Liu XR, Zhao Z, Zhang A, Shultz LD, Greiner DL, Dupont B, Hsu KC. Cell-Extrinsic MHC Class I Molecule Engagement Augments Human NK Cell Education Programmed by Cell-Intrinsic MHC Class I. *Immunity* (2016) **45**:280–291. doi:10.1016/j.immuni.2016.07.005

124. Landtwing V, Raykova A, Pezzino G, Béziat V, Marcenaro E, Graf C, Moretta A, Capaul R, Zbinden A, Ferlazzo G, et al. Cognate HLA absence in trans diminishes human NK cell education. *J Clin Invest* (2016) **126**:3772–3782. doi:10.1172/JCI86923

125. Lee N, Llano M, Carretero M, Ishitani A, Navarro F, López-Botet M, Geraghty DE. HLA-E is a major ligand for the natural killer inhibitory receptor CD94/NKG2A. *Proc Natl Acad Sci U S A* (1998) **95**:5199–204. doi:10.1073/pnas.95.9.5199

126. Boegel S, Löwer M, Bukur T, Sorn P, Castle JC, Sahin U. HLA and proteasome expression body map. *BMC Med Genomics* (2018) **11**:1–12. doi:10.1186/s12920-018-0354-x

127. Björkström NK, Riese P, Heuts F, Andersson S, Fauriat C, Ivarsson MA, Björklund AT, Flodström-Tullberg M, Michaëlsson J, Rottenberg ME, et al. Expression patterns of NKG2A, KIR, and CD57 define a process of CD56dimNK-cell differentiation uncoupled from NK-cell education. *Blood* (2010) **116**:3853–3864. doi:10.1182/blood-2010-04-281675

128. Lisovsky I, Isitman G, Song R, DaFonseca S, Tremblay-McLean A, Lebouché B, Routy J-P, Bruneau J, Bernard NF. A Higher Frequency of NKG2A $^{+}$ than of NKG2A $^{-}$ NK Cells Responds to Autologous HIV-Infected CD4 Cells irrespective of Whether or Not They Coexpress KIR3DL1. *J Virol* (2015) **89**:9909–9919. doi:10.1002/mma.5252

129. Poli A, Michel T, Thérésine M, Andrès E, Hentges F, Zimmer J. CD56 bright natural killer (NK) cells: an important NK cell subset. *Immunology* (2009) **126**:458–465. doi:10.1111/j.1365-2567.2008.03027.x

130. Ivarsson MA, Loh L, Marquardt N, Kekäläinen E, Berglin L, Björkström NK, Westgren M, Nixon DF, Michaëlsson J. Differentiation and functional regulation of human fetal NK cells. *J Clin Invest* (2013) **123**:3889–3901. doi:10.1172/JCI68989

131. Phillips JH, Hori T, Nagler A, Bhat N, Spits H, Lanier LL. Ontogeny of human natural killer (NK) cells: fetal NK cells mediate cytolytic function and express cytoplasmic CD3 epsilon,delta proteins. *J Exp Med* (1992) **175**:1055–66. Available at: http://www.ncbi.nlm.nih.gov/pubmed/1372642

132. Maciver NJ, Jacobs SR, Wieman HL, Wofford JA, Coloff JL, Rathmell JC. Glucose metabolism in lymphocytes is a regulated process with significant effects on immune cell function and survival. *J Leukoc Biol* (2008) **84**:949–57. doi:10.1189/jlb.0108024

133. Navale AM, Paranjape AN. Glucose transporters: physiological and pathological roles. *Biophys Rev* (2016) **8**:5–9. doi:10.1007/s12551-015-0186-2

134. Thorens B, Mueckler M. Glucose transporters in the 21st Century. *Am J Physiol Endocrinol Metab* (2010) **298**:E141-5. doi:10.1152/ajpendo.00712.2009

135. Mueckler M, Thorens B. The SLC2 (GLUT) family of membrane transporters. *Mol Aspects Med* (2013) **34**:121–38. doi:10.1016/j.mam.2012.07.001

136. Maratou E, Dimitriadis G, Kollias A, Boutati E, Lambadiari V, Mitrou P, Raptis SA. Glucose transporter expression on the plasma membrane of resting and activated white blood cells. *Eur J Clin Invest* (2007) **37**:282–290. doi:10.1111/j.1365-2362.2007.01786.x

137. Palmer CS, Cherry CL, Sada-Ovalle I, Singh A, Crowe SM. Glucose Metabolism in T Cells and Monocytes: New Perspectives in HIV Pathogenesis. *EBioMedicine* (2016) **6**:31–41. doi:10.1016/j.ebiom.2016.02.012

138. Palmer CS, Ostrowski M, Balderson B, Christian N, Crowe SM. Glucose metabolism regulates T cell activation, differentiation, and functions. *Front Immunol* (2015) **6**:1–6. doi:10.3389/fimmu.2015.00001

139. Frauwirth KA, Riley JL, Harris MH, Parry R V., Rathmell JC, Plas DR, Elstrom RL, June CH, Thompson CB. The CD28 signaling pathway regulates glucose metabolism. *Immunity* (2002) **16**:769–777. doi:10.1016/S1074-7613(02)00323-0

140. Finlay DK, Rosenzweig E, Sinclair L V, Feijoo-Carnero C, Hukelmann JL, Rolf J, Panteleyev AA, Okkenhaug K, Cantrell DA. PDK1 regulation of mTOR and hypoxia-inducible factor 1 integrate metabolism and migration of CD8+ T cells. *J Exp Med* (2012) **209**:2441–53. doi:10.1084/jem.20112607

141. Manel N, Kinet S, Battini JL, Kim FJ, Taylor N, Sitbon M. The HTLV receptor is an early T-cell activation marker whose expression requires de novo protein synthesis. *Blood* (2003) **101**:1913–1918. doi:10.1182/blood-2002-09-2681

142. Cammann C, Rath A, Reichl U, Lingel H, Brunner-Weinzierl M, Simeoni L, Schraven B, Lindquist JA. Early changes in the metabolic profile of activated CD8+ T cells. *BMC Cell Biol* (2016) **17**:1–11. doi:10.1186/s12860-016-0104-x

143. Wieman HL, Wofford JA, Rathmell JC. Cytokine stimulation promotes glucose uptake via phosphatidylinositol-3 kinase/Akt regulation of Glut1 activity and trafficking. *Mol Biol Cell* (2007) **18**:1437–46. doi:10.1091/mbc.e06-07-0593

144. Ward PS, Thompson CB. Signaling in control of cell growth and metabolism. *Cold Spring Harb Perspect Biol* (2012) **4**:1–15. doi:10.1101/cshperspect.a006783

145. Raff MC. Social controls on cell survival and cell death. *Nature* (1992) **356**:397–400. doi:10.1038/356397a0

146. Conlon I, Raff M. Size control in animal development. *Cell* (1999) **96**:235–244. doi:10.1016/S0092-8674(00)80563-2

147. Elmore S. Apoptosis: a review of programmed cell death. *Toxicol Pathol* (2007) **35**:495–516. doi:10.1080/01926230701320337

148. Hecht VC, Sullivan LB, Kimmerling RJ, Kim DH, Hosios AM, Stockslager MA, Stevens MM, Kang JH, Wirtz D, Vander Heiden MG, et al. Biophysical changes reduce energetic demand in growth factor-deprived lymphocytes. *J Cell Biol* (2016) **212**:439–447. doi:10.1083/jcb.201506118

149. Rathmell JC, Heiden MGV, Harris MH, Frauwirth KA, Thompson CB. In the absence of extrinsic signals, nutrient utilization by lymphocytes is insufficient to maintain either cell size or viability. *Mol Cell* (2000) **6**:683–692. doi:10.1016/S1097-2765(00)00066-6

150. Bentley J, Itchayanan D, Barnes K, McIntosh E, Tang X, Downes CP, Holman GD, Whetton AD, Owen-Lynch PJ, Baldwin SA. Interleukin-3-mediated cell survival signals include phosphatidylinositol 3-kinase-dependent translocation of the glucose transporter GLUT1 to the cell surface. *J Biol Chem* (2003) **278**:39337–39348. doi:10.1074/jbc.M305689200

151. Vander Heiden MG, Plas DR, Rathmell JC, Fox CJ, Harris MH, Thompson CB. Growth factors can influence cell growth and survival through effects on glucose metabolism. *Mol Cell Biol* (2001) **21**:5899–912. doi:10.1128/MCB.21.17.5899

152. Wofford J a, Wieman HL, Jacobs SR, Zhao Y, Rathmell JC. IL-7 promotes Glut1 trafficking and glucose uptake via STAT5-mediated activation of Akt to support T-cell survival. *Blood* (2008) **111**:2101–11. doi:10.1182/blood-2007-06-096297

153. Siska PJ, van der Windt GJW, Kishton RJ, Cohen S, Eisner W, MacIver NJ, Kater AP, Weinberg JB, Rathmell JC. Suppression of Glut1 and Glucose Metabolism by Decreased Akt/mTORC1 Signaling Drives T Cell Impairment in B Cell Leukemia. *J Immunol* (2016) **197**:2532–2540. doi:10.4049/jimmunol.1502464

154. Yu JSL, Cui W. Proliferation, survival and metabolism: the role of PI3K/AKT/mTOR signalling in pluripotency and cell fate determination. *Development* (2016) **143**:3050–3060. doi:10.1242/dev.137075

155. Shomit Sengupta1, 2, 3, Timothy R. Peterson1, 2, 3, and David M. Sabatini1, 2, 3

1Whitehead Institute for Biomedical Research, Nine Cambridge Center, Cambridge M 02142, USA, 2Howard Hughes Medical Institute, Department of Biology, Massachusetts Institute of Technology, Cambridge, MA 02139 U, 3The David H. Koch Institute for Integrative Cancer Research at MIT, 77 Massachusetts Avenue, Cambridge, MA 02139 U. NIH Public Access Regulation of the mTOR complex 1 pathway by nutrients, growth factors, and stress. *Mol Cell* (2010) **40**:310–322. doi:10.1016/j.molcel.2010.09.026.Regulation

156. Laplante M, Sabatini DM. NIH Public Access. *Cell* (2012) **149**:274–293. doi:10.1016/j.cell.2012.03.017.mTOR

157. Mizushima N, Yamamoto A, Hatano M, Kobayashi Y, Kabey Y, Suzuki K, Tokuhis T, Ohsumi Y, Yoshimori T. Dissection of autophagosome formation using Apg5-deficient mouse embryonic stem cells. *J Cell Biol* (2001) **152**:657–667. doi:10.1083/jcb.152.4.657

158. Donnelly RP, Loftus RM, Keating SE, Liou KT, Biron CA, Gardiner CM, Finlay DK. mTORC1-dependent metabolic reprogramming is a prerequisite for NK cell effector function. *J Immunol* (2014) **193**:4477–84. doi:10.4049/jimmunol.1401558

159. Klip A, Tsakiridis T, Marette A, Ortiz PA. Regulation of expression of glucose transporters by glucose: a review of studies in vivo and in cell cultures. *FASEB J* (1994) **8**:43–53. doi:10.1096/fasebj.8.1.8299889

160. Schafer JR, Salzillo TC, Chakravarti N, Kararoudi MN, Trikha P, Foltz JA, Wang R, Li S, Lee DA. Education-dependent activation of glycolysis promotes the cytolytic potency of licensed human natural killer cells. *J Allergy Clin Immunol* (2018) doi:10.1016/j.jaci.2018.06.047

161. Sun Q, Chen X, Ma J, Peng H, Wang F, Zha X, Wang Y, Jing Y, Yang H, Chen R, et al. Mammalian target of rapamycin up-regulation of pyruvate kinase isoenzyme type M2 is critical for aerobic glycolysis and tumor growth. *Proc Natl Acad Sci* (2011) **108**:4129–4134. doi:10.1073/pnas.1014769108

162. Land SC, Tee AR. Hypoxia-inducible factor 1α is regulated by the mammalian target of rapamycin (mTOR) via an mTOR signaling motif. *J Biol Chem* (2007) **282**:20534–20543. doi:10.1074/jbc.M611782200

163. Marçais A, Cherfils-Vicini J, Viant C, Degouve S, Viel S, Fenis A, Rabilloud J, Mayol K, Tavares A, Bienvenu J, et al. The metabolic checkpoint kinase mTOR is essential for IL-15 signaling during the development and activation of NK cells. *Nat Immunol* (2014) **15**:749–57. doi:10.1038/ni.2936

164. Marçais A, Marotel M, Degouve S, Koenig A, Fauteux-Daniel S, Drouillard A, Schlums H, Viel S, Besson L, Allatif O, et al. High mTOR activity is a hallmark of reactive natural killer cells and amplifies early signaling through activating receptors. *Elife* (2017) **6**:1–21. doi:10.7554/eLife.26423

165. Rathmell JC, Fox CJ, Plas DR, Hammerman PS, Cinalli RM, Thompson CB. Akt-directed glucose metabolism can prevent Bax conformation change and promote growth factor-independent survival. *Mol Cell Biol* (2003) **23**:7315–28. doi:10.1128/MCB.23.20.7315

166. Buck MD, Sowell RT, Kaech SM, Pearce EL. Metabolic Instruction of Immunity. *Cell* (2017) **169**:570–586. doi:10.1016/j.cell.2017.04.004

167. Assmann N, O'Brien KL, Donnelly RP, Dyck L, Zaiatz-Bittencourt V, Loftus RM, Heinrich P, Oefner PJ, Lynch L, Gardiner CM, et al. Srebp-controlled glucose metabolism is essential for NK cell functional responses. *Nat Immunol* (2017) **18**:1197–1206. doi:10.1038/ni.3838

168. Kelly B, O'Neill LAJ. Metabolic reprogramming in macrophages and dendritic cells in innate immunity. *Cell Res* (2015) **25**:771–84. doi:10.1038/cr.2015.68

169. Poznanski SM, Barra NG, Ashkar AA, Schertzer JD. Immunometabolism of T cells and NK cells: metabolic control of effector and regulatory function. *Inflamm Res* (2018) **67**:813–828. doi:10.1007/s00011-018-1174-3

170. Wang R, Green DR. Metabolic reprogramming and metabolic dependency in T cells. *Immunol Rev* (2012) **249**:14–26. doi:10.1111/j.1600-065X.2012.01155.x

171. O'Neill LAJ, Kishton RJ, Rathmell J. A guide to immunometabolism for immunologists. *Nat Rev Immunol* (2016) **16**:553–65. doi:10.1038/nri.2016.70

172. Pearce EL, Poffenberger MC, Chang C-H, Jones RG. Fueling immunity: insights into metabolism and lymphocyte function. *Science* (2013) **342**:1242454. doi:10.1126/science.1242454

173. Phan LM, Yeung S-CJ, Lee M-H. Cancer metabolic reprogramming: importance, main features, and potentials for precise targeted anti-cancer therapies. *Cancer Biol Med* (2014) **11**:1–19. doi:10.7497/j.issn.2095-3941.2014.01.001

174. Hanahan D, Weinberg RA. Hallmarks of cancer: the next generation. *Cell* (2011) **144**:646–74. doi:10.1016/j.cell.2011.02.013

175. Warburg O. Über den Stoffwechsel der Carcinomzelle. *Naturwissenschaften* (1924) **12**:1131–1137. doi:10.1007/BF01504608

176. WARBURG O. On the origin of cancer cells. *Science* (1956) **123**:309–14. doi:10.1126/science.123.3191.309

177. WEINHOUSE S. On respiratory impairment in cancer cells. *Science* (1956) **124**:267–9. Available at: http://www.ncbi.nlm.nih.gov/pubmed/13351638

178. Murray PJ, Rathmell J, Pearce E. SnapShot: Immunometabolism. *Cell Metab* (2015) **22**:190–190.e1. doi:10.1016/j.cmet.2015.06.014

179. Maciolek JA, Alex Pasternak J, Wilson HL. Metabolism of activated T lymphocytes. *Curr Opin Immunol* (2014) **27**:60–74. doi:10.1016/j.coi.2014.01.006

180. Kugelberg E. Immunometabolism: Complex metabolic responses to microbial stimuli. *Nat Rev Immunol* (2017) **17**:78–79. doi:10.1038/nri.2016.148

181. Keppel MP, Saucier N, Mah AY, Vogel TP, Cooper MA. Activation-Specific Metabolic Requirements for NK Cell IFN-γ Production. *J Immunol* (2015) **194**:1954–1962. doi:10.4049/jimmunol.1402099

182. Huntington ND. The unconventional expression of IL-15 and its role in NK cell homeostasis. *Immunol Cell Biol* (2014) **92**:210–213. doi:10.1038/icb.2014.1

183. Fehniger TA, Caligiuri MA, Dc W, Fehniger TA, Caligiuri MA. Interleukin 15 : biology and relevance to human disease Review article Interleukin 15 : biology and relevance to human disease. *Blood* (2001) **97**:14–32. doi:10.1182/blood.V97.1.14

184. Nandagopal N, Ali AK, Komal AK, Lee SH. The critical role of IL-15-PI3K-mTOR pathway in natural killer cell effector functions. *Front Immunol* (2014)

5:1–12. doi:10.3389/fimmu.2014.00187

185. Viel S, Marçais A, Guimaraes FS-F, Loftus R, Rabilloud J, Grau M, Degouve S, Djebali S, Sanlaville A, Charrier E, et al. TGF-β inhibits the activation and functions of NK cells by repressing the mTOR pathway. *Sci Signal* (2016) **9**:ra19. doi:10.1126/scisignal.aad1884

Auflistung der verwendeten Gefahrenstoffe nach GHS

(Gefahrensymbole, H- und P-Sätze)

Freiname	CAS-Nummer	GHS-Gefahrenstoff-kennzeichnung	H- und P-Sätze
Monensin	17090-79-8	 Giftig	H: 300 P: 264-301+310
Ethylendiamin-tetraessigsäure (EDTA)	60-00-4	 Reizend	H: 319 P: 305+351+338
Salzsäure (HCl)	7647-01-0	 Ätzend  Reizend	H: 290-314-335 P: 260-280-303+361+353-304+340+310-305+351+338
Paraform-aldehyd (PFA)	30525-89-4	 Entzündlich  Gesundheitsschädlich  Ätzend  Reizend	H: 228-302+332-315-317-318-335-350 P: 201-210-280-302+352-305+351+338
Natriumazid (NaN_3)	26628-22-8	 Umweltgefährlich  Giftig  Gesundheitsschädlich	H: 300-310-373-410 EUH: 032 P: 273-280-301+310+330-302+352-310-391-501

Eidesstattliche Versicherung

Declaration on oath

Hiermit erkläre ich, Caroline Pfeifer, an Eides statt, dass ich die vorliegende Dissertationsschrift selbst verfasst und keine anderen als die angegebenen Quellen und Hilfsmittel benutzt habe.

I, Caroline Pfeifer, hereby declare, on oath, that I have written the present dissertation by my own and have not used other than the acknowledged resources and aids.

Ort und Datum	Unterschrift
city and date	*signature*

Bestätigung der Korrektheit der englischen Sprache
Confirmation of the correctness of the English language

Hiermit erkläre ich, Christopher Thomas Ford, geboren am 30. Juli 1990 in Edinburgh, Schottland, UK, dass die Dissertation von Caroline Pfeifer mit dem Titel „Association between Natural Killer Cell Education and Cellular Glucose Metabolism in Human Natural Killer Cells" in einem korrekten Englisch verfasst wurde.

I, Christopher Thomas Ford, born on July 30th, 1990 in Edinburgh, Scotland, United Kingdom, hereby declare, that the thesis with the title "Association Between Natural Formation of Killer Cells and Cellular Glucose Metabolism in Human Natural Killer Cells" written by Caroline Pfeifer is written in grammatically correct English.

Ort und Datum *city and date*	Unterschrift *signature*

Curriculum vitae

Personal information	
Name:	Caroline Pfeifer, M.Sc.
Address:	Matthesonstraße 4, 20257 Hamburg
Date of birth:	26.03.1987 in Würzburg, Germany
Nationality:	German
Phone:	+49 (0) 176 – 457 412 26
E-mail:	carolinepfeifer@gmx.net

Professional experience	
09/2015-09/2018	**Heinrich-Pette-Institute (HPI), Leibniz-Institut for Experimental Virology, Hamburg, Germany** Graduate student in the research department of virus immunology under the supervision of Prof. Dr. Marcus Altfeld title: "Association between Natural Killer Cell Education and Cellular Glucose Metabolism in Human Natural Killer Cells"
08/2014-10/2014	**Centro de Investigatión Biomédica de Occidente in Guadalajara, México** voluntary internship as a training student at the Biomedical Research Center under the supervision of Dr. Alejandro Bravo Cuellar in the division immunology and Dr. Silvia Esperanza Flores Martinez in the division molecular medicine

academic education	
10/2011 -03/2014	**Friedrich-Alexander-University (FAU) Erlangen-Nürnberg, Germany** graduation in the master's course 'cell and molecular biology' degree: master of science (M.Sc.) master thesis at the Dermatological Institute of the University Hospital in Erlangen, Germany under the supervision of Dr. med. Andreas Baur title: 'The HIV-1 Nef Protein Induces the Cleavage of TNFα in Dendritic Cells'
10/2008-09/2011	**Friedrich-Alexander-University (FAU) Erlangen-Nürnberg, Germany** graduation in the bachelor's course 'biology' degree: bachelor of science (B.Sc.) bachelor thesis at the Virological Institute of the University Hospital in Erlangen, Germany under the direction of Prof. Dr. Thomas Stamminger title: 'Functional characterization of hybrid proteins from the human cytomegalovirus pUL69 and murine cytomegalovirus pM69'

Research experience	
Techniques	Adenoviral vector cloning, Confocal laser scanning microscopy, DNA and RNA isolation, Exosome isolation via ultracentrifugation from dendritic cells (DCs), Flow cytometry, Fluorescence-activated cell sorting (FACS), Gel electrophoresis (DNA and RNA), Immunolabeling, Immunoprecipitation, Mammalian adherent and non-adherent cell culture (K-562, 721.221, 293T, THP-1, HE-LA cells, monocytes and DCs), NK-cell degranulation assay, NK-cell isolation, PBMC isolation from whole blood samples, PCR, Protein immunoblotting, RNA-infection of DCs

Conference talks and posters	
Talk	Natural Killer Cell Symposium 2018, Hamburg Germany
Poster	NK2018 - The 17th meeting of the Society for Natural Immunity, San Antonio, Texas, USA
Poster	Natural Killer Cell Symposium 2018, Hamburg Germany

List of publications

Salzberger W, Martrus G, Bachmann K, Goebels H, Heß L, Koch M, Langeneckert A, Lunemann S, Oldhafer KJ, **Pfeifer C**, et al. Tissue-resident NK cells differ in their expression profile of the nutrient transporters Glut1, CD98 and CD71. PLoS One (2018) 13:e0201170. doi:10.1371/journal.pone.0201170

Pfeifer C, Bunders MJ. Maternal HIV infection alters the immune balance in the mother and fetus; Implications for pregnancy outcome and infant health. Curr Opin HIV AIDS (2016) 11:138–145. doi:10.1097/COH.0000000000000239

Zielke B, Wagenknecht N, **Pfeifer C**, Zielke K, Thomas M, Stamminger T. Transfer of the UAP56 Interaction Motif of Human Cytomegalovirus pUL69 to Its Murine Cytomegalovirus Homolog Converts the Protein into a Functional mRNA Export Factor That Can Substitute for pUL69 during Viral Infection. J Virol (2012) 86:7448–7453. doi:10.1128/JVI.00730-12

Skills and competences	
Language skills	German: mother tongue, English: fluent (C1), Spanish: average level (B2), French: basic knowledge (A2)
Computer skills	
Application programs	MS Office, Graph Pad Prism, FlowJo, Mendeley
	Apple OS

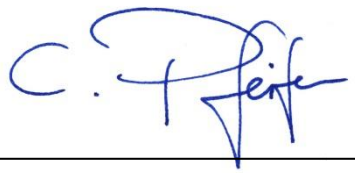

Hamburg, October the 29th, 2018

place and date

Caroline Pfeifer

Acknowledgements

Firstly, I would like to express my sincere gratitude to my doctoral supervisor and mentor **Prof. Dr. Marcus Altfeld**, who gave me the opportunity to conduct my doctoral thesis in his lab at the Heinrich Pette Institute in Hamburg. I am very grateful for his excellent scientific support and beneficial critique. I wish to thank him for the confidence he had in my work and for giving me the chance to be involved in such an interesting research topic.

My sincere thanks also goes to my second supervisor **Prof. Dr. Chris Meier** for scientific discussions and advice during the time of my Ph.D.

I would like to thank **Prof. Dr. Michael Kolbe** for being the second reviewer of my dissertation.

Very special gratitude goes to **Dr. Christian Körner** for his invaluable advice and feedback on my research and support of my work.

I gratefully acknowledge **Arne Düsedau** and **Jana Hennesen** from the flow cytometry / FACS technology platform at the Heinrich Pette Institute, for sharing their knowledge about flow cytometry with me. Thank you for your support.

I would especially like to thank all **blood donors** who gave their consent to use their blood samples for this study, as well as **Sven Peine** and everyone from the **Institute of Transfusion Medicine** at the University medical center Hamburg-Eppendorf, who were involved in the production of the buffy coats.

I want to thank **Jürgen Sauter** and **Alexander H. Schmidt** from the **DKMS** as well as everyone else who helped with the HLA-genotyping of all study participants.

I also want to thank **Laura Richert** for her statistical advice.

I wish to express my heartfelt thanks to all of my **colleagues** of the department of **virus immunology**. Thank you for your experimental help and scientific suggestions at various points of my research and especially for creating such a cooperative and enjoyable atmosphere and welcoming me so warmly as part of your team!